The Thesis Committee for Ruth Ellen Hahn
Certifies that this is the approved version of the following thesis:

Novel Cationic Surfactants for CO_2-Foam Flooding in Carbonate Reservoirs

APPROVED BY
SUPERVISING COMMITTEE:

Kishore K. Mohanty, Supervisor

Kamy Sepehrnoori

Novel Cationic Surfactants for CO_2-Foam Flooding in Carbonate Reservoirs

by

Ruth Ellen Hahn, B.S.

Thesis

Presented to the Faculty of the Graduate School of

The University of Texas at Austin

in Partial Fulfillment

of the Requirements

for the Degree of

Master of Science in Engineering

The University of Texas at Austin

August 2015

Dedication

This thesis is dedicated to my loving parents, Alice and William, and to my wonderful brother Andrew, for their love and support throughout my entire life. I would also like to dedicate it to my grandparents, Margaret and Dick Layton and Lilian and Joe Hahn, and to my Texas parents, Kathy and Aron, who have made this state home.

Acknowledgements

I would like to express my sincere thanks to my supervisor, Dr. Kishore K. Mohanty for his help and support throughout my SURI internship and my two years at the University of Texas while receiving my Master's degree. I would also like to thank Dr. Kamy Sepehrnoori for teaching me more ways to solve engineering analysis problems than I knew existed and for serving as my second reader.

I would like to extend a special thank you to the experienced research staff, Dr. Eric Dao, Dr. Krishna Panthi, and Dr. Chammi Miller. They offered invaluable assistance with my research during my time here. They were a key part of completing my degree.

I would like to extend a thank you to Barbara Messmore and Frankie Hart for always ensuring I was registered properly and taking care of the details I overlooked.

I would also like to extend a special thank you to ALL the members of Dr. Mohanty's research group, especially those in 5.106. Himanshu, Thew, Pinaki, and Shashvat, I could not have completed my degree without you guys. From our lunches to our research discussions, you were so essential to my success and to keeping my sanity. Thank you, Prateek and Himanshu for always lending a helpful hand and helping me open coreholders and troubleshoot.

Finally, I would like to thank my roommates, Roy, Andrew, Wynn, Ignacio, and Michael, for the wonderful memories I made with them and all the other friends I made along the way. They helped me enjoy graduate school to its fullest, and for that, I am immensely thankful.

Abstract

Novel Cationic Surfactants for CO_2-Foam Flooding in Carbonate Reservoirs

Ruth Ellen Hahn, M.S.E

The University of Texas at Austin, 2015

Supervisor: Kishore Mohanty

A majority of oil throughout the world is contained in carbonate reservoirs. Alkaline-Surfactant-Polymer (ASP) floods cannot be applied in many carbonate reservoirs for three main reasons: conventional alkali are not compatible with divalent ions, adsorption of anionic surfactants is high in the absence of alkali, and the permeability of the rock is often low for polymers to pass through the pores. One alternative to ASP flooding is CO_2-foam flooding. Foam flooding reduces the mobility of the CO_2 and increases the sweep efficiency. To overcome the adsorption of surfactant on the carbonate surface, cationic surfactants can be used rather than anionic surfactants. The objective of this research is to study two novel cationic surfactants for foam flooding applications. These surfactants are gemini surfactants, containing two head groups and two tail groups.

The bulk foam stability in the presence and absence of oil was studied for these surfactants and compared to conventional surfactants; these gemini surfactants showed

comparable bulk foam stability to other cationic surfactants. Corefloods in the absence of oil were performed at reservoir conditions to prove foam formation in porous media and to determine the optimum ratio of CO_2 to surfactant injection ratio. Both water-wet and oil-wet coreflood experiments were performed for the gemini surfactants. The water-wet corefloods for both surfactants recovered 6-16 %OOIP after the waterflood. The pressure drop during the water-wet foam floods was not too high, less than 15 psi/foot which is reasonable for a low permeability carbonate core. The corefloods showed results comparable with a polymer flood, with no injectivity issues, indicating that these surfactants can be used in place of polymer flooding in carbonate reservoirs. The oil-wet experiment also resulted in foam flood recovery of 13% OOIP, despite the poor wettability alteration results seen with calcite chips. With better foam stability in the presence of oil and enhanced wettability alteration, this new class of cationic surfactants could be a viable option for enhanced oil recovery in carbonate reservoirs.

Table of Contents

List of Tables xiii

List of Figures xvii

Chapter 1: Introduction 1

1.1 Use of Foam in Carbonate Reservoirs For Mobility Control 1

1.2 Research Objectives 7

1.3 Description of Chapters 8

Chapter 2: Literature Review 9

2.1 Fundamental concepts of foam 9

2.1.1 Definition of Foam 9

2.1.2 Foam Properties 10

2.1.2.1 Foam Texture 10

2.1.2.2 Foam Quality 11

2.1.2.3 Foam Rheology 12

2.1.3 Foam Generation 12

2.1.3.1 Snap-Off 12

Pre-neck snap-off 13

Neck snap-off 13

Rectilinear snap-off 14

2.1.3.2 Lamella Division 14

2.1.3.3 Leave Behind 15

2.1.4 Foam Stability 15

2.1.4.1 Presence of Oil 16

Spreading Coefficient 16

Entering Coefficient 17

Bridging Coefficient 17

2.1.4.2 Other Factors Affecting Foam Stability 18

2.2 Foam in enhanced oil recovery 18

2.2.1 Mobility Reduction 18
2.2.2 Injection Strategies: SAG vs. Co-injection 19
2.3 Gemini Surfactants 20
2.3.1 Definition 20
2.3.2 Characteristics 21
Chapter 3: Experimental Setup and Methodology 25
3.1 Materials 25
3.1.1 Oil 25
3.1.2 Surfactants 25
3.1.2.2 Commercial cationic surfactant 27
3.1.2.3 Commercial anionic surfactant 27
3.1.3 Core Sample 28
3.1.4 Formation and Injection Brine 28
3.2 Surfactant Characterization Equipment and Methodology 28
3.2.1 Aqueous Stability 28
Equipment 28
Method 29
3.2.2 Bulk Foam Stability 30
Equipment and Methodology 30
Bulk Foam Stability Results 31
3.2.3 Spreading, Entering, and Bridging Coefficients 32
Equipment 32
Methods 32
3.2.4 Adsorption 35
3.2.4.1 Anionic Surfactant Adsorption Equipment 35
3.2.4.2 Cationic Surfactant Adsorption Equipment and Materials 35
Conventional Cationic Surfactant Method 36
Gemini Cationic Surfactant Method 37
3.2.4.3 Batch Adsorption Methodology 38

3.2.5 Preliminary Wettability Alteration Studies....39
3.3 Coreflood Equipment and Methodology....39
3.3.1 Coreflood Equipment....39
Stainless Steel Accumulator....39
Syringe Pumps....40
Coreholder....40
Pressure Transducer....40
Backpressure Regulator (BPR)....41
Carbon Dioxide....41
Sandpack....41
3.3.2 Coreflood Set-Up....41
42
3.3.3 Core Measurements....43
3.3.3.1 Core Sample Measurements....43
Core Sample Preparation....43
Air Porosity....43
Air Permeability....44
Brine Saturation by Vacuum....44
Pore Volume Calculations....44
Brine Permeability....45
Initial Oil Saturation....45
Effective Oil Permeability....46
Effective Water Permeability....46
End Point Oil Relative Permeability....47
End Point Oil Relative Permeability....47
Aging....48
3.3.4 Coreflood....48
3.3.4.1 Corefloods in the Absence of Oil....48
3.3.4.2 Corefloods in the Presence of Oil....49

Chapter 4: Results 50
4.1 Results of Surfactant Characterization 50
4.1.1 Aqueous Stability 50
4.1.2 Bulk Foam Stability 56
4.1.2.1 Preliminary Bulk Foam Stability Results 56
4.1.2.2 Effect of Salinity on Bulk Foam Stability at Room Temperature and 60°C 57
GC 468 57
GC 580 60
CTAB 63
AS-40 66
4.1.2.3 Effect of Oil on Bulk Foam Stability 69
GC 468 69
GC 580 73
CTAB 76
AS-40 80
4.1.2.3 Effect of pH on Bulk Foam Stability 83
4.1.3 Spreading, Entering, and Bridging Coefficients 87
4.1.4 Adsorption 94
4.1.4.1 Anionic Surfactant Adsorption 94
4.1.4.2 Cationic Surfactant Adsorption 95
4.1.4.5 Wettability Alteration 100
4.2 Corefloods in the Absence of Oil 102
4.2.1 GC 468 102
4.2.2 GC 580 107
4.2.3 CTAB 112
4.2.4 Mobility Reduction Factor 116
4.3 Corefloods in the Presence of Oil 118
4.3.1 Coreflood 1: GC 468 with Mineral Oil (Water wet) 118
4.3.2 Coreflood 2: GC 468 with Crude A (Water Wet) 123

4.3.3 Coreflood 3: GC 468 with Crude A (Oil Wet) 128
4.3.4 Coreflood 4: GC 580 with Mineral Oil (Water wet).....132
4.3.5 Coreflood 5: GC 580 with Crude A (Water Wet).....136

Chapter 5: Conclusions and Recommendations 140
5.1 Conclusions.....140
5.2 Recommendations and Future Work 143

Appendix A.....144

Appendix B 146

References.....153

Vita…….….158

List of Tables

Table 3. 1: Oil properties. 25

Table 4. 1: Aqueous stability results of GC 468 at varying salinity and varying temperature. 51

Table 4. 2: Aqueous stability results of GC 580 at varying salinity and varying temperature. 53

Table 4. 3: Aqueous stability results of CTAB at varying salinity and varying temperature. 54

Table 4. 4: Aqueous stability result of AS-40 at varying salinity and temperature55

Table 4. 5: A summary of results of bulk foam stability for GC 468 at varying salinities at both 25^{o}C and 60^{o}C. Half-life is the time at which the height of the foam is half the height of the initial foam. No oil was present for these bulk foam stability tests. 60

Table 4. 6: A summary of results of bulk foam stability for GC 580 at varying salinities at both 25^{o}C and 60^{o}C. Half-life is the time at which the height of the foam is half the height of the initial foam. No oil was present for these bulk foam stability tests. 63

Table 4. 7: A summary of results of bulk foam stability for CTAB at varying salinities at both 25^{o}C and 60^{o}C. Half-life is the time at which the height of the foam is half the height of the initial foam. No oil was present for these bulk foam stability tests. 66

Table 4. 8: A summary of results of bulk foam stability for AS-40 at varying salinities at both 25°C and 60°C. Half-life is the time at which the height of the foam is half the height of the initial foam. No oil was present for these bulk foam stability tests. 69

Table 4.9: A summary of results of bulk foam stability for GC 468 with 1%$CaCl_2$ and 1% $MgCl_2$ in the presence of varying oils at both 25°C and 60°C. 1 wt% oil was present.....73

Table 4. 9: A summary of results of bulk foam stability for GC 580 with 4% NaCl, 1%$CaCl_2$, and 1% $MgCl_2$ in the presence of varying oils at both 25°C and 60°C. 1 wt% oil was present. 76

Table 4. 10: A summary of results of bulk foam stability for CTAB with 4% NaCl, 1%$CaCl_2$, and 1% $MgCl_2$ in the presence of oils at both 25°C and 60°C. 1 wt% oil was present. 79

Table 4. 11: A summary of results of bulk foam stability for AS-40 with 4% NaCl in the presence of varying oils at both 25°C and 60°C. 1 wt% oil was present. 83

Table 4. 12: Surface tension of each cationic surfactant at varying salinities. The measurements were performed at room temperature, therefore, the surface tension was not measured for solutions that were not aqueous stable at T=25°C.....88

Table 4. 13: Surface tension of each of the oils at room temperature. 89

Table 4. 14: IFT values for GC 468 at varying salinities with all three crude oils measured at room temperature. 90

Table 4. 15: Spreading, entering, and bridging coefficients for GC 468 at varying salinities with all three crude oils. The bolded numbers are favorable bridging coefficients. 91
Table 4. 16: IFT values for GC 580 at varying salinities with Crude A. 92
Table 4. 17: Spreading, entering, and bridging coefficients for GC 580 and Crude A. No bridging coefficients are favorable, but GC 580 with 4% NaCl, 1% $CaCl_2$, and 1% $MgCl_2$ is the closest to stable. 93
Table 4. 18: Summary of batch adsorption studies for each of the four surfactants studied at three different concentrations. All batch adsorption studies were done at 60^{o}C and at the injection brine salinity. 99
Table 4. 19: Texas Cream Limestone properties for coreflood experiments performed in the absence of oil. 103
Table 4. 20: Experimental conditions of corefloods performed in the absence of oil. 103
Table 4. 21: Core properties for Coreflood 1. 119
Table 4. 22: Experimental conditions for Coreflood 1. 119
Table 4. 23: Summary of oil recovery during Coreflood 1. 123
Table 4. 24: Texas Cream Limestone properties for Coreflood 2. 123
Table 4. 25: Experimental conditions for Coreflood 2. 124
Table 4. 26: A summary of oil recovery during Coreflood 2. 127
Table 4. 27: Texas Cream Limestone properties for Coreflood 3. 128
Table 4. 28: Experimental conditions for Coreflood 3. 128
Table 4. 29: A summary of oil recovery during Coreflood 3. 131
Table 4. 30: Texas Cream Limestone properties for Coreflood 4. 132

Table 4. 31: Experimental conditions for Coreflood 4. 132
Table 4. 32: A summary of oil recovery during Coreflood 4 135
Table 4. 33: Texas Cream Limestone properties for Coreflood 5. 136
Table 4. 34: Experimental conditions for Coreflood 5. 136
Table 4. 35: A summary of oil recovery during Coreflood 5. 139
Table A. 1: Aqueous stability GC 566 at a range of temperatures and salinities. GC 566 was only aqueously stable above 80^{o}C at low salinities. The reservoir temperature for this study was 60^{o}C; therefore, this surfactant was not studied further. 144
Table A. 2: Aqueous stability of GC 776 at a range of temperatures and salinities. GC 776 is not aqueously stable at any temperatures or salinities evaluated; therefore it was not studied further. 145

List of Figures

Figure 1. 1: Map of carbonate reservoirs around the world (Schlumberger Market Anaylsis, 2007). 2

Figure 1. 2: Areal sweep schematic of a polymer flood for mobility control (Caenn et al., 1989). 3

Figure 1. 3: Vertical sweep schematic of a polymer flood for mobility control (Caenn et al., 1989). 4

Figure 1. 4:Schematic of possible effects of foam on gas transport in porous media (Sharma and Shah, 1989). 6

Figure 2.1: A generalized foam system (Schramm, 1994) 10

Figure 2.2: Mechanism for foam generation via snap-off (Kovcek and Radke, 1994). 13

Figure 2.3: Mechanism for foam generation via lamella division (Kovscek and Radke, 1994). 14

Figure 2.4: Mechanism for foam generation via leave-behind (Kovcek and Radke, 1994). 15

Figure 2.5: Structure of gemini surfactants (a) compared to conventional surfactants (b). 21

Figure 2.6: Surface tension vs log concentration of surfactant. Below the CMC the surfactant exists as monomers; Above the CMC surfactant exists as micelles (Schramm, 1994). 22

Figure 2.7: Variation in surface tension with the surfactant concentration and a gemini surfactant with a 12- carbon tail (Zana and Xia, 2004). 23

Figure 3. 1: Chemical structure of each of the cationic gemini surfactants evaluated in this study. (a) GC 580 (b) GC 468 (c) GC 566 and (d) GC 776. 27
Figure 3. 2: Sample aqueous stability result. (a) shows a solution that is cloudy, (b) shows a sample that has a precipitate, and (c) shows a sample that is aqueously stable. 29
Figure 3. 3: Experimental set up for bulk foam stability measurements. 31
Figure 3. 4: Bulk foam stability for GC 580 at 60^{o}C. The formulation with the longest half-life was selected for coreflood experiments. 32
Figure 3. 5: Schematic of surface tension measurements. Image obtained at http://www.kruss.de/services/education-theory/glossary/pendant-drop/. 33
Figure 3. 6: Schematic of spinning drop tensiometer measurements. 34
Figure 3. 7: Calibration samples for CTAB surfactant adsorption. From left to right: 0.25 mL, 0.5, 0.75, 1.0, 1.25 mL of 0.1% CTAB 37
Figure 3. 8: The organic layer of calibration samples for GC468. From left to right: 0.5 mL, 1 mL, 2 mL, and 3 mL.....38
Figure 3. 9: Coreflood set-up. The dashed lines represent the oven boundary.....42
Figure 4. 1: Hofmann Elimination mechanism. Mechanism obtained from http://www.chem.ucalgary.ca/courses/351/Carey5th/Ch22/ch22-3-4.html. 52
Figure 4. 2: Preliminary bulk foam stability tests for GC 468. All five salinities show excellent foam formation. 57

Figure 4. 3: Bulk foam stability of GC 468 at T=25^{o}C at varying salinities. Bulk foam stability is measured as a function of foam height divided by the initial foam height. No oil was present. 58
Figure 4. 4: Bulk foam stability of GC 468 at T=60^{o}C at varying salinities. Bulk foam stability is measured as a function of foam height divided by the initial foam height. No oil was present for these bulk foam stability tests. 59
Figure 4. 5: Bulk foam stability of GC 580 at T=25^{o}C at varying salinities. Bulk foam stability is measured as a function of foam height divided by the initial foam height. No oil was present. 61
Figure 4. 6: Bulk foam stability of GC 580 at T=60^{o}C at varying salinities. Bulk foam stability is measured as a function of foam height divided by the initial foam height. No oil was present. 62
Figure 4. 7: Bulk foam stability of CTAB at T=25^{o}C at varying salinities. Bulk foam stability is measured as a function of foam height divided by the initial foam height. No oil was present. 64
Figure 4. 8: Bulk foam stability of CTAB at T=60^{o}C at varying salinities. Bulk foam stability is measured as a function of foam height divided by the initial foam height. No oil was present. 65
Figure 4. 9: Bulk foam stability of AS-40 at T=25^{o}C at varying salinities. Bulk foam stability is measured as a function of foam height divided by the initial foam height. No oil was present. 67
Figure 4. 10: Bulk foam stability of AS-40 at T=60^{o}C at varying salinities. Bulk foam stability is measured as a function of foam height divided by the initial foam height. No oil was present. 68

Figure 4. 11: Bulk foam stability of GC 468 with 1% $CaCl_2$ and 1% $MgCl_2$ at T=25^oC in the presence of oils. Bulk foam stability is measured as a function of foam height divided by the initial foam height. Three crude oils were tested in addition to mineral oil and decane.....71

Figure 4. 12: Bulk foam stability of GC 468 with 1% $CaCl_2$ and 1% $MgCl_2$ at T=60^oC in the presence of varying oils. Bulk foam stability is measured as a function of foam height divided by the initial foam height. Three crude oils were tested in addition to mineral oil and decane. 72

Figure 4. 13: Bulk foam stability of GC 580 with 4% NaCl, 1% $CaCl_2$, and 1% $MgCl_2$ at T=25^oC in the presence of varying oils. Bulk foam stability is measured as a function of foam height divided by the initial foam height. Three crude oils were tested in addition to mineral oil and decane..74

Figure 4. 14: Bulk foam stability of GC 580 with 4%NaCl, 1% $CaCl_2$, and 1% $MgCl_2$ at T=60^oC in the presence of varying oils. Bulk foam stability is measured as a function of foam height divided by the initial foam height. Three crude oils were tested in addition to mineral oil and decane..75

Figure 4. 15: Bulk foam stability of CTAB with 4% NaCl, 1% $CaCl_2$, and 1% $MgCl_2$ at T=25oC in the presence of varying oils. Bulk foam stability is measured as a function of foam height divided by the initial foam height. Three crude oils were tested in addition to mineral oil and decane..77

Figure 4. 16: Bulk foam stability of CTAB with 4% NaCl, 1% $CaCl_2$, and 1% $MgCl_2$ at T=60^oC in the presence of varying oils. Bulk foam stability is measured as a function of foam height divided by the initial foam height. Three crude oils were tested in addition to mineral oil and decane..78

Figure 4. 17: Bulk foam stability of AS-40 with 4% NaCl in the presence of varying oils at T=25^{o}C. Bulk foam stability is measured as a function of foam height divided by the initial foam height. Three crude oils were tested in addition to mineral oil and decane. 81

Figure 4. 18: Bulk foam stability of AS-40 with 4% NaCl at T=60^{o}C in the presence of varying oils. Bulk foam stability is measured as a function of foam height divided by the initial foam height. Three crude oils were tested in addition to mineral oil and decane. 82

Figure 4. 19: The bulk foam stability of GC 468 with 1%$CaCl_2$ and 1%$MgCl_2$ at varying pH at T=25^{o}C. 9.7 is the normal pH of the surfactant solution. The pH was reduced to 5 and to 4 to simulate the effect of CO_2 on the pH of the surfactant solution. 84

Figure 4. 20: The bulk foam stability of GC 580 with 4% NaCl, 1%$CaCl_2$, and 1%$MgCl_2$ at varying pH at T=25^{o}C. 9 is the normal pH of the surfactant solution. The pH was reduced to 6.6 and to 5 to simulate the effect of CO_2 on the pH of the surfactant solution. 85

Figure 4. 21: The bulk foam stability of GC 580 with 4% NaCl, 1%$CaCl_2$, and 1%$MgCl_2$ at varying pH at T=25^{o}C. 7.7 is the normal pH of the surfactant solution. The pH was reduced to 6.3 and to 5 to simulate the effect of CO_2 on the pH of the surfactant solution.....86

Figure 4. 22: Calibration curve for AS-40 using HPLC. 94

Figure 4. 23: Calibration curve for GC 468 using UV-vis. 95

Figure 4. 24: Calibration curve for GC 580 using UV-vis. 97

Figure 4. 25: Calibration curve for CTAB using UV-vis. 98

Figure 4. 26: a) Calcite chip aged in Crude A in GC 468, b) Calcite chip aged in Crude A in GC 580. 100
Figure 4. 27: a) Calcite chip aged in Crude B in GC 468. b) Calcite chip aged in Crude B in GC 580. 101
Figure 4. 28: a) Calcite chip aged in Crude C in GC 468, b) Calcite chip aged in Crude C in GC 580. 101
Figure 4. 29: Core flood experiment in the absence of oil with GC 468 with 1% $CaCl_2$ and 1% $MgCl_2$. The flow rate was 4 ft/day. The steady state pressure drop is plotted. This experiment looks at the effect of surfactant concentration on pressure drop during CO_2 and surfactant co-injection at 90% quality. 106
Figure 4. 30: Core flood experiment in the absence of oil with 0.5% GC 468 with 1%$CaCl_2$ and 1%$MgCl_2$. The flow rate was 4 ft/day. The pressure drop plotted is the pressure drop at the steady state. This experiment looks at the effect of the ratio of CO_2 to surfactant solution on the pressure drop across the core. 107
Figure 4. 31: Core flood experiment in the absence of oil with GC 580 with 4%NaCl, 1%$CaCl_2$, and 1%$MgCl_2$. The flow rate was 4 ft/day. The steady state pressure drop is plotted. This experiment looks at the effect of surfactant concentration on pressure drop during CO_2 and surfactant co-injection. 110

Figure 4. 32: Core flood experiment in the absence of oil with 0.5% GC 580 with 4%NaCl, 1%$CaCl_2$, and 1%$MgCl_2$. The flow rate was 4 ft/day. The steady state pressure drop is plotted. This experiment looks at the effect of ratio of CO_2 to surfactant during co-injection on pressure drop.112

Figure 4. 33: Core flood experiment in the absence of oil with surfactants in 4% NaCl, 1% $CaCl_2$, and 1% $MgCl_2$. The flow rate was 4 ft/day. The pressure drop plotted is the pressure drop at the steady state. CO_2 and surfactant solution are co-injected at 90% quality. CTAB is compared to the two cationic gemini surfactants, GC 468 and GC 580 at different concentrations 114

Figure 4. 34: Core flood experiment in the absence of oil with 0.5% surfactant with 4% NaCl, 1%$CaCl_2$, and 1%$MgCl_2$. The flow rate was 4 ft/day. The pressure drop plotted is at the steady state. This experiment looks at the effect of ratio of CO_2 to surfactant solution during co-injection on pressure drop. CTAB is compared to the two cationic gemini surfactants, GC 468 and GC 580.....115

Figure 4. 35: The mobility reduction factor is compared for all three cationic surfactants. The effect of surfactant concentration is also shown. .117

Figure 4. 36: The mobility reduction factor is compared for all three cationic surfactants. The effect of CO_2 and surfactant ratio is also shown. .118

Figure 4. 37: The pressure drop and oil recovery are shown as a function of pore volumes injected for Coreflood 1. Brine is injected at 1 ft/day, followed by brine injection at 5 ft/day, surfactant injection at 1 ft/day, and finally a foam injection at 86% quality at 1 ft/day. 121

Figure 4. 38: The oil, water, and gas cuts during Coreflood 1. 122
Figure 4. 39: The pressure drop and oil recovery are shown as a function of pore volumes injected for Coreflood 2. Brine is injected at 1 ft/day, followed by brine injection at 5 ft/day, surfactant injection at 1 ft/day, and finally a foam injection at 86% quality at 1 ft/day. 125
Figure 4. 40: The oil, water, and gas cuts during Coreflood 2. 127
Figure 4. 41: The pressure drop and oil recovery are shown as a function of pore volumes injected for Coreflood 3. Brine is injected at 1 ft/day, followed by brine injection at 4 ft/day (because this coreholder should not be subjected to more than 400 psi), surfactant injection at 1 ft/day, and finally a foam injection at 86% quality at 1 ft/day.....130
Figure 4. 42: The oil, water, and gas cuts during Coreflood 3. 131
Figure 4. 43: The pressure drop and oil recovery are shown as a function of pore volumes injected for Coreflood 4. Brine is injected at 1 ft/day, followed by brine injection at 5 ft/day, surfactant injection at 1 ft/day, and finally a foam injection at 86% quality at 1 ft/day. Since the 1 ft/day foam flood did not recover much, the foam flood rate was increased to 4 ft/day.134
Figure 4. 44: The oil, water, and gas cuts during Coreflood 4. 135
Figure 4. 45: The pressure drop and oil recovery are shown as a function of pore volumes injected for Coreflood 5. Brine is injected at 1 ft/day, followed by brine injection at 5 ft/day, surfactant injection at 1 ft/day, and finally a foam injection at 86% quality at 1 ft/day. 138
Figure B. 1: Bulk foam stability results of 0.25% GC 468 with 1% $CaCl_2$ and 1% $MgCl_2$ at T=60^{o}C. No oil was present. 146

Figure B. 2: Bulk foam stability results of 0.25% GC 580 with 4% NaCl, 1% $CaCl_2$, and 1% $MgCl_2$ at T=25^{o}C in the presence of 1 wt% decane. 147
Figure B. 3: Bulk foam stability results of 0.25% GC 580 with 4% NaCl, 1% CaCl2, and 1% MgCl2 at T=25^{o}C. No oil was present.....148
Figure B. 4: Bulk foam stability results of 0.25% GC 580 with 4% NaCl, 1% $CaCl_2$, and 1% $MgCl_2$ at T=25^{o}C in the presence of 1 wt% mineral oil. ...149
Figure B. 5: Bulk foam stability results of 0.25% GC 580 with 4% NaCl, 1% $CaCl_2$, and 1% $MgCl_2$ at T=25^{o}C in the presence of 1 wt% Crude A.....150
151
Figure B. 6: Bulk foam stability of 0.25% CTAB with 4% NaCl, 1% $CaCl_2$, and 1% $MgCl_2$ at T=60^{o}C. No oil was present. 151
Figure B. 7: Bulk foam stability of 0.25% AS-40 at T=60^{o}C. No salt is present and no oil is present 152

Chapter 1: Introduction

The first chapter of this thesis discusses the motivation behind foam flooding with novel cationic gemini surfactants for chemical enhanced oil recovery (EOR). It provides the importance of this research in terms of oil recovery in carbonate reservoirs. This chapter also contains the research objectives of this thesis and an overview of the remaining chapters.

1.1 Use of Foam in Carbonate Reservoirs For Mobility Control

Carbonate hydrocarbon-containing reservoirs are more prominent than sandstone reservoirs, with an estimate that more than 40% of the gas reserves and 60% of the oil reserves are found in carbonate reservoirs worldwide (Schlumberger Market Analysis, 2007). Figure 1.1 shows a map of the distribution of carbonate reservoirs across the world. It is estimated that 80% of these carbonate reservoirs are mixed-wet to oil-wet compared to sandstones with are predominantly water-wet. The negatively charged carboxylic acid anions found in the oil are attracted to the carbonate surface which has a positive zeta potential (Seethepalli et al, 2004). Due to the high affinity of oil to the carbonate rock surface, waterfloods often have low recovery factors (the ratio of recoverable oil to the original oil in place), averaging 35% (Schlumberger, 2007). Additionally, due to the heterogeneity of carbonate reservoirs, secondary recovery, either immiscible gas flooding or waterflooding, can have recovery factors as low as 10% (Montaron, 2005). The remaining oil after secondary recovery is either residual oil trapped in the swept portion of the reservoir or oil bypassed in the unswept portions of the reservoir.

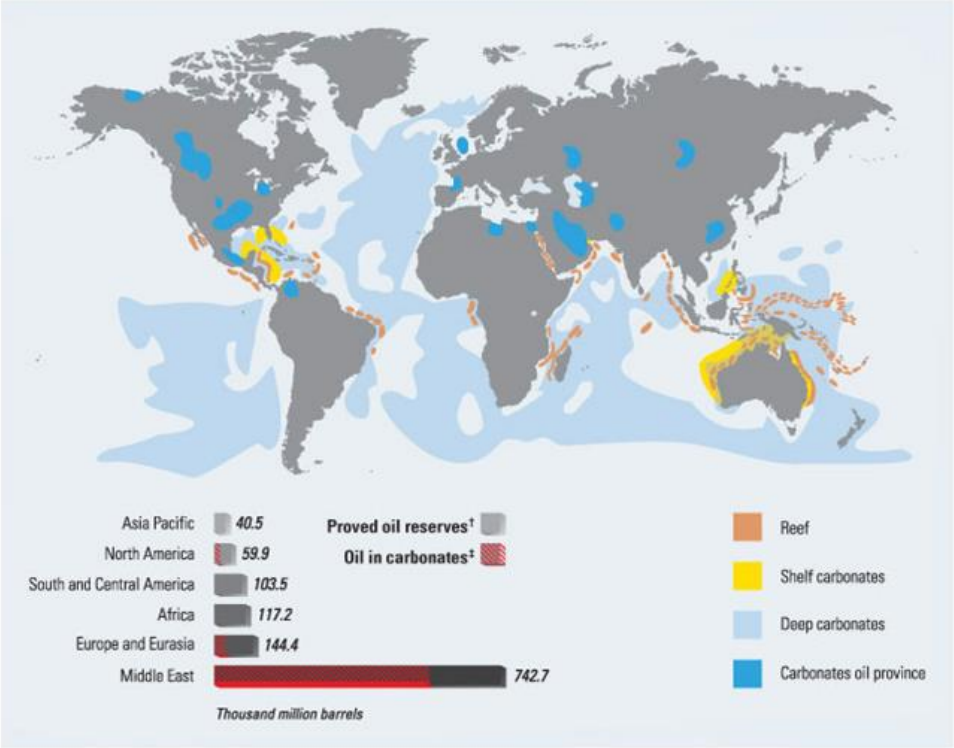

Distribution of oil from carbonate sources around the world.

† BP Statistical Review, 2007

‡ Schlumberger Market Analysis, 2007

Figure 1. 1: Map of carbonate reservoirs around the world (Schlumberger Market Anaylsis, 2007).

In order to increase the recovery of the remaining oil, a tertiary flood must be performed. Tertiary recovery techniques include injection of solvents, surfactants, polymers, and a combination of surfactants and polymers (ASP). Polymer flooding is among the most common tertiary techniques, with over 40 years of commercial applications (Pope, 2007). Polymer flooding increases the viscosity of the injected water, contributing to mobility control and stability, reducing viscous fingering and contacting the oil previously bypassed during a water or gas flood. This increases the sweep

efficiency. Figure 1.2 shows how a decrease in mobility ratio can dramatically improve the areal sweep efficiency of a typical polymer flood, and Figure 1.3 shows how a decrease in mobility ratio can improve the vertical sweep efficiency of a typical polymer flood.

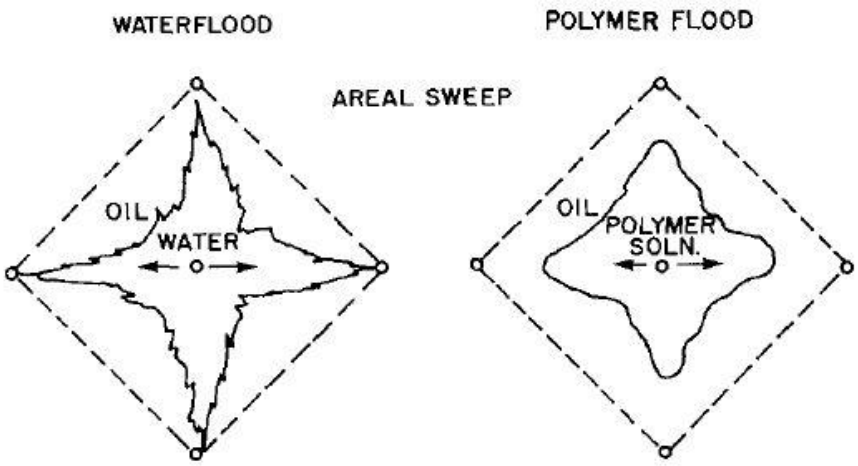

Figure 1. 2: Areal sweep schematic of a polymer flood for mobility control (Caenn et al., 1989).

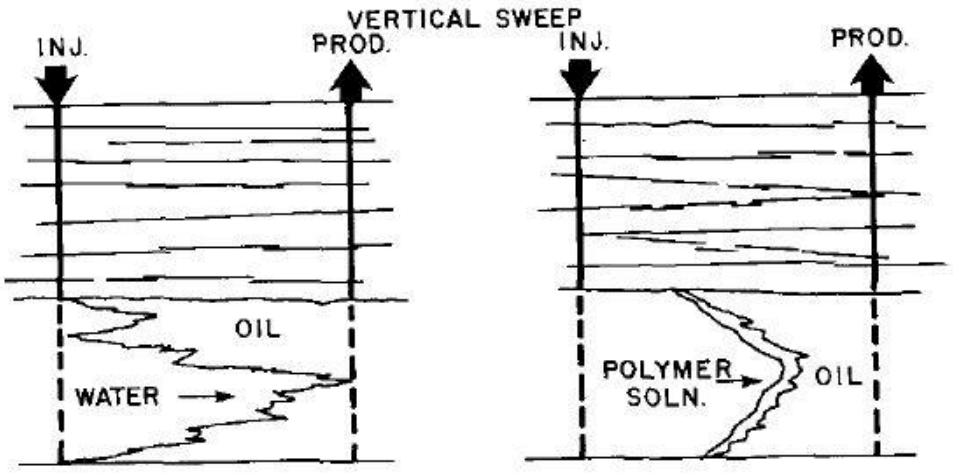

Figure 1. 3: Vertical sweep schematic of a polymer flood for mobility control (Caenn et al., 1989).

However, oil recovery due to polymer floods in carbonate reservoirs is relatively low, typically 0-13%, with an average of 5% recovery (Lake, 1989). Polymer floods are not ideal for carbonate reservoirs due to poor injectivity. Poor injectivity may be caused by incompatibility between the injection brine and the polymer, by incompatibility between the formation brine and the polymer, low permeability, and due to contamination in the surface facilities (Caenn et al, 1989). To ensure appropriate injectivity, it is recommended that the reservoir has a permeability of at least 20 mD (Lyons and Plisga, 2011). Many carbonate reservoirs have permeabilities smaller than 20 mD. In addition, carbonate reservoirs often contain hard brine which reduces polymer viscosity and increases adsorption. Another shortcoming of polymer flooding in carbonate reservoirs is the highly variable pore size distribution associated with carbonates compared to sandstones. Polymers have a large molecular size and are sometimes larger than the smaller pores in porous carbonate media. The small pores that cannot be entered by

polymers are called inaccessible pore volume. Due to inaccessible pore volume, the polymer injection will sweep even less of the swept zone, reducing the amount of oil contacted and recovered during a polymer flood. As a result of large polymer adsorption, inaccessible pore volume, poor injectivity in low permeability reservoirs, and viscosity reduction from hard brines, polymer flooding is not always the most viable method for mobility control in carbonate reservoirs.

In addition to the problems mentioned above with polymer floods, the alkaline and surfactant floods also pose obstacles in carbonate reservoirs during ASP floods. Typically, anionic surfactants are used to achieve ultra-low IFT conditions between the surfactant and oil. Anionic surfactants, due to their negative charge, adsorb more on the carbonate rock surface. To reduce adsorption, alkali is added to increase the pH of surfactant solution. If gypsum is present in the carbonate reservoir, however, the alkalis can precipitate and form calcium carbonate, leading to permeability reduction and loss of alkali (Sharma et al 2014). From well logs alone, it cannot be determined if gypsum is present in a carbonate reservoir. Due to potential plugging from calcum carbonate precipitation during an alkali flood and polymer plugging in low permeability regions, an alternate method of tertiary oil recovery is necessary for some carbonate reservoirs.

An alternative method of mobility control for tertiary recovery is foam flooding. Foam has been studied as a candidate for improving sweep efficiency and mobility control from as early as the 1970s. In addition, foam can be used as a gas-blocking agent to divert gas away from high permeability swept regions into unswept regions. Foams, either as gas-blocking agents or as mobility control agents, are appealing due to their low unit cost. The chemicals used to form foam are relatively inexpensive, used in low concentration, and used in low liquid to gas ratios. Some other advantages of foam are

that they are shear-thinning fluids contributing to decent injectivity, they are offer more effective mobility control in far-wellbore regions, and their low density can be exploited to block the high regions that have already been swept by gas. As a result of reducing the mobility of the injected gas, foam decreases the channeling that is typically associated with high mobility ratios and decreases gravity override which is typical of gas flooding. Figure 1.4 shows how foam flooding can increase the sweep efficiency in three scenarios: gravity override, viscous fingering/channeling, and rapid flow through high permeability zones.

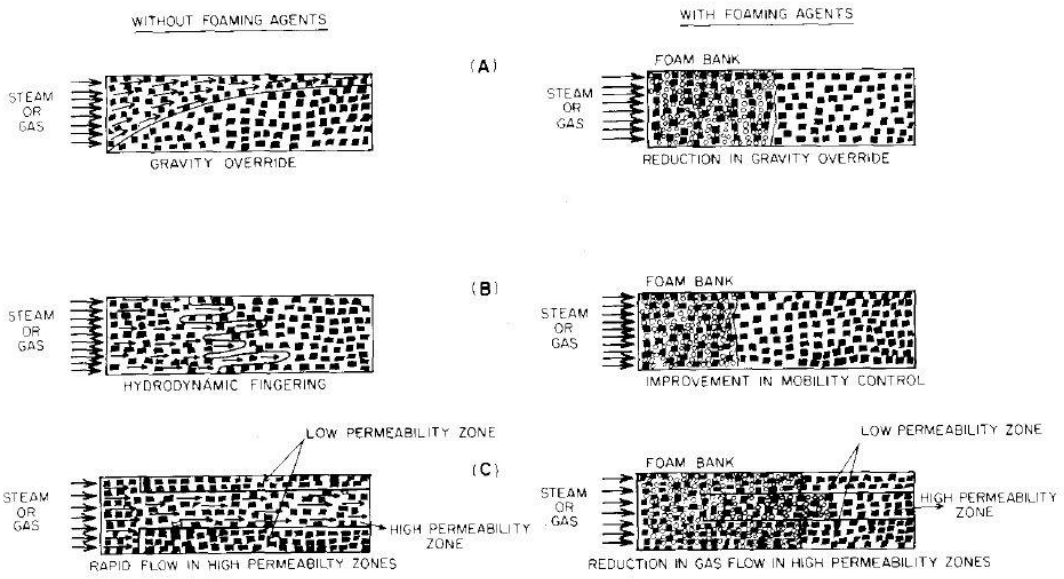

Figure 1. 4:Schematic of possible effects of foam on gas transport in porous media (Sharma and Shah, 1989).

Likewise, it has been shown by Sharma et al (1982), foam increases the saturation of trapped gas, and therefore, results in lower oil saturation. The increased trap gas

saturation results in a higher pressure gradient that further reduces the gas mobility. When using a surfactant as a foaming agent, the surfactant reduces the oil-water interfactial tension and also facilitates the wettability alteration from oil-wet to mixed-wet carbonate surfaces.

1.2 RESEARCH OBJECTIVES

The goal of this research was to test novel cationic surfactants for CO_2 foam flooding in carbonate reservoirs as an alternative to polymer flooding. The goal was to create a foam that increases the viscosity of the injection fluid, reduces the mobility ratio, and directs gas to unswept regions. Cationic surfactants were studied rather than anionic surfactants to reduce the amount of surfactant adsorption on the carbonate surface. Four gemini surfactants with foaming capabilities were studied at varying concentrations, salinity, and quality to determine the feasibility of foam flooding to reduce the mobility ratio. The effects of salinity, temperature, pH, surfactant concentration, and the presence of oil were tested on the bulk phase of foam for two cationic gemini surfactants. The surfactants were tested in a Texas Cream limestone in the absence of oil to determine that foam was forming and being propagated through the core. They were also tested in the presence of oil, both oil-wet and water-wet systems, to determine how much oil could be recovered in tertiary mode. The two cationic gemini surfactants were compared to anionic and cationic conventional surfactants that also display foaming capabilities.

1.3 Description of Chapters

The second chapter provides a literature review on the fundamental theories of foam generation and destruction, foam as a method for EOR, and the distinguishing features of cationic gemini surfactants. The third chapter discusses the materials and methods used to test the viability of the novel surfactants for CO_2 foam flooding. The fourth chapter discusses the results of the experiments performed. The final chapter discusses the conclusions reached from the experiments and suggestions for future work to make these novel surfactants more feasible for enhanced oil recovery.

Chapter 2: Literature Review

This chapter provides a brief background on the fundamental principles of foam theory and applications. It is important to note, that not all aspects of foam will be covered in this section. The aspects relating to the viability of foam for chemical Enhanced Oil Recovery (EOR), however, will be addressed in this chapter. This chapter will include the basic principles of foam, in addition to an introduction of foam in chemical EOR. Lastly, this chapter will include the fundamental differences between gemini surfactants and conventional surfactants.

2.1 FUNDAMENTAL CONCEPTS OF FOAM

This section discusses the fundamental concepts of foam including the definition of foam, the properties of foam, the generation of foam, and foam stability.

2.1.1 Definition of Foam

Foam is often defined as a dispersion of gas in a continuous liquid phase (Friedmann 1991, Kovscek and Radke 1994, Falls 1989, Schramm 1994). The gas phase is made discontinuous by liquid films called "lamellae." The lamella is defined as a thin liquid film with interfaces on both sides of the liquid phase. It is connected to other lamellae. The liquid phase generally contains a surfactant to stabilize the lamellae by surfactant adsorption at the gas/liquid interface (Kovscek and Radke 1994). The liquid phase can also contain macromolecules or solid particles as an alternative to surfactants as a foaming agent. The foaming agents lower the surface tension and form protective films to prevent coalescence with other bubbles (Schramm 1994). As seen in the Figure 2.1, a bulk foam structure is contained on the bottom by a liquid phase and on the top by

a gas phase. At a microscopic level, the gas phase is separated from the thin film liquid phase by a 2-D interface.

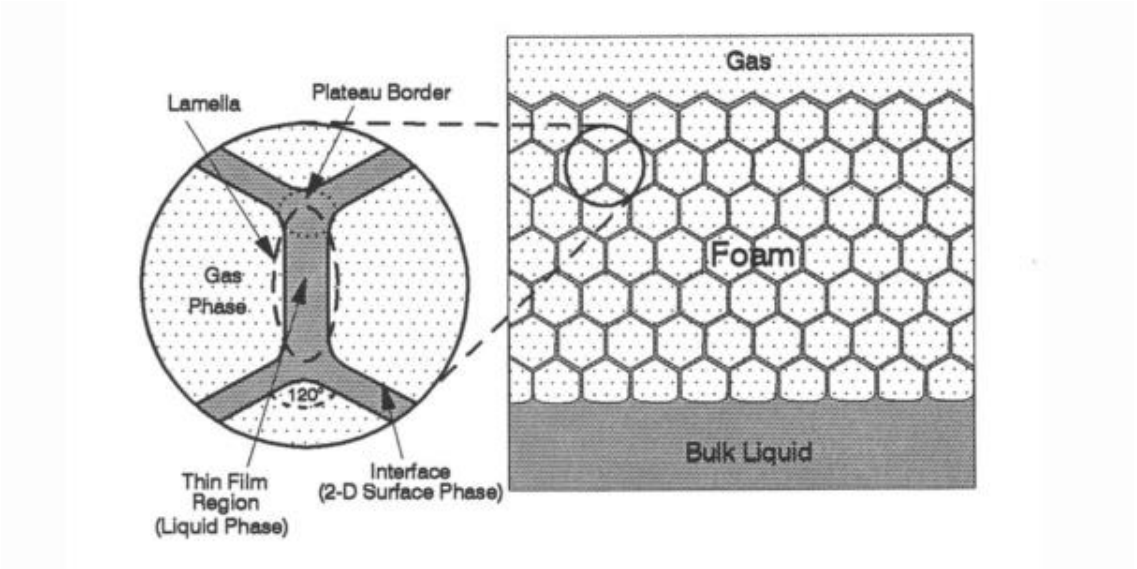

Figure 2.1: A generalized foam system (Schramm, 1994)

2.1.2 Foam Properties

Foams vary based on the following three properties: texture, quality, and rheology.

2.1.2.1 Foam Texture

Foam texture refers the bubble size and bubble size distribution. It is widely agreed that finer bubble sizes result in more stable foam (Nguyen 2000). Not only does foam bubble size affect the stability of the foam, but it also affects the viscosity of the foam phase. When the volume occupied by the foam is significantly larger than the individual bubbles, it is called bulk foam (Rossen 1996). However, in porous media, foam bubbles span one or more pore bodies, preventing a free flow of gas from traveling

the pore channels through a rock. Friedmann (1991) found that bubble size and bubble size distribution range decrease with an increase in surfactant concentration; bubble size and bubble size distribution also decreased with an increase in system pressure. In addition to surfactant concentration and pressure, foam texture depends on type of surfactant, pore structure, and foam quality.

2.1.2.2 Foam Quality

Foam quality is defined as the volume of gas contained in the foam, and can be expressed as a fraction or a percentage. In the bulk phase, foam quality is expressed by the following equation:

$$Foam\ Quality(\%) = \frac{gas\ volume}{gas\ volume + liquid\ volume} \times 100. \quad (2.1)$$

In coreflood experiments, foam quality is expressed as a ratio of the injection rates, as seen in the following equation:

$$Foam\ Quality\ (\%) = \frac{injection\ gas\ rate}{injection\ gas\ rate + injection\ liquid\ rate} \times 100. \quad (2.2)$$

Foam quality is one of the most widely disagreed upon parameter affecting mobility. Marsden (1986) found that increasing foam quality caused a decrease in foam mobility. Whereas, Lee (1991) found that foam mobility decreased with decreasing foam quality. However, most sources do not study foam below 40% quality or above 95% quality because mobility reduction cannot be achieved (Bullen 1976, Chang 1998, Hutchins 2005) due to foam instability outside of this range.

2.1.2.3 Foam Rheology

Foams are shear-thinning fluids. Since foam viscosity cannot be measured, foam viscosity is either approximated using apparent viscosities or by foam mobility. Foam mobility is defined as the ratio of effective permeability to apparent viscosity. In a typical water-wet system, the relative mobility of a liquid phase is calculated as a function of saturation and is independent of whether the gas exists as foam (Falls 1989). If the gas phase is continuous, the foam merely reduces the cross-sectional area that gas flows through, resulting in a reduction of relative permeability. If the gas phase is discontinuous, however, the relative permeability is decreased, and the foam also has a larger apparent viscosity, reducing the gas mobility. In porous media, the apparent viscosity of foam depends on the bubble size of the foam. The smaller the foam bubbles, the more lamellae there are to be transported through the porous media and the greater the resistance to flow (Hirasaki and Lawson). Falls (1989) found that the apparent gas viscosity increases by an order or magnitude, if the ratio of bubble size to average pore size decreases two-fold.

2.1.3 Foam Generation

There are three mechanisms in which foam can be generated in porous media: snap-off, division, and leave-behind. These mechanisms have been thoroughly studied and are fundamental to understanding foam behavior in porous media.

2.1.3.1 Snap-Off

Snap-off is the most significant mechanism for foam generation in porous media. In order for snap-off to occur, the porous media must have a body-to-throat ratio larger than two (Kovscek and Radke 1994) and the capillary pressure must be low, meaning the

liquid saturation is high (Falls 1989). Snap-off occurs when the capillary pressure is larger than the entry pressure, and gas enters the pore body, as seen in Figure 2.2. If a surfactant is not present, the bubbles formed via snap-off will quickly coalesce and a continuous gas phase could exist.

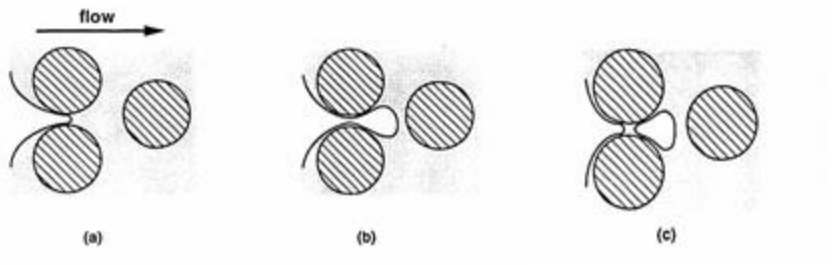

Figure 2.2: Mechanism for foam generation via snap-off (Kovcek and Radke, 1994).

Chambers and Radke divide snap-off into three types: pre-neck, neck snap-off, and rectilinear snap-off.

Pre-neck snap-off

Pre-neck snap-off occurs when a gas bubble completely blocks a pore throat. When the capillary pressure is large enough to push the accumulation of liquid upstream to the throat, it results in a smaller bubble than the original bubble (Nguyen 2000).

Neck snap-off

Neck Snap-off (also known as roof snap-off) occurs during a drainage displacement. The negative capillary pressure drives the liquid in the pore body to flow into the pore throat where it snaps-off.

Rectilinear snap-off

Rectilinear snap-off is a similar mechanism to neck snap-off but is most likely to occur in relatively long and straight pores.

2.1.3.2 Lamella Division

Lamella division occurs when a lamella splits into two separate lamellae. This occurs when the lamella is stretched around a branch point, as seen in Figure 2.3. When division occurs, the new lamellae are smaller than the original lamella. The frequency of lamellae division is a function of density of flowing bubbles, gas velocity, bubble sizes, branch points, and capillary pressure (Falls 1989).

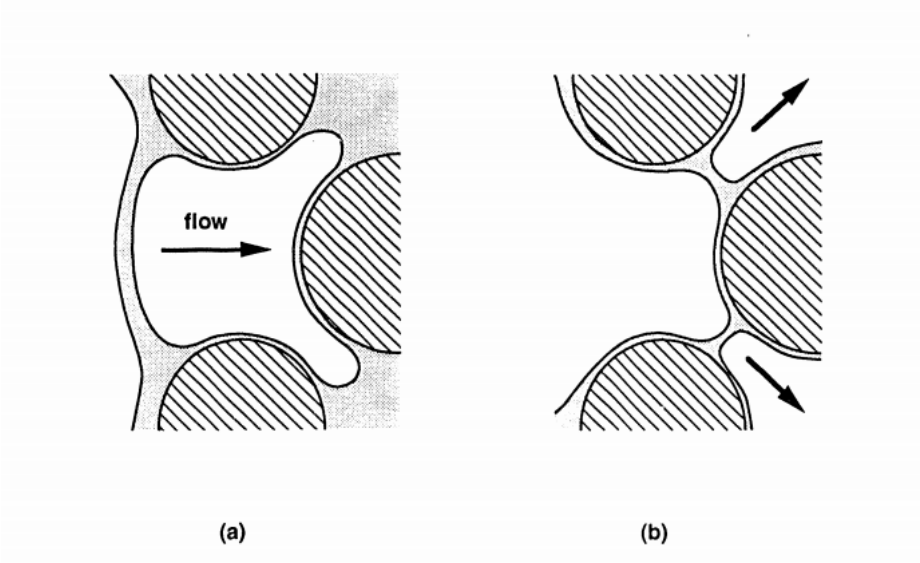

Figure 2.3: Mechanism for foam generation via lamella division (Kovscek and Radke, 1994).

2.1.3.3 Leave Behind

Unlike snap-off and division which generate lamellae perpendicular to the flow, leave-behind generates lamellae parallel to the flow. Leave-behind occurs when a wetting phase is displaced by a non-wetting phase, and the two wet surfaces bridge together to form a lamella. As two gas menisci converge downstream, a lens is left behind, and it may drain to a lamella, as seen in Figure 2.4. Leave-behind further reduces gas permeability by blocking gas flow paths (Nguyen 2000 and Friedmann et al 1991).

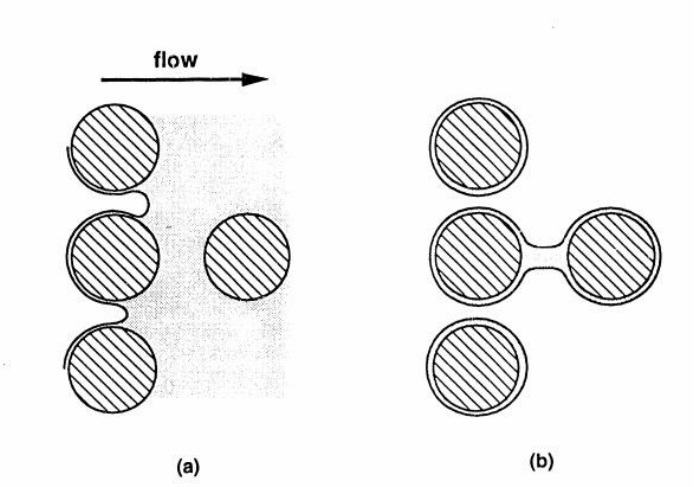

Figure 2.4: Mechanism for foam generation via leave-behind (Kovcek and Radke, 1994).

2.1.4 Foam Stability

Once foam has been generated, it can be destroyed by two general mechanisms: capillary suction coalescence and gas diffusion. Capillary suction coalescence is widely accepted as the principal mechanism for lamella destruction. Capillary suction is influenced by liquid saturations, rock permeability, and surfactant concentration. When two bubbles come into contact, the liquid film separating them begins to thin and

eventually ruptures and bubbles coalesce. Gas diffusion affects trapped bubbles, primarily, and is less common in porous media because the bubble radius of curvature is related to pore throats and pore bodies rather than bubble volume. Gas on the concave side of a foam bubble has a lower potential than the gas on the convex size of a foam bubble. Therefore, gas dissolves through the liquid film and diffuses to the concave side. Eventually, the bubble will shrink enough until it disappears (Chambers and Radke 1990).

2.1.4.1 Presence of Oil

The addition of other phases, especially oil, can be detrimental to both the generation and the stability of foam. The amount of foam destabilization due to the presence of oil depends on the oil-, surfactant-, and aqueous-phase compositions (Farajzedah 2012). In ideal environments, it is possible to make surfactant foams that last on the order of months and years (Schramm 1994). Whether or not oil will destabilize foam depends on the spreading, entering, and bridging coefficients of the gas/surfactant/oil interactions.

Spreading Coefficient

When a drop of oil contacts the gas-liquid interface, the oil drop can either spread to form a film over the gas-liquid interface, or it can form a bead on the surface. The film is formed when the oil has a strong affinity for the new phase; a bead is formed when the oil has a weak affinity for the new phase. The spreading coefficient S is expressed as a function of the interfacial tension of oil, gas, and surfactant with respect to each other as seen in the equation below. If the spreading coefficient, S, is positive, it is predicted that

the oil drop will spread spontaneously over the foam. This is generally sufficient for defoaming, and foam instability,

$$S = \gamma s_{/G} - \gamma s_{/O} - \gamma o_{/G}. \quad (2.6)$$

Entering Coefficient

When an insoluble agent, such as oil, is dispersed in the interior of a foam lamella, it can enter gas-liquid interface. If the oil enters, entering coefficient, E, is positive, a new gas-oil interface is created, and some oil-surfactant and some previous gas-surfactant interfaces are destroyed. This can cause the interfacial film to lose its foam stabilizing capability. However, oil entering does not always cause foam to destabilize (Schramm 1994). If E is negative, the oil theoretically is ejected from the lamellar surface and does not destabilize the foam. The entering coefficient is defined by the following equation:

$$E = \gamma s_{/G} + \gamma s_{/O} - \gamma o_{/G}. \quad (2.4)$$

Bridging Coefficient

If oil enters the gas-liquid interface but does not spread, it is possible that the oil will bridge adjacent foam bubbles. When the bridging coefficient, B, is positive, the film is unstable; if B is negative, the film is stable. The bridging coefficient is defined in the equation below:

$$B = (\gamma s_{/G})^2 + (\gamma s_{/O})^2 + (\gamma o_{/G})^2. \quad (2.5)$$

The most stable foams are formed when the entering coefficient is negative, and the lamella number is low (Farajzedah 2012).

2.1.4.2 Other Factors Affecting Foam Stability

Other factors that affect foam stability are temperature, surfactant concentration, salinity, and presence of solid particles. The presence of solid particles can either be beneficial or detrimental to foam stability. If the particles are not water-wet, they gather at the interfaces in the foam, enhancing the mechanical stability of the lamellae. Dispersed particles can also influence the stability by enhancing the bulk viscosity, and thus, enhancing the stability (Schramm 1994). At concentrations below critical micelle concentration (CMC), an increase of concentration causes a decrease in interfacial tension and stabilizes the foam. An increase in surfactant concentration significantly above CMC is thought to contribute to increasing foam stability based on a different mechanism—ordered microstructure formation in lamellae (Nikolov et al. 1986). Salinity can have either a detrimental or a stabilizing effect on foam depending on type of surfactant, the salinity, concentration and the presence of divalent ions. Above the critical micelle concentration, foam stability is relatively insensitive to pH change (Liu 2005). Generally, studies have found that foam stability decreases with an increasing temperature (Kapetas 2015, Chen et al 2012, Spirov et al 2012) due to a decrease in drainage time, thus a faster rate of foam destruction.

2.2 FOAM IN ENHANCED OIL RECOVERY

This section discusses how foam can be utilized for methods of enhanced oil recovery.

2.2.1 Mobility Reduction

Although gas floods are popular for enhanced oil recovery, the low viscosity of gas results in early gas breakthrough, poor sweep efficiency, viscous fingering, and

channeling that results in low overall recoveries, sometimes only 10 to 20% (Lee 1991). Because gases have much higher mobilities than oil and water, gases tend to override the formation or channel through oil in a formation. This decreases the amount of oil that is contacted by gas and expedites gas breakthrough, causing poor sweep efficiency. Mobility ratio, M, is defined as the mobility of the displacing phase divided by the mobility of the displaced phase, oil, as seen in the equation below:

$$M = \frac{k_{rg}\mu_o}{k_{ro}\mu_g}. \tag{2.6}$$

The gas displacement process can be improved if the mobility ratio is decreased. The mobility ratio can be decreased if the gas viscosity is increased or the relative permeability of gas is decreased. Both of these can be achieved through foam. Foam decreases the relative permeability of gas by blocking the pores through which the gas can flow; it also diverts flow from higher permeability zones to lower-permeability unswept zones. Lastly, foam improves oil recovery by reducing the capillary forces due to lower interfacial tensions resulting from the presence of a surfactant.

2.2.2 Injection Strategies: SAG vs. Co-injection

Foam can either be injected in alternating slugs of surfactant solution and gas, or foam can be pre-formed in surface facilities and injected into the well. The efficiency of the injection method depends on the type of foam flood. For steam-foam injections, it is less practical to sequentially inject surfactant and gas in alternating slugs because the steam depletes the top section due to gravity segregation. It is more beneficial to inject surfactant, steam and a non-condensible gas concurrently. A strong foam can be formed at the surface using a foam generator, and a loose foam is likely to be generated in the

tubing due to turbulence during injection (Friedmann 1991). Another time in which a co-injection is more desirable than an alternating injection is when foam is needed near wellbore in a heterogeneous reservoir. Co-injection is the only way to ensure that gas and liquid both enter the same region. Generally, the gas mobility is more reduced during co-injection than for SAG injection (Farajzedah 2012). The significance of snap-off to lamella mobilization and generation, however, implies that an alternating surfactant and gas injection strategy may be more beneficial than co-injection. In addition, alternating slugs of surfactant and gas improves the injectivity and reduces the likelihood of corrosion due to gas/water contact in the injection facilities and pipelines.

2.3 GEMINI SURFACTANTS

This section discusses aspects of gemini surfactants including the definition and the characteristics of gemini surfactants.

2.3.1 Definition

Conventional surfactants have a single hydrophilic head group and a single hydrophobic tail. Gemini surfactants, however, are a class of surfactant that contain more than one hydrophobic tail and hydrophilic head groups separated by a rigid spacer chain. This rigid spacer is what differentiates a gemini surfactant from a conventional surfactant. The spacer prevents the two chains within a single gemini molecule from interacting with each other. A schematic representation of a gemini surfactant compared to a conventional surfactant can be seen in Figure 2.5.

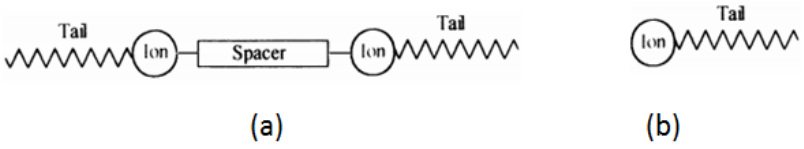

Figure 2.5: Structure of gemini surfactants (a) compared to conventional surfactants (b).

2.3.2 Characteristics

Gemini surfactants are thought to have many advantages over conventional surfactants. Gemini surfactants have more surface activity and a lower packing parameter than conventional surfactants (Diamant 2003, Hait and Moulik 2002). The tighter packing of gemini surfactants generates a more cohesive and stable interfacial film, indicating greater emulsion and foam stability (Hait and Moulik 2002). The foaming properties of gemini surfactants depend on the length of spacer and hydrophobic tails, like conventional surfactants. However, Kim et al. (1996) found that certain cationic gemini surfactants form comparable amounts of foam compared to DTAB, and in some cases comparable to SDS. Likewise, geminis have a lower sensitivity to Ca^{2+} and Mg^{2+}, making them more applicable in scenarios with hard brines present. Increased surface activity means that less surfactant is needed to perform a specific task. Menger and Littau (1993) found that gemini surfactants are more efficient at reducing surface tension than conventional surfactants by 3 orders of magnitude.

In addition to being more surface active and reducing surface tension, gemini surfactants also have a much lower critical micelle concentration (CMC). CMC is the minimum concentration, above which the surfactant aggregates to form micelles. CMC can be determined by plotting the surface tension versus log concentration of the

surfactant. The plot is linear until the CMC; after the CMC, the slope of the plot diminishes, as seen in Figure 2.6. Figure 2.7 shows the CMC curve of a gemini surfactant compared to a conventional surfactant.

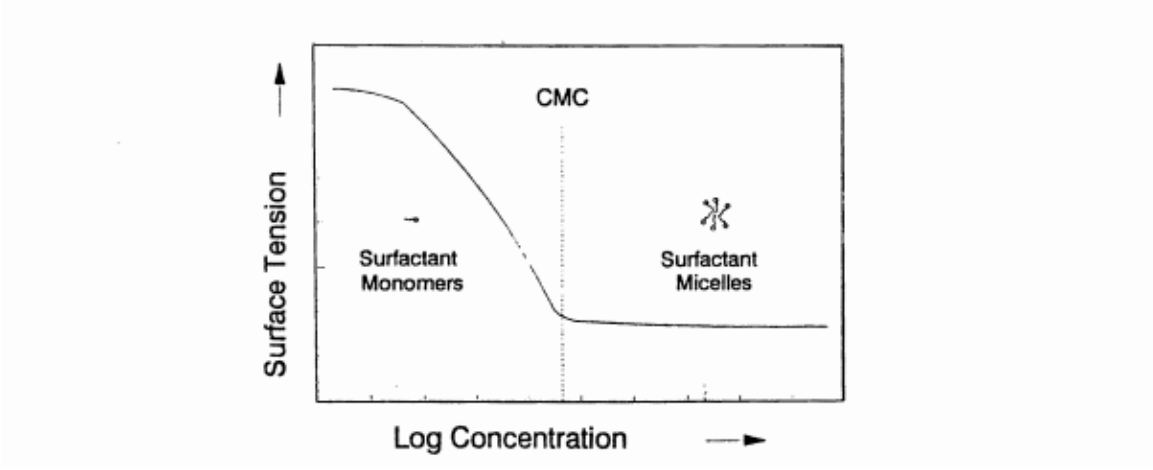

Figure 2.6: Surface tension vs log concentration of surfactant. Below the CMC the surfactant exists as monomers; Above the CMC surfactant exists as micelles (Schramm, 1994).

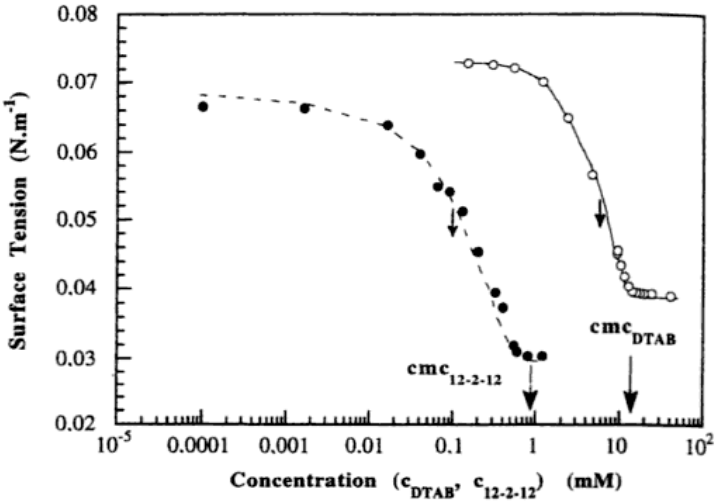

Figure 2.7: Variation in surface tension with the surfactant concentration and a gemini surfactant with a 12- carbon tail (Zana and Xia, 2004).

Hait and Moulik (2002) found that CMC values are not sensitive to the polarity of short spacers and that the CMC value generally decreases with increasing hydrophobic chain length. Longer spacers contribute to overall hydrophobicity of the surfactant, therefore, reducing the monomer solubility and increasing the monomer's tendency to self-assemble. Unlike conventional surfactants, gemini surfactant CMC values are more sensitive to changes in hydrophobic tail length. As a result of lower CMC values and the tubular shape of their aggregates, Engberts et al (1996) found that cationic geminis have better oil solubilization than conventional surfactants. In addition to better solubilizing properties than conventional surfactants, gemini surfactants also increase wetting, have a higher tolerance to multivalent metallic ions, promote emulsification of oil in water, and have a stronger antimicrobial ability. Some classes of gemini surfactants can be

synthesized at a reasonable cost, making them a viable option for multiple industries: agricultural, biological, and petroleum.

Chapter 3: Experimental Setup and Methodology

This chapter contains the materials and equipment used in experiments, as well as the methodology and experimental procedure for experiments conducted.

3.1 MATERIALS

This subsection discusses the materials used to perform all of the experiments performed in this study.

3.1.1 Oil

Several oils, including crude and light chain oils, were used during foam stability tests and interfacial tension measurements. Table 3.1 contains the density and viscosity of each oil. For core flood experiments with oil present, two different oils were used. Crude A was used for oil-wet cores, and mineral oil was used for water-wet cores. Note that Crude A was a dead oil diluted to 110 cP using approximately 15% toluene.

Oil	Viscosity (cP) (T=25^{o}C)	Density (g/mL)
Crude A	110	0.90
Crude B	200	0.89
Crude C	52	0.87
Mineral Oil	34.5	0.86
Decane	0.92	0.73

Table 3. 1: Oil properties.

3.1.2 Surfactants

Six different surfactants were used in this study. Four novel cationic gemini surfactants (coined GC 468, GC 580, GC 566, and GC 776) were synthesized in our

laboratory, and two commercial surfactants, a cationic and an anionic, were used for comparison purposes. GC 468 is a cationic gemini surfactant with 12 carbons in each hydrophobic tail with 3 carbons in the spacer, seen in Figure 3.1 (a), and GC 580 is a cationic gemini surfactant with 16 carbons in each hydrophobic tail with 3 carbons in the spacer, seen in Figure 3.1 (b). GC 566 is a cationic gemini surfactant with 14 carbons in each hydrophobic tail with 6 carbons in the spacer, seen in Figure 3.1 (c). GC 776 is a cationic gemini surfactant with 24 carbons in each hydrophobic tail and 3 carbons in the spacer, seen in Figure 3.1 (d).

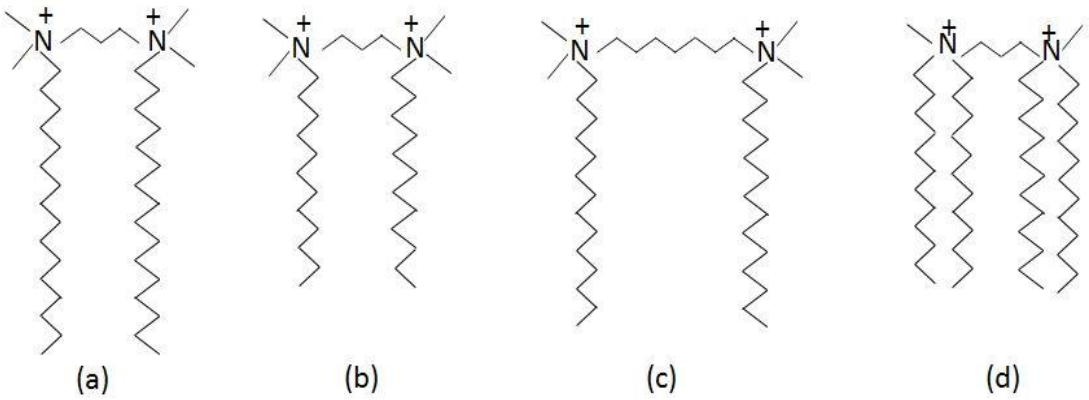

Figure 3. 1: Chemical structure of each of the cationic gemini surfactants evaluated in this study. (a) GC 580 (b) GC 468 (c) GC 566 and (d) GC 776.

GC 566 and GC 776 did not pass initial aqueous stability tests at any temperature or salinity, so they were not used in the remainder of the study. GC 468, GC 580, and the two commercial surfactants were used in foam stability, interfacial tension measurements, and core floods.

3.1.2.2 Commercial cationic surfactant

98% pure Cetyltrimethylammonium bromide (CTAB) from MP Biomedicals, LLC was used as the commercial cationic surfactant.

3.1.2.3 Commercial anionic surfactant

Bioterg ® AS-40, sodium C14-16 olefin sulfonate, with 38.86% active contents from Stepan was used as the commercial anionic surfactant.

3.1.3 Core Sample

Outcrops of Texas Cream limestone were used for batch adsorption studies and core floods. The limestone samples were 1.5 inches in diameter and 12 inches in length, with brine permeability of 10-40 mD and porosity of 22-30%.

3.1.4 Formation and Injection Brine

Formation and injection brine were composed of Calcium Chloride Dihydrate, Magnesium Chloride Hexahydrate, and Sodium Chloride. All three chemicals were from Fischer Scientific™ with purity greater than 99%. The formation brine for each core flood was 4% NaCl, 1%$CaCl_2$, and 1%$MgCl_2$. The injection brine salinity is dependent upon the bulk foam stability and aqueous stability of the surfactant at varying temperatures and salinities.

3.2 Surfactant Characterization Equipment and Methodology

This section discusses the equipment and methodology for surfactant characterization. The surfactants were characterized by aqueous stability tests, bulk foam stability, spreading coefficients, entering coefficients, bridging coefficients, and adsorption.

3.2.1 Aqueous Stability

Equipment

Aqueous stability tests were performed using 20 mL clear glass vials. An oven was used to change the temperature of the system.

Method

The surfactants were first characterized by testing their aqueous stability at various temperatures and salinities. A surfactant and brine solution is considered aqueously stable if the solution is clear, homogeneous, and contains only one phase. If the surfactant injection solution is not clear, significant phase trapping occurs, and the surfactant is considered lost to adsorption. Sample aqueous stability results can be seen in Figure 3.2. The sample results show a sample that is cloudy, therefore not aqueously stable, a sample that has a solid precipitate, also not stable, and a clear aqueously stable solution. Results of the aqueous stability tests of each surfactant can be found in the results section (Chapter 4).

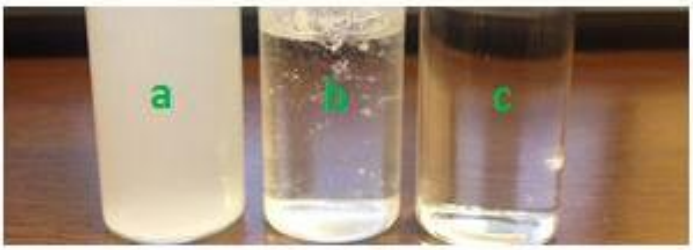

Figure 3. 2: Sample aqueous stability result. (a) shows a solution that is cloudy, (b) shows a sample that has a precipitate, and (c) shows a sample that is aqueously stable.

3.2.2 Bulk Foam Stability

Equipment and Methodology

Preliminary bulk foam stability was measured using 5 mL of surfactant in 15 mL plastic centrifuge tubes. The tube was shaken by hand for 5 seconds, and the decay of foam was measured as a function of time. This was to quickly evaluate the foaming capabilities of surfactants at various temperatures, salinities, and pH. More precise bulk foam stability experiments were performed using the setup seen in Figure 3.3. Air was injected into the bottom of 30 mL of surfactant solution in a glass, graduated cylinder through a 26 gauge syringe for approximately 10 seconds. The airflow was stopped, and the top of the graduated cylinder was covered using parafilm to prevent external air from affecting the bulk foam stability. The decay of foam height was measured as a function of time. The temperature of the surfactant solution could be changed using the water bath. For foam stability in the presence of oil, after airflow was stopped, 1 wt% of oil was sprayed onto the top of the foam, and the graduated cylinder was covered. The foam decay was measured as a function of time.

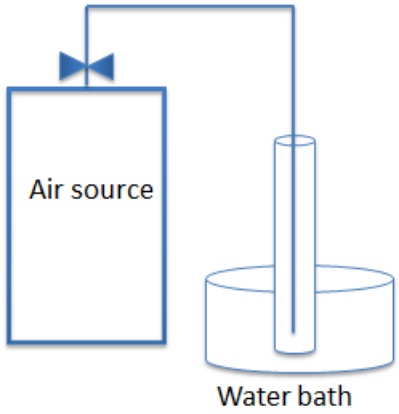

Figure 3. 3: Experimental set up for bulk foam stability measurements.

Bulk Foam Stability Results

Bulk foam stability was used to select the salinity to use during coreflood experiments. The salinity that resulted in the longest half-life (h/h_o=0.5) was selected. Likewise, bulk foam stability was used to select the oil to use in coreflood experiments. The oil that destabilized the foam the least was selected. Sample results from bulk foam stability of GC 580 at different salinities are shown in Figure 3.4. As seen in the figure, the foam corresponding to 4%NaCl + 1%$CaCl_2$ + 1%$MgCl_2$ was the most stable at 60^{o}C and this salinity was chosen for all GC 580 corefloods at 60^{o}C. The remainder of the bulk foam stability results can be seen in the Chapter 4.

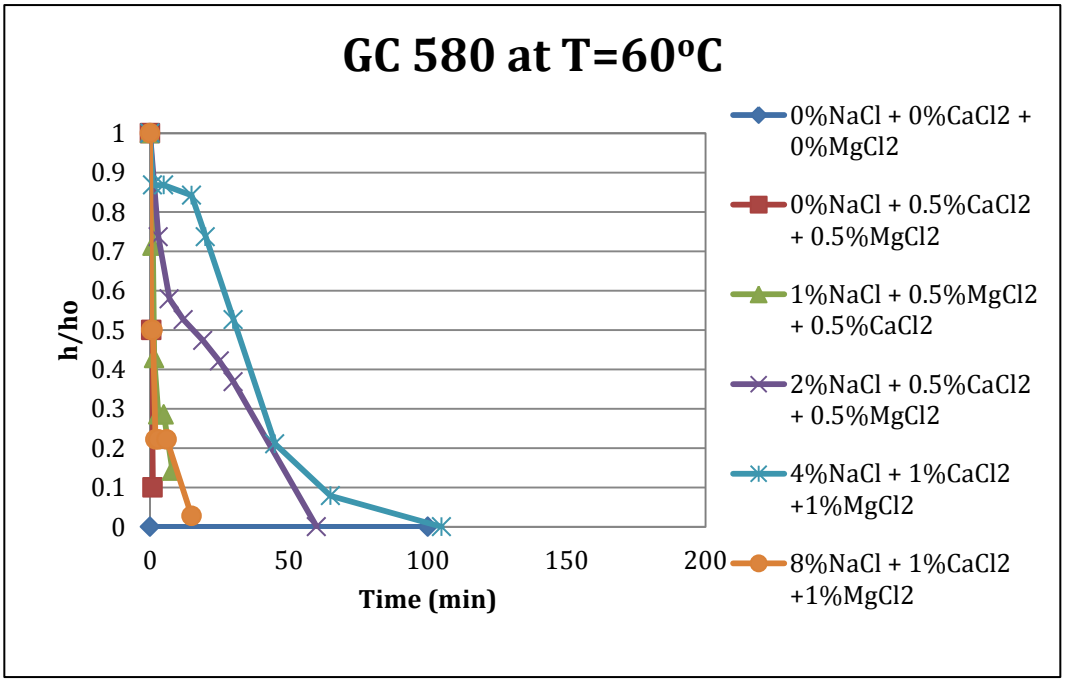

Figure 3. 4: Bulk foam stability for GC 580 at 60°C. The formulation with the longest half-life was selected for coreflood experiments.

3.2.3 Spreading, Entering, and Bridging Coefficients

Equipment

To measure spreading, entering, and bridging coefficients, the following interfacial tensions needed to be measured: oil/surfactant, oil/gas, and surfactant/gas. The oil/gas and surfactant/gas surface tensions were measured using a Ramé-Hart Contact Angle Goniometer. The interfacial tension between surfactant and oil was measured using a spinning drop interfacial tensiometer provided by TEMCO™.

Methods

The surface tensions (surfactant/gas and oil/gas) were measured using a pendant drop method using the goniometer. Since the liquid phase is more dense than the external gas phase, a hanging pendant was used. A drop of liquid large enough to be stable, but

not so large the drop releases from the needle, was allowed to equilibrate for 10 minutes. A schematic of the pendant drop method can be seen in Figure 3.5. The goniometer then took 10 measurements of the surface tension, shape factor, radius of curvature, contact angle, etc. over 10 seconds. The surface tension of the hanging drop was calculated using the Young-Laplace equation,

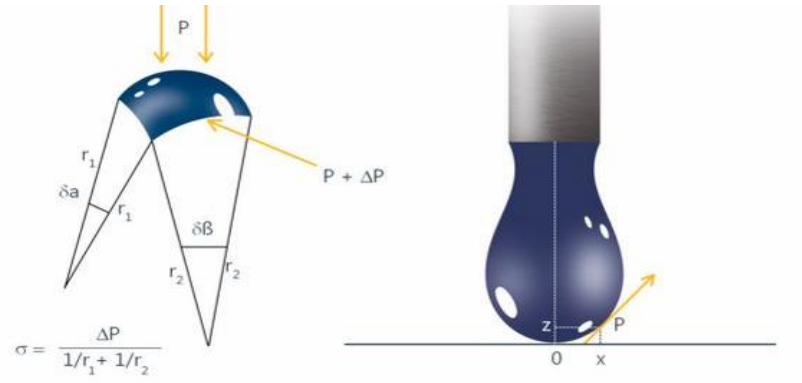

Figure 3. 5: Schematic of surface tension measurements. Image obtained at http://www.kruss.de/services/education-theory/glossary/pendant-drop/.

$$\Delta P = \sigma \times \left(\frac{1}{r_1} + \frac{1}{r_2}\right). \tag{3.1}$$

The average surface tension was recorded. For each sample, this process was performed five times to reduce error from drop size variations.

The interfacial tension between oil and surfactant was measured using the spinning drop tensiometer. Solutions of 80% surfactant and 20% oil by volume were mixed and allowed to equilibrate for three days. Each solution was then placed in a rotating capillary tube. The less dense fluid migrates to the center of the drop and

equilibrium is reached. A schematic of the two fluids at equilibrium within the capillary tube can be seen in Figure 3.6.

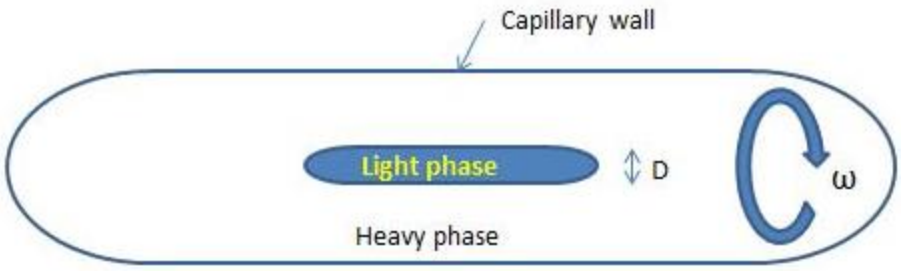

Figure 3. 6: Schematic of spinning drop tensiometer measurements.

The equilibrium shape of the drop is determined by interfacial tension and the pressure difference at the interface caused by the density differences and centrifugal force. From the, the interfacial tension between the two immiscible fluids can be calculated using Vonnegut's equation.

$$\gamma = \frac{r^3 \times \omega^2 \times \Delta\rho}{4} \tag{3.2}$$

In Vonnegut's equation, γ is the surfactant/oil interfacial tension, r is the radius of the lighter phase, ω is the angular velocity of the rotating capillary tube, and $\Delta\rho$ is the density difference between the two fluids.

Using the interfacial tensions measured using the spinning drop tensiometer and the surface tensions measured using the goniometer, the spreading (S), entering (E), and bridging (B) coefficients were calculated using the following equations:

$$S = \gamma_{S/G} - \gamma_{S/O} - \gamma_{O/G}, \tag{3.3}$$

$$E = \gamma s_{/G} + \gamma s_{/O} - \gamma o_{/G}, \quad (3.4)$$

$$B = (\gamma s_{/G})^2 + (\gamma s_{/O})^2 + (\gamma o_{/G})^2, \quad (3.5)$$

In the equations above, $\gamma s_{/G}$ is the interfacial tension between surfactant and gas, $\gamma s_{/O}$ is the interfacial tension between surfactant and oil, and $\gamma o_{/G}$ is the interfacial tension between oil and gas. The gas in each of these equations was air.

3.2.4 Adsorption

3.2.4.1 Anionic Surfactant Adsorption Equipment

The adsorption of anionic surfactants was measured using a High Performance Liquid Chromatograph (HPLC). A Dionex Ultimate™ 3000 HPLC was used to measure the adsorption of anionic surfactants in batch adsorption studies. HPLC measures retention time of each compound present in a sample and can be calibrated with known concentrations of surfactant to determine concentration of surfactant present in the sample. However, since this HPLC does not have the appropriate column to measure cationic surfactants, a different method for determining cationic concentration had to be determined.

3.2.4.2 Cationic Surfactant Adsorption Equipment and Materials

The concentration of cationic surfactants before and after batch adsorption studies was determined using a modified method of Wang and Langley's original method (1977). In this method the following materials are used: chloroform, 0.1 weight % solution of

methyl orange, a buffer solution of 125 mL 0.5M citric acid and 125 mL of 0.2M disodium hydrogen orthophosphate, and 0.1 weight % cationic surfactant. The cationic surfactant forms a complex with the methyl orange and moves to the organic (chloroform) layer. The organic layer can be separated from the aqueous layer, where it can be analyzed by a Varian UV-vis. The methyl orange peak appears around 420 nm wavelength.

Conventional Cationic Surfactant Method

For conventional cationic surfactants, the surfactant and methyl orange form a 1:1 complex as dictated by the equation below:

$$Cationic\ surf^{+}(aq) + MO^{-}(aq) \leftrightarrow [Cationic\ surf - MO](org). \quad (3.6)$$

A calibration curve for surfactant concentration and absorbance was generated by making standards using 0.25 mL, 0.5 mL, 0.75 mL, 1 mL, and 1.25 mL of 0.1% CTAB. Each sample was diluted to 50 mL using DI water and stirred for 10 minutes. One mL of 0.1 weight % methyl orange was added to each sample. Five mL of the buffer solution was added to each solution. The solution was stirred for 10 minutes. Twenty mL of chloroform was added, and the solutions are stirred for two hours. The solutions sat overnight to make the separation between organic and aqueous layers more defined. After sitting overnight, a visible difference in color could be seen in each sample, as shown in Figure 3.7. The organic layer was separated, diluted 1:10 using chloroform, and analyzed using a UV-vis.

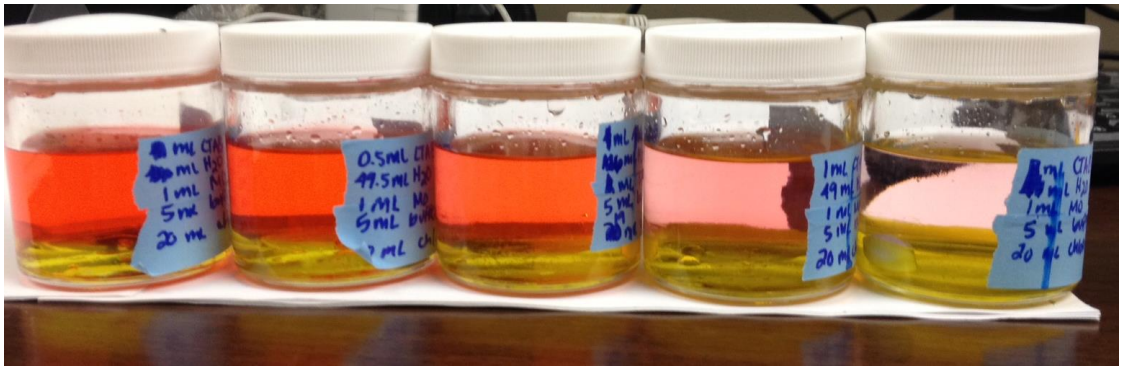

Figure 3. 7: Calibration samples for CTAB surfactant adsorption. From left to right: 0.25 mL, 0.5, 0.75, 1.0, 1.25 mL of 0.1% CTAB

Gemini Cationic Surfactant Method

For cationic gemini surfactants, two molecules of methyl orange bind with one molecule of the gemini surfactant, as seen in the equation below:

$$cationic\ surf\ (aq) + 2MO^{-}\ (aq) \leftrightarrow [MO - Cationic\ surf - MO](org). \quad (3.7)$$

A calibration curve for surfactant concentration and absorbance was added by making standards using 0.5 mL, 1 mL, 2mL, and 3mL of 0.1% cationic gemini surfactant. Each sample was diluted to 50 mL using DI water. Two mL of 0.1% methyl orange solution and 5mL buffer solution were added to each sample. As with the conventional surfactant method, the solutions were stirred for 10 minutes. Twenty mL of chloroform was added, and the solutions are stirred for two hours. The solutions sat overnight to make the separation between organic and aqueous layers more defined. The organic layer was separated from the aqueous layer and diluted 1:10 with chloroform. A visible

difference in color could be seen in each sample, as seen in Figure 3.8. The organic layer was analyzed using UV-Vis.

Figure 3. 8: The organic layer of calibration samples for GC468. From left to right: 0.5 mL, 1 mL, 2 mL, and 3 mL.

3.2.4.3 Batch Adsorption Methodology

To perform batch adsorption experiments, Texas Cream Limestone was crushed and filtered using 200 mesh. Four grams of the crushed limestone were placed in a glass vial, and eight grams of the surfactant solution at appropriate concentration and salinity were added to the vial. The vial was shaken twice daily for three days and stored at reservoir temperature, 60^{o}C. The anionic surfactants were then prepared for HPLC measurements, while the cationic surfactants were prepared as discussed in 3.4.3. The adsorption of the surfactant (q) was expressed as mg/g and calculated using the following equation:

$$q = \frac{m_{solution} \times (C_o - C)}{m_{carbonate}} \times 10^{-3}, \quad (3.8)$$

where q is the adsorption (mg/g), C_o is the initial surfactant concentration (ppm), C is the final surfactant concentration (ppm), $m_{solution}$ is the mass of the surfactant solution (g), and $m_{carbonate}$ is the mass of the crushed limestone (g).

3.2.5 Preliminary Wettability Alteration Studies

Preliminary wettability alteration tests were conducted to study the effect of cationic Gemini surfactants on the wettability of oil-aged calcite chips with Crude Oil A. Calcite chips were polished and aged in formation brine for one day at 80°C. The calcite chip was then aged in Crude Oil A for one week at 80°C. After one week of aging, the calcite chip was placed in injection brine at reservoir temperature for one day. The following day, the calcite chip was placed in injection surfactant solution at reservoir temperature. It was observed that oil left the calcite surface. Contact angle of the oil on the calcite surface can be measured using the Goniometer to determine the wettability of the surface.

3.3 COREFLOOD EQUIPMENT AND METHODOLOGY

This section discusses the equipment and methodology for performing coreflood experiments.

3.3.1 Coreflood Equipment

Stainless Steel Accumulator

TEMCO™ stainless steel accumulators were used to store and transfer the CO_2, oil, and surfactant to the coreholder. The accumulators have a piston. Water is injected from the pump into the bottom of the accumulator, where the floating piston displaces the

injection fluid. An accumulator with 1L capacity was used to store CO_2, and an accumulator with 350 mL capacity was used to store surfactant or oil.

Syringe Pumps

Three Teledyne™ ISCO 500D syringe pumps were used during the coreflood procedures to apply an overburden pressure, to inject the aqueous phase, and to inject the CO_2. CO_2 and surfactant were placed in accumulators, and the syringe pumps were used to pump the fluid from the accumulator to the core.

Coreholder

A TEMCO™ coreholder was used for core floods both in the presence and absence of oil. The core holder was mounted vertically, and fluids were injected from the top. Brine at 400 psi was used as an overburden fluid to compress and seal the Viton rubber sleeve in which the core was placed. The pressure drop across the core was measured using a pressure transducer connected to the inlet and outlet of the core holder.

Pressure Transducer

Honeywell™ transducers were used to record pressure drops across the core. A pressure transducer records the pressure drop as a voltage, sends the voltage to a Data Acquisition Card connected to LabView, which records the voltages in tabular form. The voltage can be converted to pressure using a calibration curve.

Backpressure Regulator (BPR)

A Swagelok mechanical backpressure regulator was used at the outlet of the apparatus to maintain a constant upstream pressure and to reduce the effect of gas expansion at the core outlet. The backpressure regulator was set to 100 psi.

Carbon Dioxide

CO_2 greater than 99.9% purity from Praxair was used for foam floods.

Sandpack

A 6-inch long sandpack was made using carbonate sand packed into a 0.5-inch metal tube. Surfactant and CO_2 were coinjected into the bottom of the sandpack to form foam before entering the coreholder.

3.3.2 Coreflood Set-Up

The equipment discussed in 3.3.1 were assembled to form a coreflood set-up, as seen in Figure 3.9. The coreholder, accumulator containing the surfactant, and sandpack were placed inside a convection oven set at 60^{o}C, the reservoir temperature. The CO_2 is pumped through 20 feet of metal tubing, allowing the CO_2 to heat to reservoir temperature before entering the core. The surfactant was stored in an accumulator in the oven and could either go through the sandpack before entering the core or enter the core directly. The effluent fluid and CO_2 is collected outside the oven. At the sandpack outlet, the CO_2 and surfactant could either bypass the core or go directly into the core. At the beginning of the foam flood, core was bypassed until the CO_2 and surfactant coinjection

had a stabilized pressure. Visual cells were placed directly outside the sandpack and directly outside the core outlet to verify foam was forming in the sandpack and in-situ in the core and to determine if oil was preventing in-situ foam formation in the core.

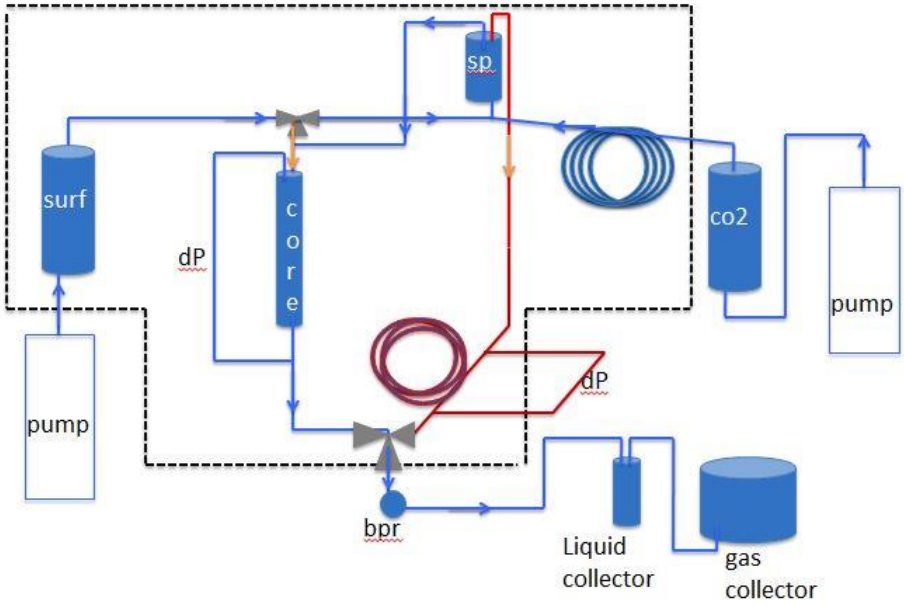

Figure 3. 9: Coreflood set-up. The dashed lines represent the oven boundary.

3.3.3 Core Measurements

This section discusses how core samples were prepared and characterized in addition to discussing coreflood procedure.

3.3.3.1 Core Sample Measurements

Core Sample Preparation

Texas Cream limestone cores that were 1.5 inches in diameter and 12 inches long were used for all coreflood experiments. The core samples were dried in an overnight before use. The dry weight, length and diameter were measured before applying a shrinking plastic layer around the core to prevent fluids from flowing out of the core along the length of the core. The core was then placed in the coreholder, and an overburden pressure of 500 psi was applied.

Air Porosity

Air porosity measurements were used to calculate the pore volume of the core sample. A pump filled with air was connected to the coreholder containing the core. A pressure gauge and a valve were in between the pump and the coreholder. While the coreholder was closed at both the outlet and inlet, a pressure and volume for the pump were recorded as the initial condition. The valve in between the pump and coreholder was opened, and the new pump pressure and volume was recorded. Twenty mL of air was pumped into the coreholder, and the new pump pressure and volume was recorded. Using Boyle's Law, the volume of the void space can be calculated.

$$(P_1V_1 + P_2V_2)_i = (P_1V_1 + P_2V_2)_f. \tag{3.9}$$

Air Permeability

After the pore volume was calculated, air was injected into the core at different rates. The steady state pressure of each flow rate was recorded, and the permeability to air was calculated using Darcy's law.

$$q = \frac{-kA(P_O^2 - P_i^2)}{2\mu P_o}. \quad (3.10)$$

q is the flow rate of the brine, A is the cross-sectional area of the core, μ is the viscosity of the air, P_o is the outlet pressure, P_i is the inlet pressure, and L is the length of the core.

Brine Saturation by Vacuum

After air porosity and air permeability were measured, the core was then vacuum saturated with brine. The core was connected to a vacuum pump. CO_2 was injected into the core; then the core was vacuumed to -14.7psi. This was repeated three times. After the CO_2 was stopped, the core was vacuumed for a few hours. CO_2 was used in case all the gases were not removed during the vacuum process, because CO_2 is miscible with brine unlike air. After the core was saturated, brine was injected into the core at a constant pressure of 100 psi. Pore volume was estimated by change in pump volume during saturation process.

Pore Volume Calculations

The pore volume of the core from air porosity measurements and brine saturation was confirmed using a brine tracer test. During the brine tracer test, a brine four times the salinity of the brine originally in the core was injected at a constant flow. Two pore

volumes of the higher salinity brine were injected into the core. The effluent was collected in 5 mL samples, and the salinity was measured using a refractometer. The brine salinity was normalized and plotted with respect to injected volume. The pore volume of the core for a non-vuggy core is the volume that corresponds to the normalized value of 0.5.

Brine Permeability

The formation brine was injected into the core at varying rates. The steady state pressure was recorded for each flow rate. Brine permeability was calculated using Darcy's law and the slope of a plot of pressure versus rate.

$$q = \frac{-kA\Delta P}{\mu L}, \tag{3.11}$$

q is the flow rate of the brine, A is the cross-sectional area of the core, ΔP is the pressure drop across the core, μ is the viscosity of the brine, and L is the length of the core.

Initial Oil Saturation

During oil saturation, oil was injected into the core at constant pressure displacing the brine that was previously in the core. Oil was injected until no more water was produced. The oil saturation was estimated using the equation below.

$$S_{oi} = \frac{V_{water\ produced}}{V_P}, \tag{3.12}$$

S_{oi} is the initial oil saturation, $V_{water\ produced}$ is the volume of water that is displaced by the oil and V_P is the pore volume of the core.

Effective Oil Permeability

Once the core is at residual water saturation, after oil saturation, the effective oil permeability can be measured. Oil was injected at a constant flow rate until the pressure drop across the core was stabilized at reservoir temperature. The effective oil permeability was calculated using Darcy's law with respect to oil using the equation below.

$$q_o = \frac{-k_o A \Delta P}{\mu_o L}, \tag{3.13}$$

k_o is the effective oil permeability, q_o is the flow rate of the oil, A is the cross-sectional area of the core, ΔP is the pressure drop across the core, L is the length of the core, and μ_o is the viscosity of the oil.

Effective Water Permeability

Effective water permeability was calculated at the end of the waterflood when no more oil was being produced and the pressure drop was stable across the core. The effective water permeability was calculated at residual oil saturation using the following equation:

$$q_w = \frac{-k_w A \Delta P}{\mu_w L}, \tag{3.14}$$

k_w is the effective water permeability at residual oil saturation, qw is the flow rate of the water, A is the cross-sectional area of the core, ΔP is the pressure drop across the core, L is the length of the core, and μ_w is the viscosity of the water.

End Point Oil Relative Permeability

The end point relative permeability of oil was calculated by dividing the effective oil permeability at residual water saturation calculated in Equation 3.13 by the brine permeability at 100% water saturation calculated in Equation 3.11. The calculation for oil end point relative permeability was calculated using the equation below.

$$k_{ro} = \frac{k_o}{k_{w@SW=100\%}}, \tag{3.15}$$

k_{ro} is the oil relative permeability at endpoint, k_o is the effective oil permeability, and $k_{w@SW=100\%}$ is the brine permeability at 100% brine saturation.

End Point Oil Relative Permeability

The end point relative permeability of water was calculated similarly, dividing the effective permeability of water by the brine permeability at 100% brine saturation using the equation below. The effective permeability of water was calculated at residual oil saturation at the end of the waterflood using equation 3.14.

$$k_{rw} = \frac{k_w}{k_{w@SW=100\%}}, \tag{3.16}$$

k_{rw} is the water relative permeability at endpoint, k_w is the effective water permeability, and $k_{w@SW=100\%}$ is the brine permeability at 100% brine saturation.

Aging

After the core was saturated with oil, it was placed in a glass container and filled with Crude Oil A. The container was placed in an oven set at 80^{o}C for three weeks, allowing the core to change from water wet to oil wet.

3.3.4 Coreflood

Two types of corefloods were conducted in this study. The first set of corefloods performed were in the absence of oil to determine whether or not foam formed in porous media and the effects of surfactant concentration and quality on foam formation. The second type of coreflood performed was a foam flood at a set surfactant concentration and quality in the presence of oil to determine the viability of the surfactant formulation as an effective enhanced oil recovery technique.

3.3.4.1 Corefloods in the Absence of Oil

Corefloods in the absence of oil were performed for all four surfactants; GC580, GC468, CTAB, and Bioterg. The primary objective of these floods was to determine the pressure drop across the core. After the core was saturated with brine, a tracer test was conducted, and brine permeability was measured, a waterflood was performed at 4 ft/day until the pressure drop across the core stabilized. CO_2 was then injected at 4 ft/day until the pressure drop was stabilized. Following the CO_2 injection, brine and CO_2 were co-

injected at 90% quality until steady state was reached. Next, a pore volume of surfactant was injected to satisfy surfactant adsorption. The surfactant was then co-injected with CO_2 at 90% quality and 4 ft/day. If the pressure drop for CO_2 and surfactant co-injection was larger than co-injection of brine and CO_2, it was assumed that foam was formed. Three different surfactant concentrations were co-injected with CO_2: 0.1 wt%, 0.25 wt%, and 0.5 wt%. Finally, 0.5 wt% surfactant and CO_2 were co-injected at varying qualities: 70%, 75%, 80%, 85%, 90%, and 95% to determine the optimum foam quality for each surfactant.

3.3.4.2 Corefloods in the Presence of Oil

After the core had been characterized and saturated with oil, a waterflood was performed on the core to determine secondary recovery. The waterflood was conducted at 1 ft/day until no more oil was produced and pressure drop was stabilized. Effluent samples were collected to calculate cumulative oil recovery and oil saturation as a function of pore volumes of injected water. Waterflood injection was increased to 5 ft/day to make sure there was no more oil production due to capillary end effects. After the waterflood was completed, one pore volume of surfactant solution was injected at 1 ft/day to satisfy adsorption. Next, 0.5% surfactant was co-injected with CO_2 at the optimal quality as determined by the coreflood experiments in the absence of oil. Initially, the coinjection bypassed the core until the pressure stabilized, then the foam flood was redirected into the core. The surfactant and CO_2 co-injection was performed at 1 ft/day. The effluent samples were collected, and the oil cut, residual oil saturations, and cumulative oil production were determined using the following equations:

$$f_o = \frac{V_{oil}}{V_{oil}+V_{water}}. \quad (3.17)$$

In the oil cut equation above, f_o is the oil cut, V_{oil} is the effluent oil volume, and V_{water} is the effluent water volume.

$$N_p = \frac{\sum V_{oil}}{V_p}. \quad (3.18)$$

In the cumulative oil production equation above, N_p is the cumulative oil produced, V_{oil} is the effluent oil volume, and V_p is the pore volume.

Chapter 4: Results

This chapter contains the results of the experiments done on the surfactants to determine aqueous stability, foamability, adsorption, and bulk foam stability, as well as results of the foam capabilities of the surfactants in porous media both in the absence and the presence of oil.

4.1 Results of Surfactant Characterization

4.1.1 Aqueous Stability

he aqueous stability of each of the surfactants can be seen in Tables 4.1 to 4.4. The surfactants were tested at different salinities and different temperatures. In these tables, “Clear” indicates that the surfactant solution was clear and aqueously stable, “Hazy” indicates that the solution was hazy and not aqueously stable, “Cloudy” indicates that the solution was cloudy and not aqueously stable, and “P” indicates that part of the solution precipitated out of solution.

%NaCl	%$CaCl_2$ + %$MgCl_2$	25°C	40°C	60°C	80°C	100°C	120°C
0	1+1	Clear	Clear	Clear	Clear	Clear	Clear
1	1+1	Clear	Clear	Clear	Clear	Clear	Clear
4	1+1	Clear	Clear	Clear	Clear	Clear	Clear
8	1+1	Clear	Clear	Clear	Clear	Clear	Clear
10	1+1	Hazy	Hazy	Clear	Clear	Hazy	Cloudy
15	1+1	Hazy	Hazy	Hazy	Hazy	Hazy	Cloudy

Table 4. 1: Aqueous stability results of GC 468 at varying salinity and varying temperature.

As seen in Table 4.1, GC 468 has excellent aqueous stability in the presence of divalent and monovalent ions at a range of temperatures. At 60°C, GC 468 is stable up to 15% NaCl with 1% $CaCl_2$ and 1%$MgCl_2$. Temperatures above 120°C have not been tested yet, so the upper limit of temperature on aqueous stability has not been determined yet. It is thought that the solution will still be stable at higher temperatures. However, there is the possibility for Hofmann elimination. Hofmann elimination is a mechanism where a base removes an accessible proton, causing a two carbons to become double bonded, and forcing a neutral amine to disconnect from the carbon. The mechanism is illustrated in Figure 4.1. Further studies should be performed to determine the temperature required for Hofmann elimination for this surfactant.

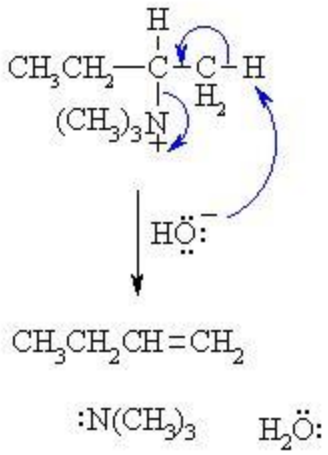

Figure 4. 1: Hofmann Elimination mechanism. Mechanism obtained from http://www.chem.ucalgary.ca/courses/351/Carey5th/Ch22/ch22-3-4.html.

%NaCl	%$CaCl_2$ + %$MgCl_2$	25°C	40°C	60°C	80°C	100°C	120°C
0	1+1	Clear	Clear	Clear	Clear	Clear	Clear
1	1+1	Clear	Clear	Clear	Clear	Clear	Clear
4	1+1	Hazy	Hazy	Clear	Clear	Clear	Clear
8	1+1	Hazy	Hazy	Hazy	Clear	Clear	Hazy
10	1+1	Cloudy	Hazy	Hazy	Clear	Hazy	Hazy
15	1+1	Cloudy	Hazy	Hazy	P	P	P

Table 4. 2: Aqueous stability results of GC 580 at varying salinity and varying temperature.

As seen in Table 4.2, GC 580 has a smaller range of aqueous stability than GC 468. This is because GC 580 has four more carbons in each tail, making the surfactant more hydrophobic and less soluble in water. At lower salinities, however, below 8% NaCl and 1% $CaCl_2$ and 1% $MgCl_2$ and below, GC 580 has excellent aqueous stability from 60°C up to 120°C. Aqueous stability has not yet been tested above 120°C so the upper limit of aqueous stability for all salinities has not been determined. As with GC 468, further temperature studies should be performed to determine the temperature at which Hofmann elimination occurs. However, since some Hofmann elimination reactions require the presence of a strong base and temperatures up to 400°C (Jimenez et al., 2001), it is unlikely that Hofmann elimination will occur for the gemini surfactants at reservoir conditions.

%NaCl	%$CaCl_2$+ %$MgCl_2$	25°C	40°C	60°C	80°C	100°C	120°C
0	1+1	Clear	Clear	Clear	Clear	Clear	Clear
1	1+1	Clear	Clear	Clear	Clear	Clear	Clear
4	1+1	Clear	Clear	Clear	Clear	Clear	Clear
8	1+1	Clear	Clear	Clear	Clear	Clear	Clear
10	1+1	Clear	Clear	Clear	Clear	Clear	Clear
15	1+1	Clear	Clear	Clear	Clear	Clear	Clear

Table 4. 3: Aqueous stability results of CTAB at varying salinity and varying temperature.

As seen in Table 4.3, CTAB has excellent aqueous stability, especially at room temperature in the presence of monovalent and divalent ions. As the temperature increases, the aqueous stability is not affected. CTAB has better aqueous stability than the gemini surfactants at room temperature, but at lower salinities (less than 10% NaCl and 1%$CaCl_2$ and 1%$MgCl_2$) the cationic gemini surfactants have comparable stability, meaning the gemini surfactants could be used for similar applications as CTAB. Additionally, two other cationic gemini surfactants were tested for aqueous stability. Since neither of them were aqueously stable at any temperature or salinity tested, they were not included in the rest of this study. A table of these results can be found in the

Appendix A. The aqueous stability of anionic surfactant AS-40 was also tested, as seen in Table 4.4.

%NaCl	%$CaCl_2$ + %$MgCl_2$	25°C	40°C	60°C	80°C	100°C	120°C
0	1+1	Clear	Clear	Hazy	Hazy	Hazy	Hazy
1	1+1	Hazy	Hazy	Hazy	Hazy	Hazy	Hazy
4	1+1	Hazy	Hazy	Hazy	Hazy	Hazy	Hazy
8	1+1	Hazy	Hazy	Hazy	Hazy	Hazy	Hazy
10	1+1	Cloudy	Hazy	Hazy	Hazy	Hazy	Hazy
15	1+1	Cloudy	Hazy	Hazy	Hazy	Hazy	Hazy

Table 4. 4: Aqueous stability result of AS-40 at varying salinity and temperature

AS-40 has poor aqueously stable in the presence of divalent ions at most of the temperatures or salinities tested without the addition of a co-solvent. Since most anionic surfactants are not stable without the addition of co-solvents in the presence of divalent ions, cationic gemini surfactants could be utilized more than the anionic surfactants in harsh salinity reservoirs. The novel cationic gemini surfactants both have a broader range of aqueous stability than AS-40 in the absence of co-solvents.

4.1.2 Bulk Foam Stability

This section contains the results from foam stability experiments. Preliminary foam stability experiments were performed by shaking tubes containing surfactants to ensure that the surfactant at varying salinities was capable of forming foam. After foamability was determined, GC 468, GC 580, CTAB, and AS-40 were tested for the bulk foam stability at varying salinities and in the presence of varying oils at room temperature and 60^{o}C. The bulk foam stability was inferred from the height of the foam column (h) in a graduated cylinder compared to the initial foam height (h_o) as a function of time. To compare foam stability, the half-life (time to achieve $h/h_o=0.5$) was evaluated for each surfactant.

4.1.2.1 Preliminary Bulk Foam Stability Results

Preliminary bulk foam stability experiments were performed by placing 5 mL of surfactant solution with varying salinities in centrifuge tubes and shaking the tubes by hand to form foam. Figure 4.1 shows the preliminary effect of GC 468 at five different salnities: 0%, 1% $CaCl_2$ + 1% $MgCl_2$, 1% NaCl + 1% $CaCl_2$ + 1% $MgCl_2$, 4% NaCl + 1% $CaCl_2$ + 1% $MgCl_2$, and 8% NaCl + 1% $CaCl_2$ + 1% $MgCl_2$. As seen in the figure, foam was formed for each of the salinities. The same experiment was performed with GC 580, CTAB, and AS-40. Foam formation was seen for all four surfactants at these salinities.

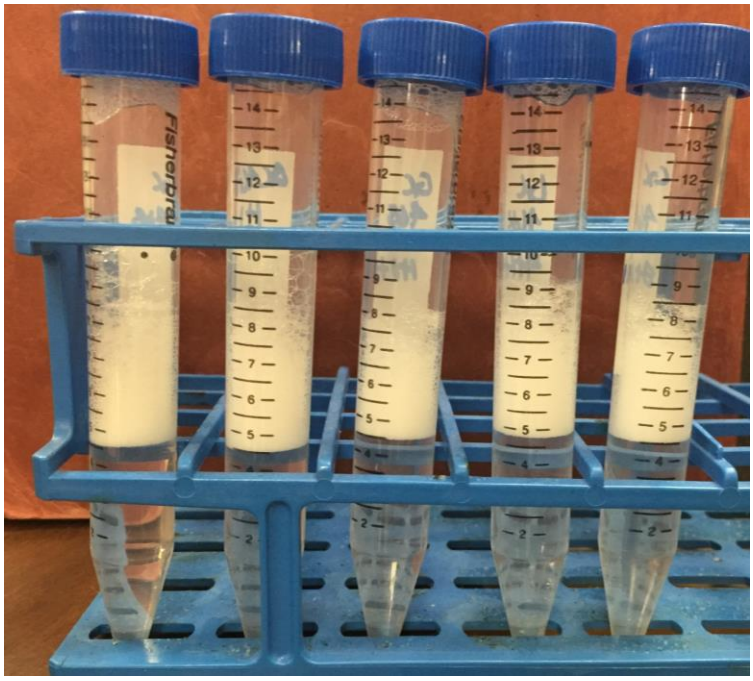

Figure 4. 2: Preliminary bulk foam stability tests for GC 468. All five salinities show excellent foam formation.

4.1.2.2 Effect of Salinity on Bulk Foam Stability at Room Temperature and 60^{o}C

GC 468

Figure 4.3 contains the bulk foam stability of GC 468 at varying salinities at room temperature. As seen in the figure below, increasing the salinity has a destabilizing effect on the bulk foam stability. Above 30,000 ppm, the half-life of the foam is less than 200 minutes. At 60^{o}C, however, the bulk foam stability of GC 468 at all salinities was dramatically reduced, and the most stable foam was with a salinity of 20,000 ppm, as seen in Figure 4.4. Bulk foam stability experiments were performed 3 times, and the median bulk foam experiment was plotted. The variability of the bulk foam stability results can be seen in Appendix B.

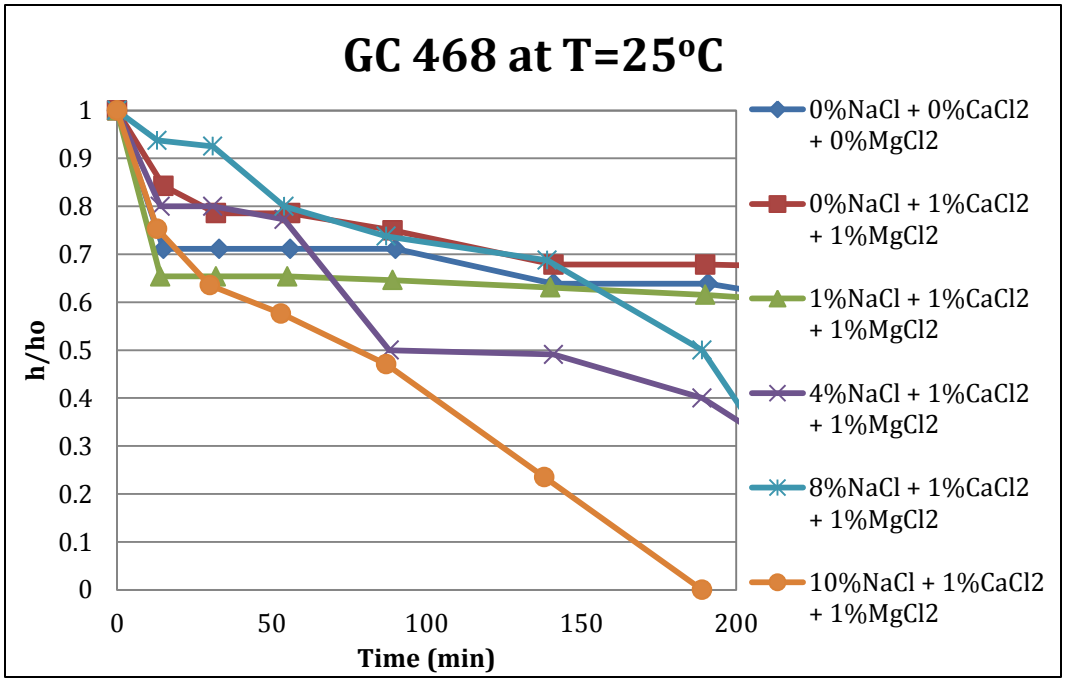

Figure 4. 3: Bulk foam stability of GC 468 at T=25°C at varying salinities. Bulk foam stability is measured as a function of foam height divided by the initial foam height. No oil was present.

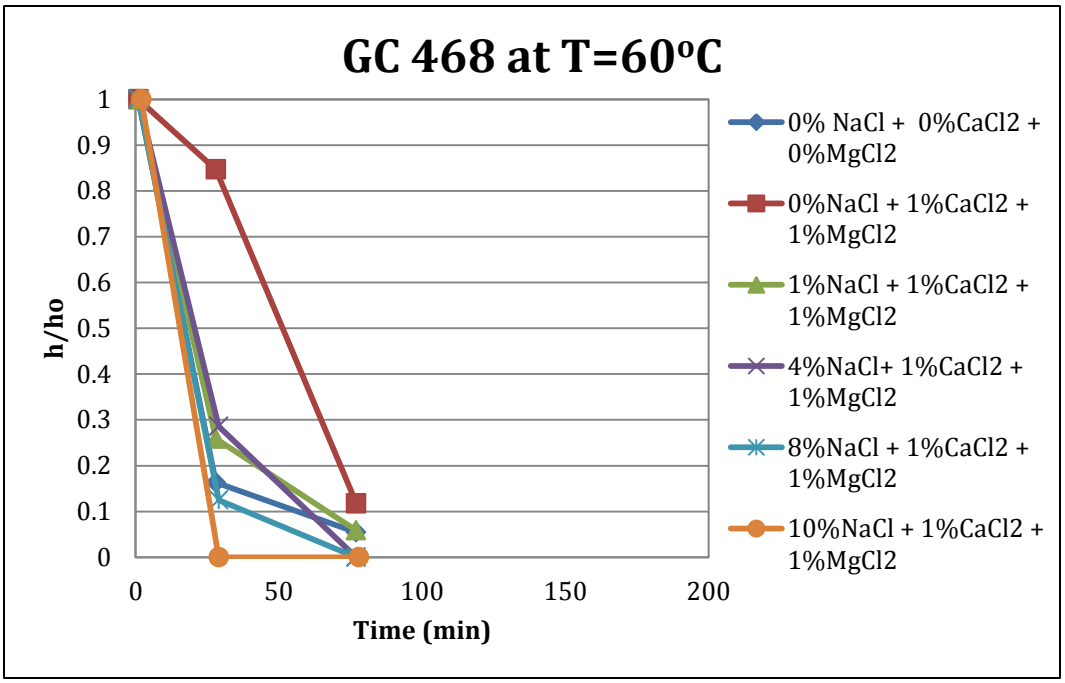

Figure 4. 4: Bulk foam stability of GC 468 at T=60°C at varying salinities. Bulk foam stability is measured as a function of foam height divided by the initial foam height. No oil was present for these bulk foam stability tests.

Salinity	Half-life at T=25°C	Half-life at T=60°C
0%	308 min	17 min
1%$MgCl_2$ + 1%$CaCl_2$	312 min	77 min
1% NaCl + 1%$MgCl_2$ + 1%$CaCl_2$	288 min	19 min
4% NaCl + 1%$MgCl_2$ + 1%$CaCl_2$	88 min	21 min
8% NaCl + 1%$MgCl_2$ + 1%$CaCl_2$	189 min	17 min
10% NaCl + 1%$MgCl_2$ + 1%$CaCl_2$	44 min	15 min

Table 4. 5: A summary of results of bulk foam stability for GC 468 at varying salinities at both 25°C and 60°C. Half-life is the time at which the height of the foam is half the height of the initial foam. No oil was present for these bulk foam stability tests.

Table 4.5 contains a summary of the half-life of GC 468 foam at varying salinities at both room temperature and at 60°C. Since the foam experiments in porous media were conducted at 60°C, the formulation of 1%$MgCl_2$ and 1% $CaCl_2$ with 0.5% GC 468 was selected.

GC 580

Figure 4.5 contains the bulk foam stability of GC 580 at varying salinities at room temperature. As seen in the figure below, the effect of salinity is more complicated than with GC 468. No foam is formed at 0 ppm salinity which suggests that ions are needed at the liquid interface to form lamella. The most stable foam is formed with 30,000 ppm. However, as more ions are added, the foam stability remains about the same at room

temperature. As with GC 468, at 60°C the bulk foam stability of GC 580 at all salinities was dramatically reduced, as seen in Figure 4.6. At 60°C, the bulk foam stability increases with increasing salinity until 60,000 ppm then decreases with increasing salinity above 60,000 ppm.

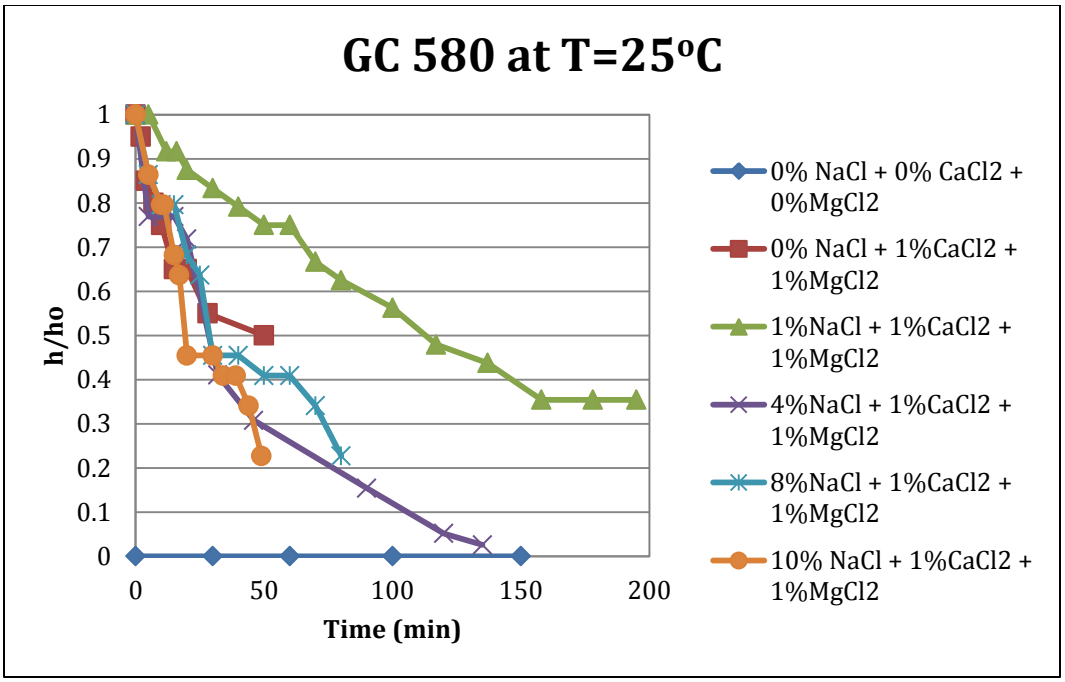

Figure 4. 5: Bulk foam stability of GC 580 at T=25°C at varying salinities. Bulk foam stability is measured as a function of foam height divided by the initial foam height. No oil was present.

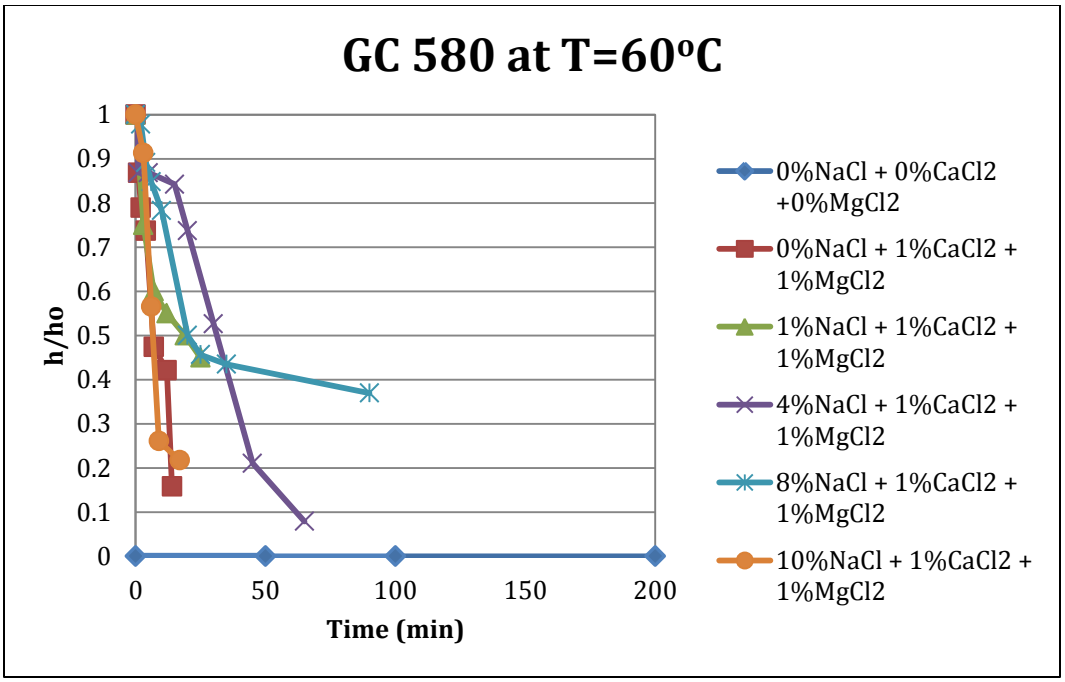

Figure 4. 6: Bulk foam stability of GC 580 at T=60°C at varying salinities. Bulk foam stability is measured as a function of foam height divided by the initial foam height. No oil was present.

Salinity	GC 580 at T=25°C	GC 580 at T=60°C
0%	0 min	0 min
1%$MgCl_2$ + 1%$CaCl_2$	50 min	7 min
1% NaCl + 1%$MgCl_2$ + 1%$CaCl_2$	113 min	19 min
4% NaCl + 1%$MgCl_2$ + 1%$CaCl_2$	28 min	31 min
8% NaCl + 1%$MgCl_2$ + 1%$CaCl_2$	28 min	20 min
10% NaCl + 1%$MgCl_2$ + 1%$CaCl_2$	19 min	7 min

Table 4. 6: A summary of results of bulk foam stability for GC 580 at varying salinities at both 25°C and 60°C. Half-life is the time at which the height of the foam is half the height of the initial foam. No oil was present for these bulk foam stability tests.

Table 4.6 contains a summary of the half-life of GC 580 foam at varying salinities at both room temperature and at 60°C. Since the foam experiments in porous media were conducted at 60°C, the formulation of 4% NaCl, 1%$MgCl_2$, and 1% $CaCl_2$, with 0.5% GC 580 was selected. During the coreflood experiments, however, a new batch of GC 580 had to be synthesized. The new batch of GC 580 has slightly different aqueous stability results, and the formulation had to be changed to 0.5% GC 580 with 2%NaCl, 0.5% $CaCl_2$, and 0.5% $MgCl_2$. Brief bulk foam stability tests were performed on this new formulation and had similar half-lives as the 4% NaCl, 1% $CaCl_2$, and 1% $MgCl_2$.

CTAB

Figure 4.7 contains the bulk foam stability of CTAB at varying salinities at room temperature. As seen in this figure, no trend between salinity and bulk foam stability at room temperature exists for CTAB. At 60°C, however, the bulk foam stability of CTAB

at all salinities was dramatically reduced, and once again, no trend exists between salinity and bulk foam stability as seen in Figure 4.8. In general, the higher salinities have higher bulk foam stability at 60°C with 100,000 ppm having the longest half-life with 120,000 ppm having almost the same half-life.

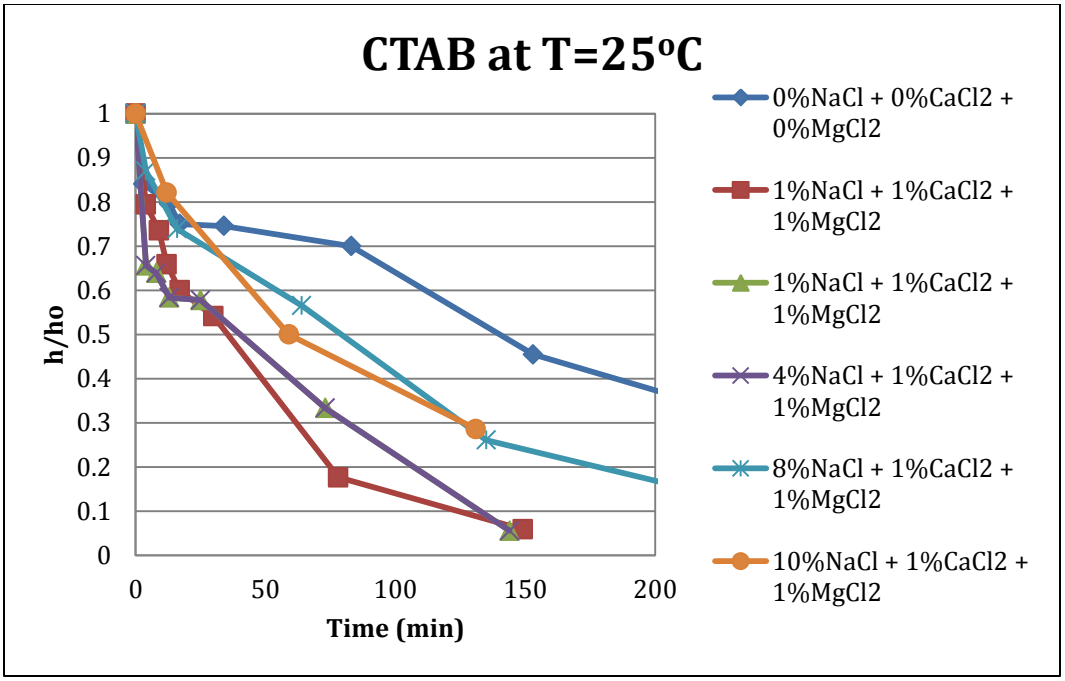

Figure 4. 7: Bulk foam stability of CTAB at T=25°C at varying salinities. Bulk foam stability is measured as a function of foam height divided by the initial foam height. No oil was present.

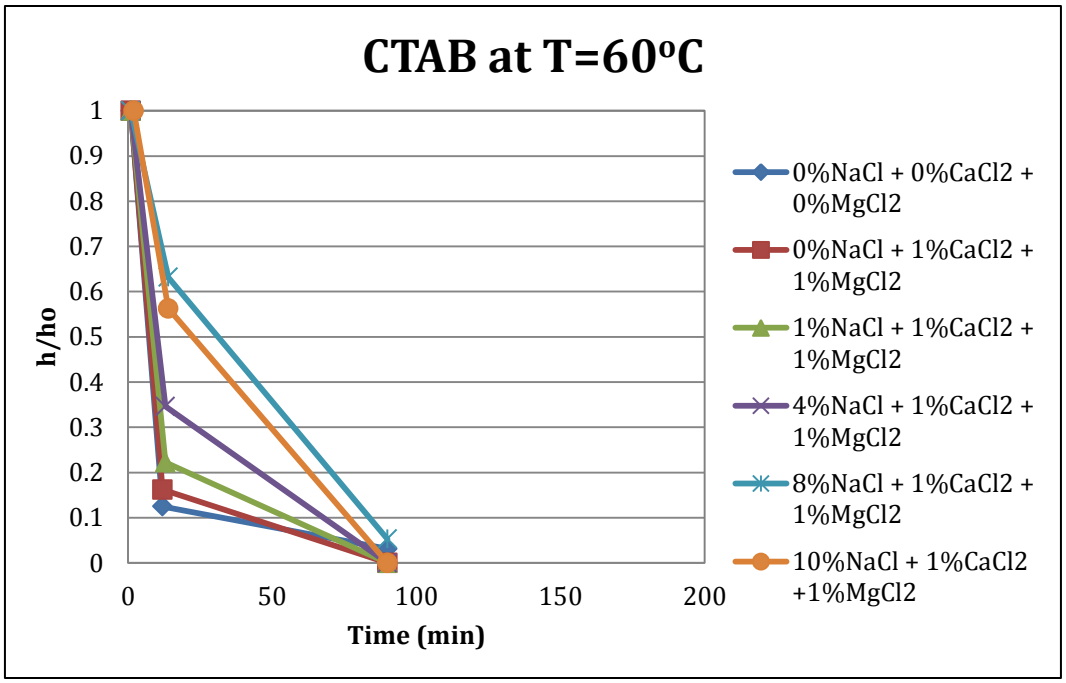

Figure 4. 8: Bulk foam stability of CTAB at T=60°C at varying salinities. Bulk foam stability is measured as a function of foam height divided by the initial foam height. No oil was present.

Salinity	CTAB at T=25°C	CTAB at T=60°C
0%	140 min	7 min
1%$MgCl_2$ + 1%$CaCl_2$	35 min	7 min
1% NaCl + 1%$MgCl_2$ + 1%$CaCl_2$	40 min	9 min
4% NaCl + 1%$MgCl_2$ + 1%$CaCl_2$	72 min	10 min
8% NaCl + 1%$MgCl_2$ + 1%$CaCl_2$	79 min	31 min
10% NaCl + 1%$MgCl_2$ + 1%$CaCl_2$	59 min	20 min

Table 4. 7: A summary of results of bulk foam stability for CTAB at varying salinities at both 25°C and 60°C. Half-life is the time at which the height of the foam is half the height of the initial foam. No oil was present for these bulk foam stability tests.

Table 4.7 contains a summary of the half-life of CTAB foam at varying salinities at both room temperature and at 60°C. Since CTAB was used as a comparison for the cationic Gemini surfactants, the same formulation for GC 580 was used for CTAB in the porous media experiments. The formulation of 4% NaCl, 1%$MgCl_2$, and 1% $CaCl_2$, with 0.5% CTAB was selected.

AS-40

Figure 4.9 contains the bulk foam stability of AS-40 at varying salinities at room temperature. As seen in the figure below, no trend between salinity and bulk foam stability at room temperature exists for AS-40. At 60°C, however, the bulk foam stability of AS-40 at all salinities was dramatically reduced, and once again, no trend exists between salinity and bulk foam stability as seen in Figure 4.10. At both room temperature and 60°C, AS-40 has significantly longer half-lives at all salinities than the cationic

surfactants. However, since AS-40 has a negative charge, it will be adsorbed on the carbonate surface at a much larger quantity than the cationic surfactants without the use of alkalis to reduce adsorption. Also, since AS-40 is not aqueously stable in the presence of divalence ions, AS-40 cannot be used without the addition of a co-solvent.

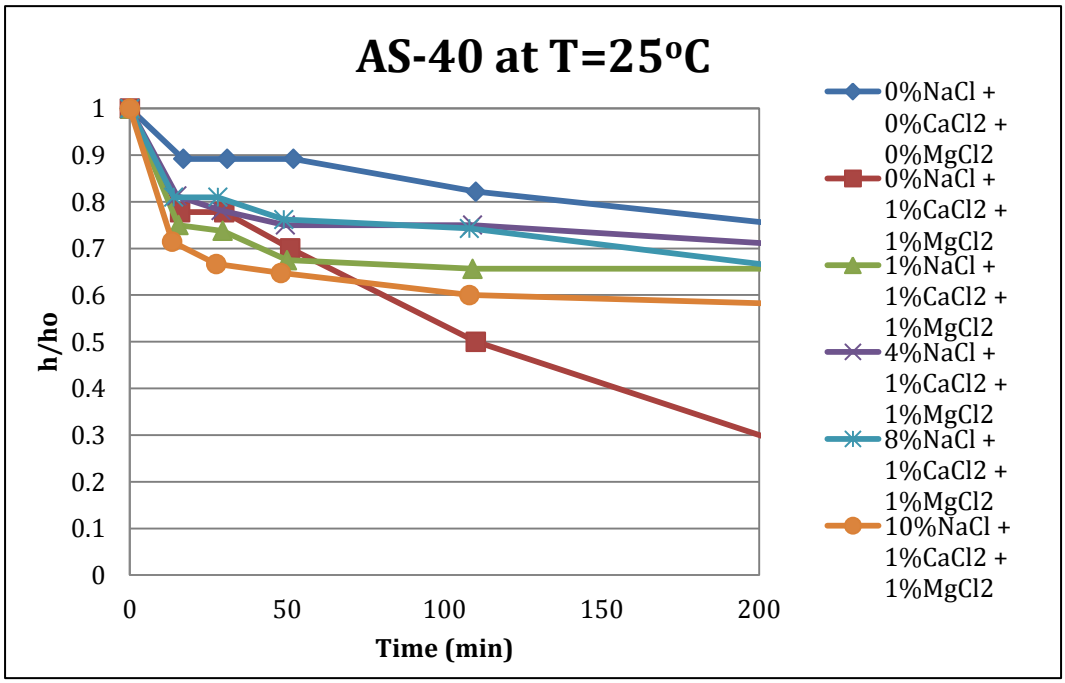

Figure 4. 9: Bulk foam stability of AS-40 at T=25°C at varying salinities. Bulk foam stability is measured as a function of foam height divided by the initial foam height. No oil was present.

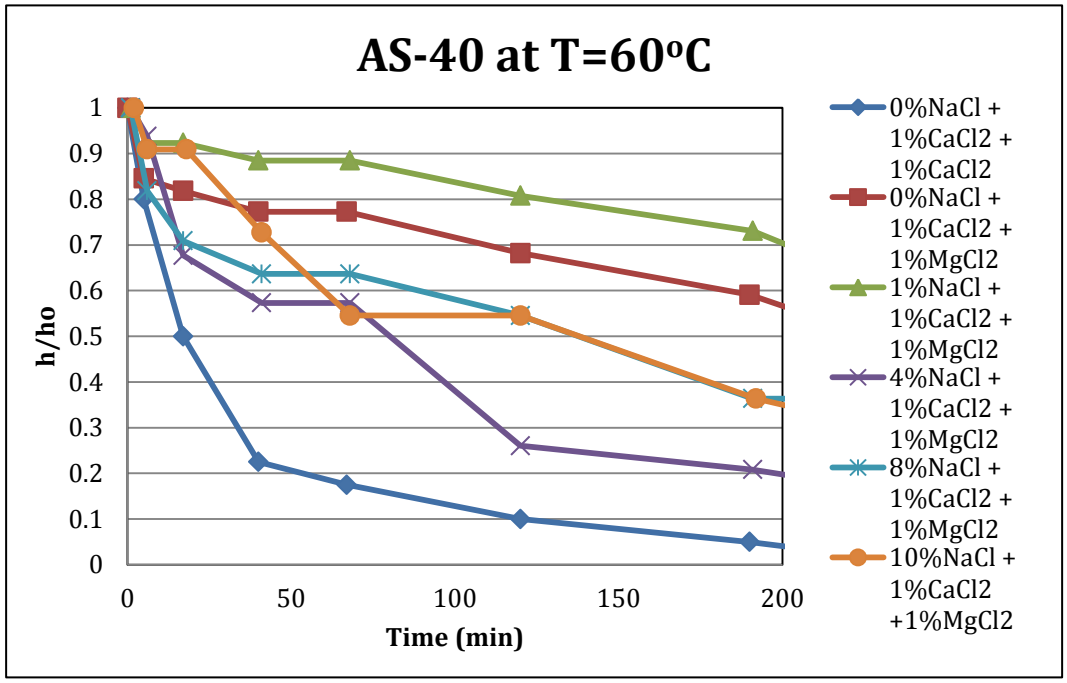

Figure 4. 10: Bulk foam stability of AS-40 at T=60°C at varying salinities. Bulk foam stability is measured as a function of foam height divided by the initial foam height. No oil was present.

Salinity	AS-40 at T=25°C	AS-40 at T=60°C
0%	476 min	17min
1%$MgCl_2$ + 1%$CaCl_2$	110 min	227 min
1% NaCl + 1%$MgCl_2$ + 1%$CaCl_2$	402 min	325 min
4% NaCl + 1%$MgCl_2$ + 1%$CaCl_2$	624 min	80 min
8% NaCl + 1%$MgCl_2$ + 1%$CaCl_2$	402 min	138 min
10% NaCl + 1%$MgCl_2$ + 1%$CaCl_2$	291 min	138 min

Table 4. 8: A summary of results of bulk foam stability for AS-40 at varying salinities at both 25°C and 60°C. Half-life is the time at which the height of the foam is half the height of the initial foam. No oil was present for these bulk foam stability tests.

Table 4.8 contains a summary of the half-life of AS-40 foam at varying salinities at both room temperature and at 60°C. Despite longer half-lives, these surfactant solutions cannot be used in porous media because the solutions were not aqueously stable at room temperature or 60°C without the addition of a cosolvent. Due to time constraints, aqueous instability, and adsorption on carbonate rocks, AS-40 was not tested in porous media.

4.1.2.3 Effect of Oil on Bulk Foam Stability

GC 468

Figure 4.11 contains the bulk foam stability of GC 468 with 1% $CaCl_2$ and 1% $MgCl_2$ in the presence of 1 wt% of varying oils at T=25°C. As seen in the figure below Crude A has the least destabilizing effect on the foam stability. Crude C also does not destabilize the foam as much as mineral oil, decane, and Crude B. These results are

slightly different than Schramm and Novosad's study where it was found that the more viscous oils have less of destabilizing effects on the foam (Homme, 1996). Crude B was the most viscous oil with a viscosity of 200 cP, but it had the second most destabilizing effect on the bulk foam. As with the bulk foam stability tests without the presence of oil, the increased temperature to 60^{o}C greatly reduced the half-life regardless of which oil was present, as seen in Figure 4.12. Similar to room temperature, all oils reduced the half-life of the foam in bulk phase at 60^{o}C, but Crude A had the least destabilizing effect on the foam. Like at room temperature, mineral oil, decane, and Crude B are the worst for the bulk foam stability. An explanation for why Crude A is the least destabilizing will be discussed in Section 4.1.3 where the spreading, entering, and bridging coefficients are analyzed.

Table 4.9 contains a summary of the half-life of GC 468 foam in the presence of different at both room temperature and at 60^{o}C. For core floods, Crude A was selected because it had the least destabilizing effect on the foam. Crude A decreases the half-life by only 13% at 60^{o}C; whereas, Crude B and Crude C reduce the half-life of the foam by 83% and 71%, respectively.

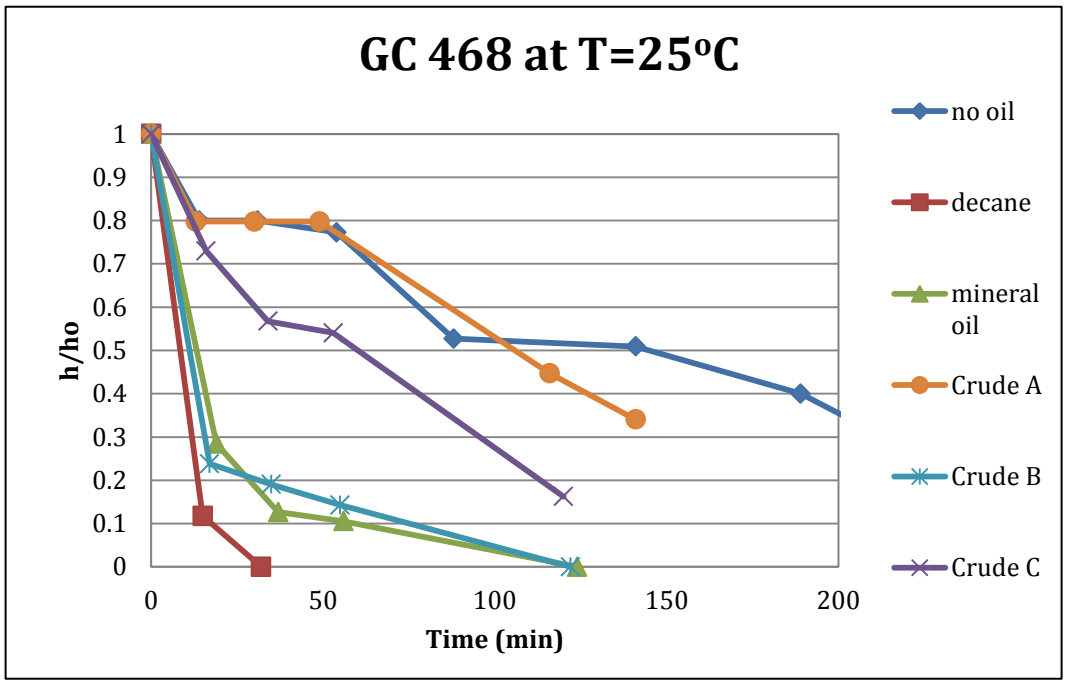

Figure 4. 11: Bulk foam stability of GC 468 with 1% $CaCl_2$ and 1% $MgCl_2$ at T=25°C in the presence of oils. Bulk foam stability is measured as a function of foam height divided by the initial foam height. Three crude oils were tested in addition to mineral oil and decane.

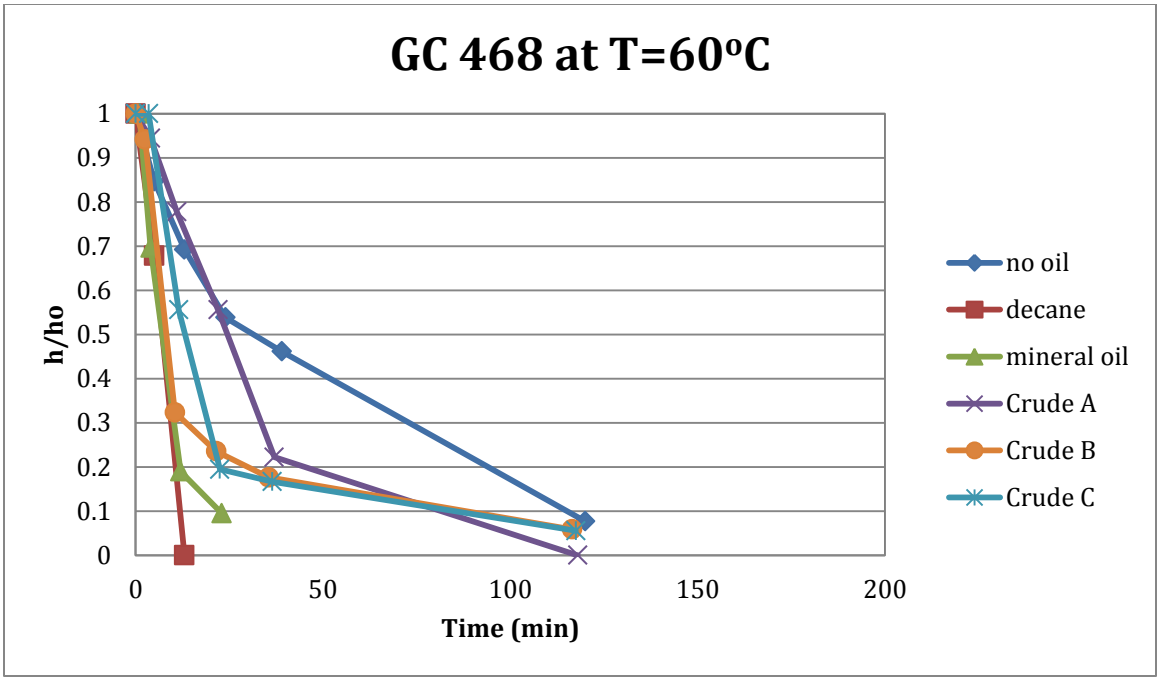

Figure 4. 12: Bulk foam stability of GC 468 with 1% $CaCl_2$ and 1% $MgCl_2$ at T=60°C in the presence of varying oils. Bulk foam stability is measured as a function of foam height divided by the initial foam height. Three crude oils were tested in addition to mineral oil and decane.

Oil	GC 468 at T=25°C	GC 468 at T=60°C
No oil	145 min	46 min
Decane	8.5 min	7 min
Mineral oil	32 min	7 min
Crude A	106 min	40 min
Crude B	11 min	8 min
Crude C	60 min	13 min

Table 4.9: A summary of results of bulk foam stability for GC 468 with 1%$CaCl_2$ and 1% $MgCl_2$ in the presence of varying oils at both 25°C and 60°C. 1 wt% oil was present.

GC 580

Figure 4.13 contains the bulk foam stability results of GC 580 with 4% NaCl, 1% $CaCl_2$, and 1% $MgCl_2$ in the presence of 1 wt% of oils at room temperature. As seen in the figure, the presence of oil reduces the stability of the foam. As with GC 468, mineral oil and decane have the greatest reduction of foam half-life. Mineral oil destabilizes GC 580 more than it destabilizes GC 468. A 98% decrease in half-life is seen when 1wt% mineral oil is introduced to GC 580 in the bulk foam phase; whereas, an 80% decrease in half-life is seen when mineral oil is introduced to GC 468 foam. Like GC 468, Crude A destabilizes GC 580 foam the least. A similar trend is seen at 60°C, as seen in Figure 4.14. All of the oils destabilize the foam, but Crude A destabilizes GC 580 the least; the explanation will be discussed in Section 4.1.3 while the spreading, entering, and bridging

coefficients are analyzed. Mineral oil, Decane, Crude B, and Crude C all decrease the half-life of the bulk foam by over 90%.

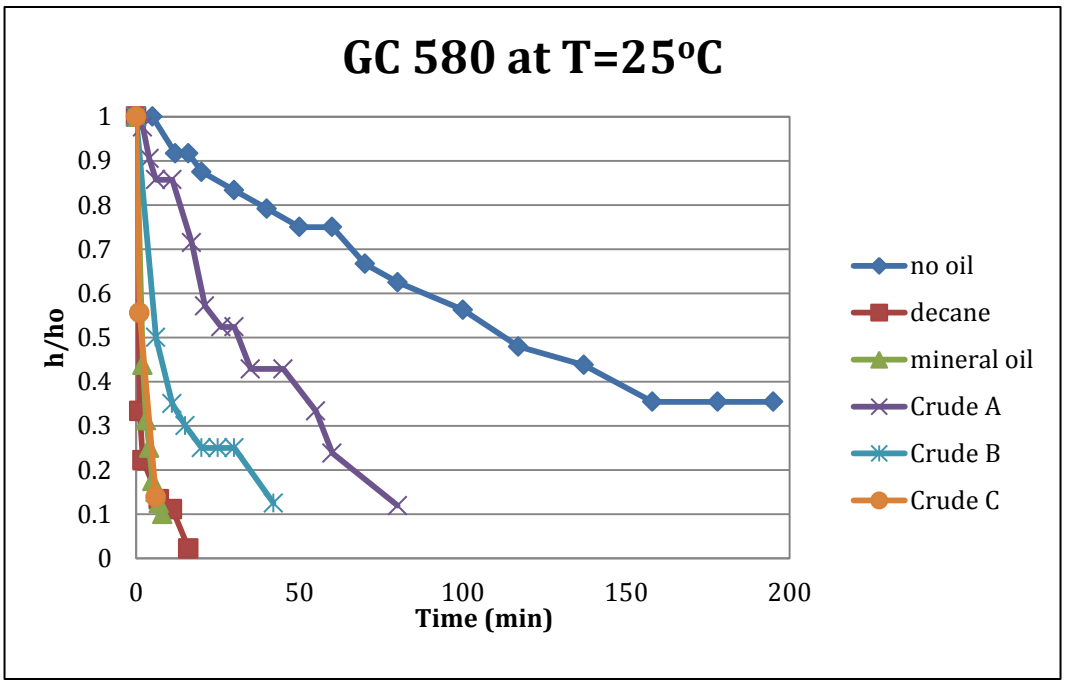

Figure 4. 13: Bulk foam stability of GC 580 with 4% NaCl, 1% $CaCl_2$, and 1% $MgCl_2$ at T=25°C in the presence of varying oils. Bulk foam stability is measured as a function of foam height divided by the initial foam height. Three crude oils were tested in addition to mineral oil and decane.

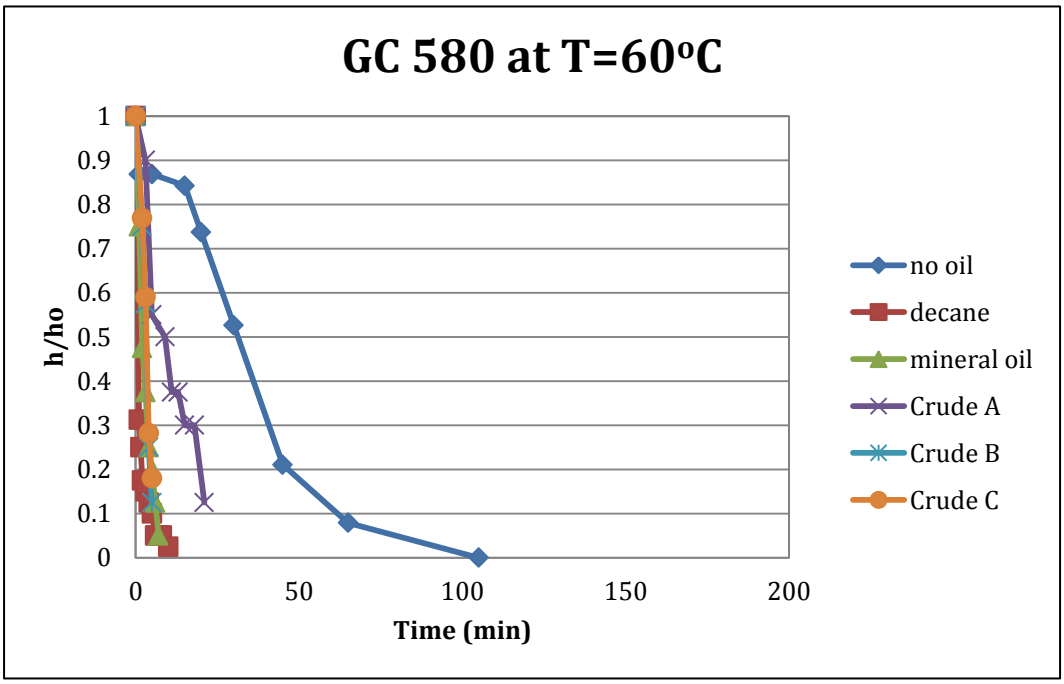

Figure 4. 14: Bulk foam stability of GC 580 with 4%NaCl, 1% $CaCl_2$, and 1% $MgCl_2$ at T=60°C in the presence of varying oils. Bulk foam stability is measured as a function of foam height divided by the initial foam height. Three crude oils were tested in addition to mineral oil and decane.

Oil	GC 580 at T=25°C	GC 580 at T=60°C
No oil	113 min	31 min
Decane	1 min	1 min
Mineral oil	2 min	2 min
Crude A	31 min	9 min
Crude B	6 min	3 min
Crude C	2 min	3 min

Table 4. 9: A summary of results of bulk foam stability for GC 580 with 4% NaCl, 1%$CaCl_2$, and 1% $MgCl_2$ in the presence of varying oils at both 25°C and 60°C. 1 wt% oil was present.

Table 4.10 contains a summary of the half-life of GC 580 foam in the presence of different at both room temperature and at 60°C. For core floods, Crude A was selected because it had the least destabilizing effect on the foam. Crude A decreased the half-life at 60°C by 70%; whereas, Crude B and Crude C reduce the half-life of the foam by over 90%. All three crudes destabilized GC 580 more than they destabilized GC 468.

CTAB

Figure 4.15 contains the results of bulk foam stability of CTAB with 4% NaCl, 1% $CaCl_2$, and 1% $MgCl_2$ in the presence of 1 wt% of oils at room temperature. As seen in the figure, the presence oil destabilizes CTAB foam. Crude A and Crude C destabilize the foam less than Crude B, mineral oil, and decane. Crude A only reduces the half-life by 13 minutes at room temperature. Like GC 468 and GC 580, decane and mineral oil

have the most destabilizing effects on the CTAB foam stability, indicating that these cationic gemini surfactants have comparable foam stability in the presence of oil as seen with conventional cationic surfactants. Figure 4.16 contains the bulk foam stability of CTAB with 4% NaCl, 1% $CaCl_2$, and 1% $MgCl_2$ at 60°C. At 60°C, all oils have a similar destabilizing effect on the foam stability. However, Crude B has the least destabilizing effect with only a decrease in foam half-life by 58%, while Crude A and Crude C both decrease the half-life by 65%.

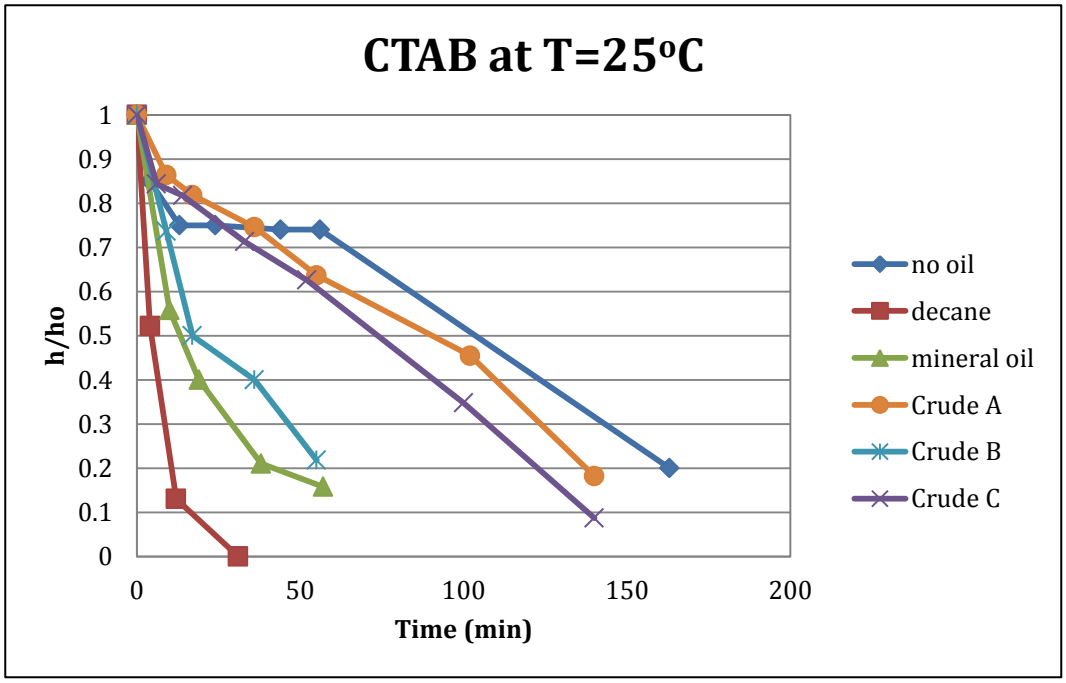

Figure 4. 15: Bulk foam stability of CTAB with 4% NaCl, 1% $CaCl_2$, and 1% $MgCl_2$ at T=25°C in the presence of varying oils. Bulk foam stability is measured as a function of foam height divided by the initial foam height. Three crude oils were tested in addition to mineral oil and decane.

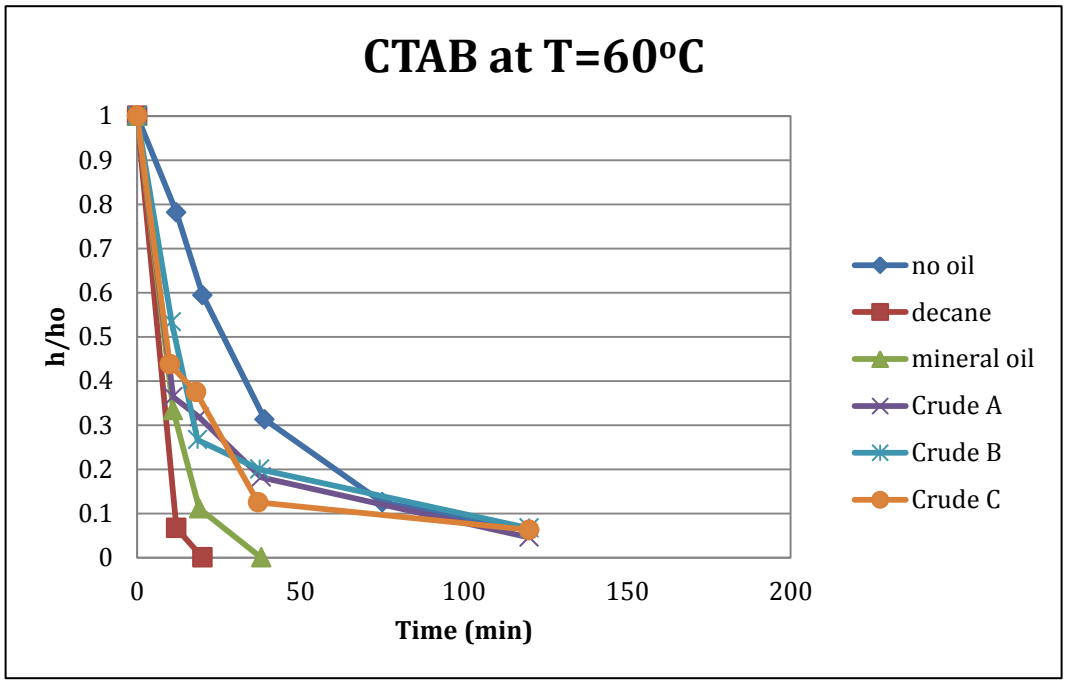

Figure 4. 16: Bulk foam stability of CTAB with 4% NaCl, 1% $CaCl_2$, and 1% $MgCl_2$ at T=60°C in the presence of varying oils. Bulk foam stability is measured as a function of foam height divided by the initial foam height. Three crude oils were tested in addition to mineral oil and decane.

Oil	CTAB at T=25°C	CTAB at T=60°C
No oil	103 min	26 min
Decane	4 min	6 min
Mineral oil	13 min	8 min
Crude A	90 min	9 min
Crude B	17 min	11 min
Crude C	74 min	9 min

Table 4. 10: A summary of results of bulk foam stability for CTAB with 4% NaCl, 1%$CaCl_2$, and 1% $MgCl_2$ in the presence of oils at both 25°C and 60°C. 1 wt% oil was present.

Table 4.11 contains a summary of the half-life of CTAB foam in the presence of different at both room temperature and at 60°C. In general, the half-life of CTAB in the presence of all oils at room temperature and 60°C is shorter than GC 468 and comparable to GC 580, indicating that these cationic gemini surfactants have potential for foam flooding. Due to time constraints, CTAB was not used for foam floods in the presence of oil; however, its foaming ability in porous media was tested in the absence of oil and will be compared to the cationic gemini surfactants in Section 4.1.5. Tsau and Grigg (1997) found that the stability of foam in the bulk phase can be correlated with foam in porous media. They found that surfactants with greater bulk foam stability also resulted in more mobility reduction during foam displacement. Using this correlation, we can assume that our cationic gemini surfactants will perform as well or better than the conventional cationic surfactant CTAB.

AS-40

Figure 4.16 contains the bulk foam stability of AS-40 with 4% NaCl in the presence of 1 wt% of varying oils at room temperature. As seen in the figure, all oils have a destabilizing effect on the foam stability. As with the cationic surfactants, decane has the most destabilizing effect on the foam stability. Unlike the cationic surfactants for which Crude A is the least destabilizing, Crude C has the least destabilizing effect on AS-40 at both room temperature and 60^{o}C. Figure 4.18 contains the bulk foam stability of AS-40 with 4% NaCl in the presence of 1 wt% of varying oils at 60^{o}C. As seen in the figure, the presence of any oil has a destabilizing effect on foam half-life. Like at room temperature, Crude C has the least destabilizing effect on AS-40 at 60^{o}C, and decane has the most destabilizing effect on the foam.

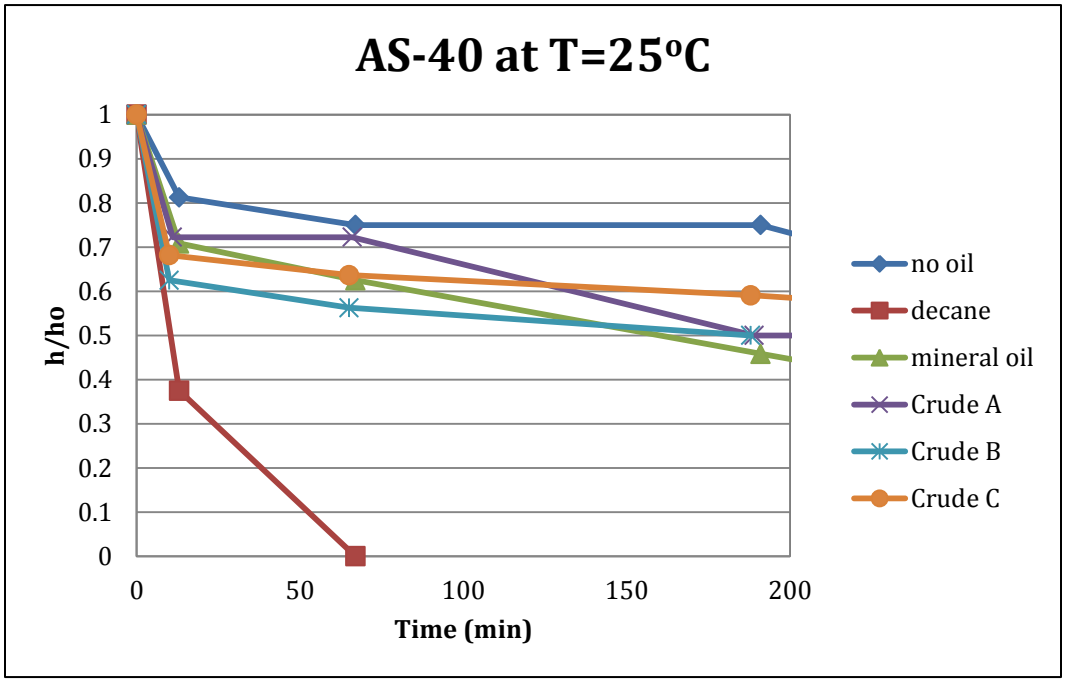

Figure 4. 17: Bulk foam stability of AS-40 with 4% NaCl in the presence of varying oils at T=25°C. Bulk foam stability is measured as a function of foam height divided by the initial foam height. Three crude oils were tested in addition to mineral oil and decane.

Table 4.12 contains a summary of the half-life of AS-40 foam in the presence of different at both room temperature and at 60°C. As seen in the table, AS-40 has longer half-lives than all three cationic surfactants. However, due to adsorption on the carbonate surface, using a cationic surfactant would be more beneficial than using an anionic surfactant. Surfactant adsorption will be discussed in Section 4.1.4.

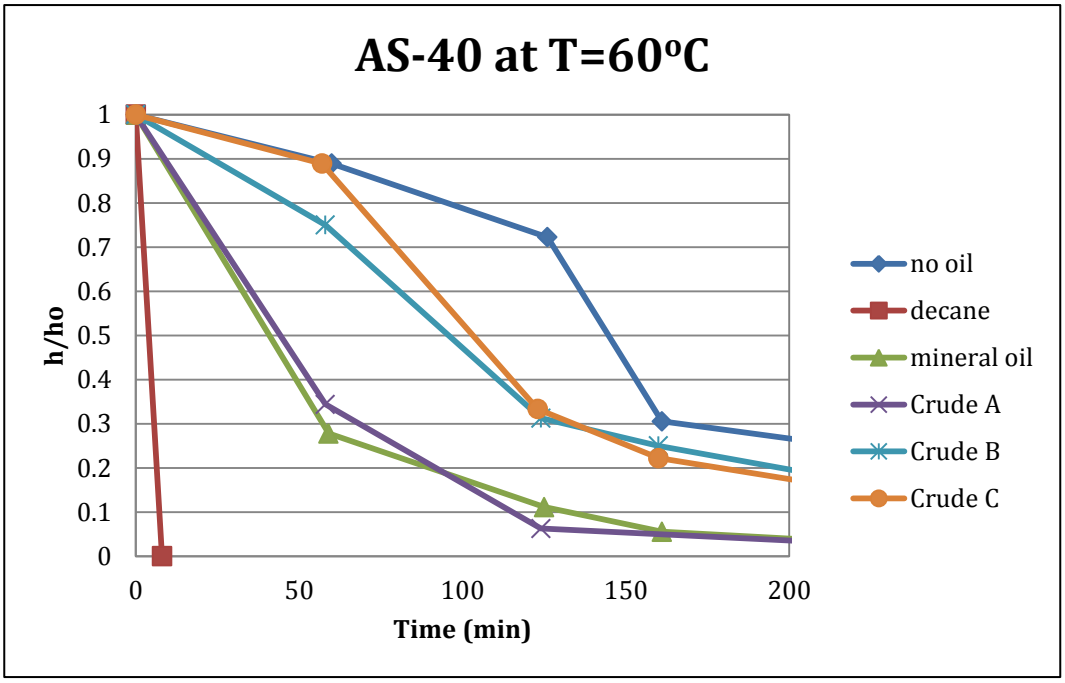

Figure 4. 18: Bulk foam stability of AS-40 with 4% NaCl at T=60°C in the presence of varying oils. Bulk foam stability is measured as a function of foam height divided by the initial foam height. Three crude oils were tested in addition to mineral oil and decane.

Oil	AS-40 at T=25°C	AS-40 at T=60°C
No oil	320 min	145 min
Decane	10 min	22 min
Mineral oil	160 min	41 min
Crude A	189 min	44 min
Crude B	188 min	95 min
Crude C	283 min	103 min

Table 4. 11: A summary of results of bulk foam stability for AS-40 with 4% NaCl in the presence of varying oils at both 25°C and 60°C. 1 wt% oil was present.

4.1.2.3 Effect of pH on Bulk Foam Stability

For CO_2 foam, CO_2 reduces the pH of surfactant solutions and it is necessary to determine the effects of pH on bulk foam stability. The pH was varied by adding hydrochloric acid to the surfactant solution before passing air to form foam in these laboratory experiments. The effects of pH on bulk foam stability were studied at room temperature for the three surfactant solutions that were used during porous media foaming experiments. Figure 4.19 shows the effect of pH on 0.25% GC 468 with 1%$CaCl_2$ and 1% $MgCl_2$. As seen in the figure, pH has little to no effect on the half-life of GC 468 bulk foam.

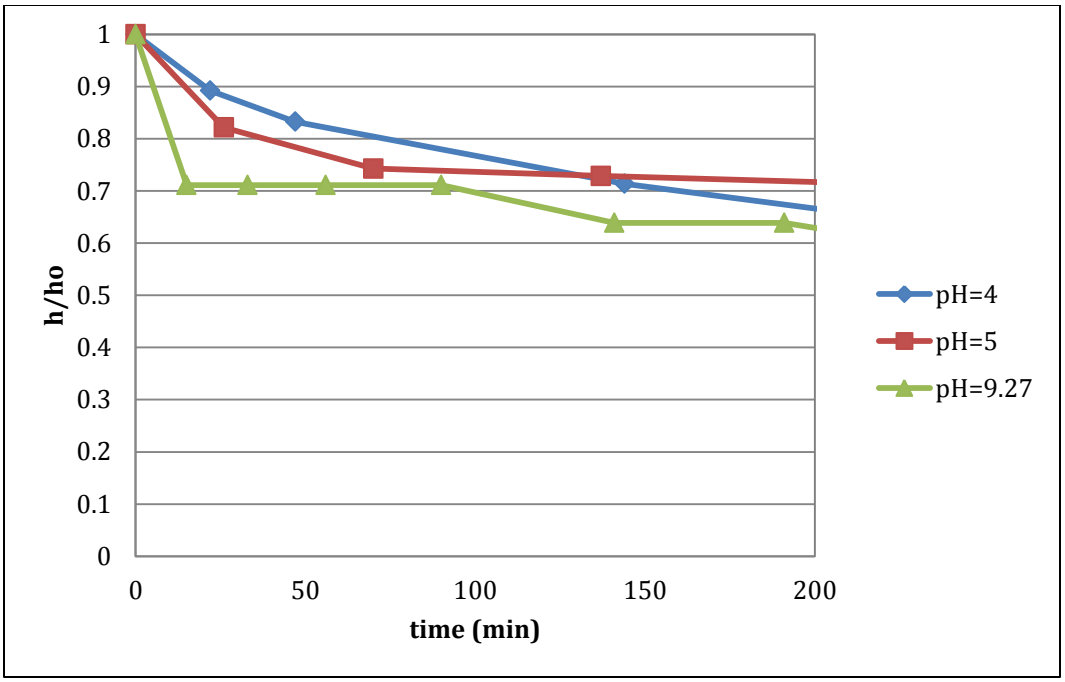

Figure 4. 19: The bulk foam stability of GC 468 with 1%$CaCl_2$ and 1%$MgCl_2$ at varying pH at T=25°C. 9.7 is the normal pH of the surfactant solution. The pH was reduced to 5 and to 4 to simulate the effect of CO_2 on the pH of the surfactant solution.

The effect of pH on the bulk foam stability was also determined for GC 580 with 4% NaCl, 1% $CaCl_2$, and 1% $MgCl_2$. As seen in Figure 4.20, pH also has little to no effect on the bulk foam stability of GC 580.

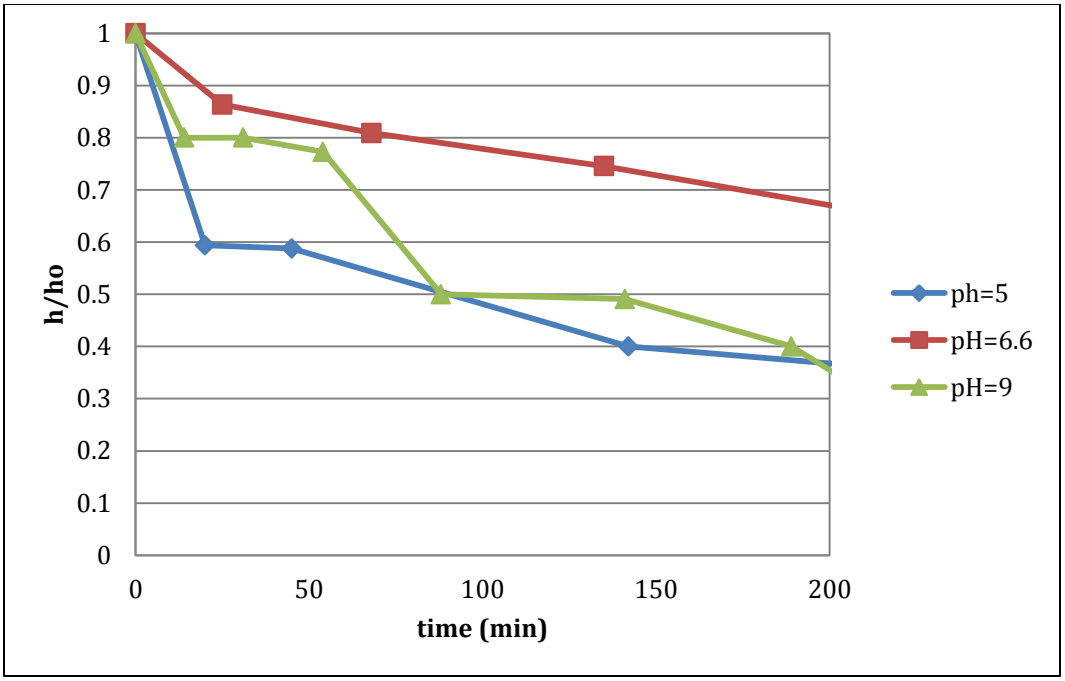

Figure 4. 20: The bulk foam stability of GC 580 with 4% NaCl, 1%$CaCl_2$, and 1%$MgCl_2$ at varying pH at T=25^{o}C. 9 is the normal pH of the surfactant solution. The pH was reduced to 6.6 and to 5 to simulate the effect of CO_2 on the pH of the surfactant solution.

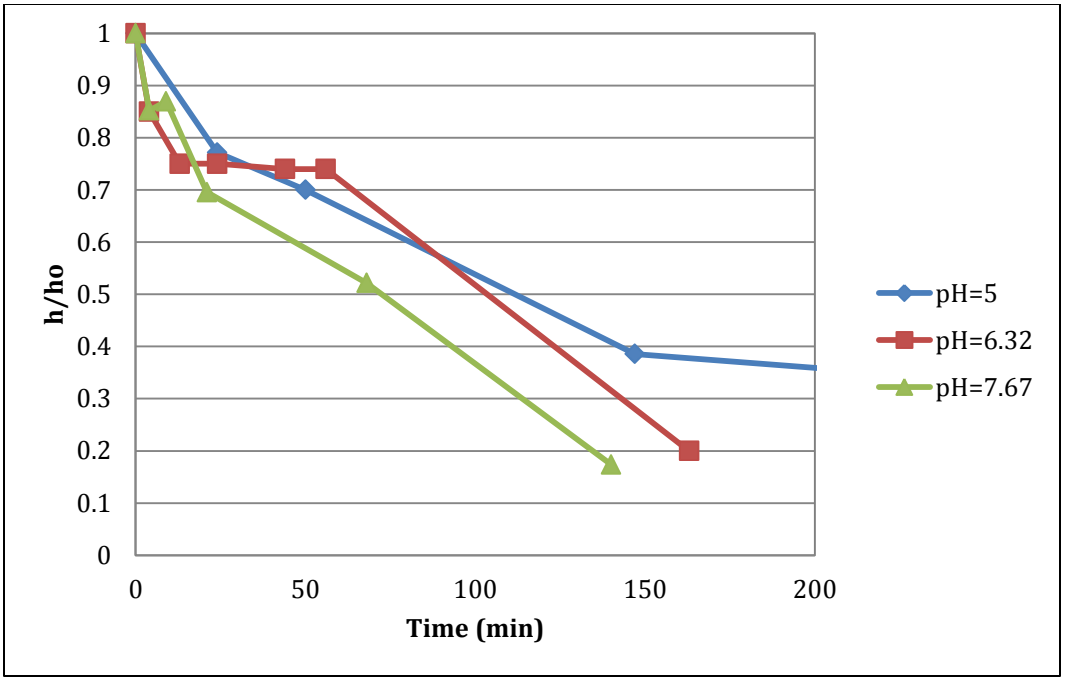

Figure 4. 21: The bulk foam stability of GC 580 with 4% NaCl, 1%$CaCl_2$, and 1%$MgCl_2$ at varying pH at T=25°C. 7.7 is the normal pH of the surfactant solution. The pH was reduced to 6.3 and to 5 to simulate the effect of CO_2 on the pH of the surfactant solution.

Lastly, the effect of pH on the bulk foam stability of CTAB with 4% NaCl, 1% $CaCl_2$, and 1% $MgCl_2$ was tested. The results of this bulk foam stability test are shown in Figure 4.21. Unlike GC 468 and GC 580, it appears that decreasing the pH has a beneficial effect on the half-life of CTAB bulk foam. However, the difference between the half-life at pH 5 and pH 6.3 is small, only 8 minutes. The difference between pH 7.67 and pH 5 is more significant with a difference of almost 40 minutes, approximately 35% shorter of a half-life. From these pH tests, it is apparent that the pH changes from CO_2 will not have a detrimental effect on foam stability in the porous medium during core flood experiments.

4.1.3 Spreading, Entering, and Bridging Coefficients

The surface tensions of oils/gas and aqueous surfactant solutions/gas were measured using the goniometer. To ensure that the Pendant drop method was accurate for surface tension measurements, the surface tension of water and mineral oil with respect to air were measured. The surface tension of water was 70.3 dynes/cm, which is within 5% error of the documented value of 71.97 dynes/cm. Likewise, the surface tension of decane using the goniometer was found to be 24.27 dynes/cm which is supposed to be 23.83 dynes/cm. However, the measured value of mineral oil/air surface tension was 22.1 dynes/cm, which is significantly different than the surface tension value found in the MSDS for mineral oil of 34 dynes/cm. Therefore, some of the crude oil surface tension measurements may be subject to experimental error. Since the goniometer in our lab could only measure surfactant/air and oil/air surface tensions at room temperature, the spreading, entering, and bridging coefficients were only calculated at room temperature. Surface tension and interfacial tension measurements were only taken at salinities in which the surfactant was aqueously stable. The spreading (S), entering (E), and bridging (B) coefficients were calculated using the following three equations.

$$S = \gamma_{G/S} - \gamma_{O/S} - \gamma_{G/O} \,, \tag{4.1}$$

$$E = \gamma_{G/S} + \gamma_{O/S} - \gamma_{G/O} \,, \tag{4.2}$$

$$\mathrm{B} = \gamma_{G/S}2 + \gamma_{O/S}2 - \gamma_{G/O}2 \quad . \tag{4.3}$$

The surface tension for each of the cationic surfactants was measured at varying salinities at room temperature. Table 4.13 summarizes the surface tensions of GC 468, GC 580, and CTAB. The surface tension of each of the oils was also measured, and the results are shown in Table 4.14. As seen in Equation 4.3, if the surface tension of the

surfactant solution is greater than the surface tension of the oil, the bridging coefficient will be positive because the IFT of surfactant and oil cannot be negative.

Salinity	Surface Tension GC 468 (dynes/cm)	Surface Tension GC 580 (dynes/cm)	Surface Tension CTAB (dynes/cm)
0%	30.6	36.3	32.6
1%$CaCl_2$ + 1%$MgCl_2$	31.2	40.8	32.0
1%NaCl + 1%$CaCl_2$ + 1%$MgCl_2$	30.4	39.2	33.8
4%NaCl + 1%$CaCl_2$ + 1%$MgCl_2$	31.9	35.1	31.9
8%NaCl + 1%$CaCl_2$ + 1%$MgCl_2$	30.2	Not aq. stable	32.5
10%NaCl + 1%$CaCl_2$ + 1%$MgCl_2$	Not aq. stable	Not aq. stable	30.6

Table 4. 12: Surface tension of each cationic surfactant at varying salinities. The measurements were performed at room temperature, therefore, the surface tension was not measured for solutions that were not aqueous stable at T=25^{o}C.

Oil	Surface Tension (dynes/cm)
Decane	24.3
Mineral Oil	22.1
Crude A	31.3
Crude B	24.8
Crude C	23.0

Table 4. 13: Surface tension of each of the oils at room temperature.

From the bridging coefficient number, it is evident that the bridging coefficient will only be favorable (B<0) for surfactant/gas/oil systems where the surface tension of oil is greater than the surface tension of the surfactant summed with the interfacial tension of the oil and surfactant. As seen in Table 4.13 and Table 4.14, regardless of IFT between oil and surfactant, Crude A is the only oil for which a negative bridging coefficient is feasible. This explains why Crude A has the least destabilizing effect on bulk foam stability for the cationic surfactants studied. To show that only Crude A can result in a favorable bridging coefficient, the IFT values for GC 468 were calculated for all salinities with all three crude oils. The results can be seen in Table 4.15.

GC 468	IFT with Crude A (dynes/cm)	IFT with Crude B (dynes/cm)	IFT with Crude C (dynes/cm)
0% NaCl + 0% $CaCl_2$ + 0% $MgCl_2$	0.38	1.15	0.15
0% NaCl + 1% $CaCl_2$ + 1% $MgCl_2$	0.14	0.12	0.14
1% NaCl + 1% $CaCl_2$ + 1% $MgCl_2$	0.13	0.13	0.12
4% NaCl + 1% $CaCl_2$ + 1% $MgCl_2$	0.11	0.33	0.76
8% NaCl + 1% $CaCl_2$ + 1% $MgCl_2$	0.17	0.14	0.11

Table 4. 14: IFT values for GC 468 at varying salinities with all three crude oils measured at room temperature.

For mineral oil and decane, only one IFT value was measured to determine the order of magnitude of the IFT between surfactant and oil. The IFT between GC 468 and decane is greater than 5 dynes/cm, and the IFT between GC 468 and mineral oil is greater than 10 dynes/cm. The spreading, entering, and bridging coefficients were tested for all GC 468 salinities with all three crude oils. The results are shown in Table 4.16.

GC 468	Crude A S	Crude A E	Crude A B	Crude B S	Crude B E	Crude B B	Crude C S	Crude C E	Crude C B
0	-1.05	-0.28	**-40.9**	7.5	7.8	410.3	5.7	8.0	374.4
0+1+1	-0.20	0.07	**-4.1**	8.3	8.5	457.3	7.3	7.6	410.0
1+1+1	-1.06	-0.80	**-57.3**	5.8	6.1	308.6	6.5	6.7	449.5
4+1+1	0.44	0.67	35.2	8.1	9.6	487.2	7.7	8.4	449.5
8+1+1	-1.3	-0.98	**-70.5**	7.0	7.3	380.8	6.2	6.5	343.6

Table 4. 15: Spreading, entering, and bridging coefficients for GC 468 at varying salinities with all three crude oils. The bolded numbers are favorable bridging coefficients.

As seen in Table 4. 16, the bridging coefficient is favorable for foam stability for GC 468 and Crude A, which was confirmed during bulk foam stability tests. The positive entering coefficients theoretically are not favorable for foam stability. However, Kruglyakov and Vilkova (1999) found that the spreading and entering coefficients are not good criteria for antifoam determining factors. Farajzadeh et al. (2012) suggests that the bridging coefficient is more correct in predicting foam stability than the spreading and entering coefficients.

The bridging, spreading, and entering coefficients were calculated for GC 580 and Crude A. The IFT values for GC 580 at varying salinities with Crude A can be seen in Table 4.17. As seen in the table, the IFT values for Crude A and GC 580 are low, less than 1 dynes/cm, but not ultra-low IFT like the surfactants used in ASP flooding.

GC 580	IFT with Crude A (dynes/cm)
0% NaCl + 0% $CaCl_2$ + 0% $MgCl_2$	0.77
0% NaCl + 1% $CaCl_2$ + 1% $MgCl_2$	0.645
1% NaCl + 1% $CaCl_2$ + 1% $MgCl_2$	0.59
4% NaCl + 1% $CaCl_2$ + 1% $MgCl_2$	0.535

Table 4. 16: IFT values for GC 580 at varying salinities with Crude A.

Even though Crude A, has the highest surface tension and is the most likely to result in a favorable bridging coefficient, the surface tension of GC 580 is larger than the surface tension than Crude A and results in unfavorable bridging coefficients, as seen in Table 4.18. Since Crude B and Crude C have even lower surface tension values than Crude A, the bridging coefficients will be much larger, and therefore, more unfavorable than Crude A. Even though Crude A and GC 580 do not exist in a stable foam system, Crude A has lower bridging coefficients than Crude B and Crude C and is less unstable than Crude B and Crude C. GC 580 with 4% NaCl, 1% $CaCl_2$, and 1% $MgCl_2$ has the lowest bridging coefficient and is less unfavorable than the other formulations. This is also seen during the bulk foam stability tests, where GC 580 with 4% NaCl, 1% $CaCl_2$, and 1% $MgCl_2$ is the most favorable salinity for bulk foam stability.

GC 580	Crude A S	Crude A E	Crude A B
0	4.2	5.8	339.2
0+1+1	8.9	10.2	688.7
1+1+1	7.2	8.4	553.4
4+1+1	3.3	4.3	253.2

Table 4. 17: Spreading, entering, and bridging coefficients for GC 580 and Crude A. No bridging coefficients are favorable, but GC 580 with 4% NaCl, 1% $CaCl_2$, and 1% $MgCl_2$ is the closest to stable.

As with GC 580, the surface tension for CTAB at all salinities is larger than the surface tension for mineral oil, decane, and all three crude oils. Because the surface tension of CTAB is larger than the surface tension of the oils, the bridging coefficient, regardless of the IFT measurements, will be positive, and therefore unfavorable. Since Crude A has the highest surface tension of the oils tested, it will result in the bridging coefficients closest to zero and be the least destabilizing of the oils on the CTAB foam, which was seen during the bulk foam stability tests with oil.

4.1.4 Adsorption

The adsorption of 0.1%, 0.5%, and 1% GC 468, GC 580, CTAB, and AS-40 were determined using batch adsorption experiments.

4.1.4.1 Anionic Surfactant Adsorption

A calibration curve for AS-40 was generated by using HPLC to calculate the area for calibration samples of 0.01 wt%, 0.03 wt%, 0.05 wt%, and 0.1 wt% of AS-40 solutions. The calibration curve can be seen in Figure 4.22.

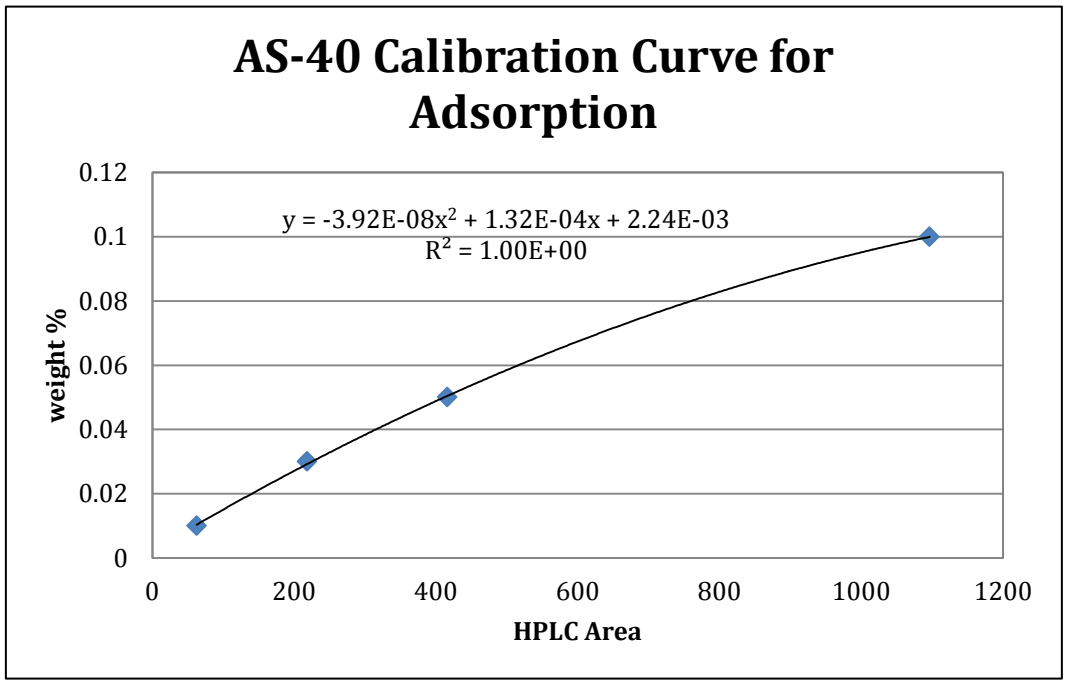

Figure 4. 22: Calibration curve for AS-40 using HPLC.

Batch adsorption experiments were performed on AS-40 samples of 0.1 wt%, 0.25 wt%, and 0.5 wt%, and the HPLC area was 8.8, 308.2, and 842.3, respectively. Using the calibration curve to determine the amount of surfactant remaining and Equation 3.8, it was determined that the adsorption for AS-40 was 0.15, 0.19, and 0.26 mg/g,

respectively. The adsorption of AS-40 shows Langmuir type behavior, increasing adsorption with increasing concentrations until the CMC of the surfactant, at which point the adsorption should remain constant with increases in concentration, which is expected for surfactant adsorption on carbonate reservoirs.

4.1.4.2 Cationic Surfactant Adsorption

Calibration curves for GC 468, GC 580, and CTAB were generated using the titration method discussed in Chapter 3 for cationic adsorption. Calibration samples for GC 468 were generated by measuring UV-vis for 0.001, 0.002, 0.004, 0.006, and 0.008 weight % solutions. The calibration curve for GC 468 can be seen in Figure 4.23.

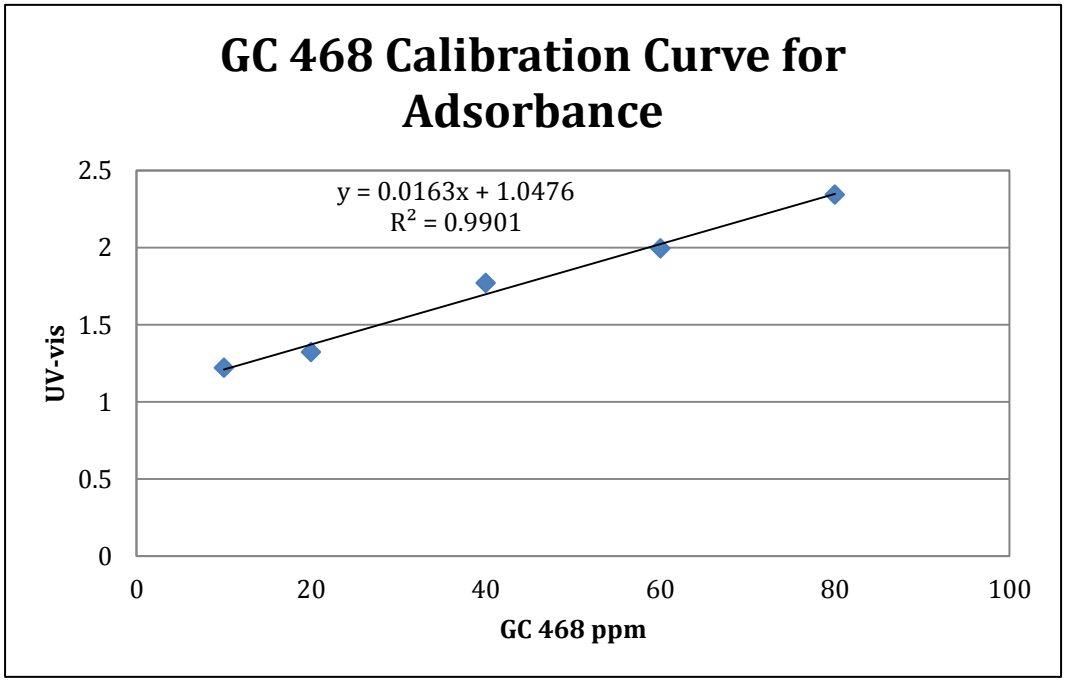

Figure 4. 23: Calibration curve for GC 468 using UV-vis.

After generating the calibration curve, adsorption was measured for GC 468 solutions of 0.1, 0.5, and 1 wt% surfactant; the UV-vis absorbance was 1.09, 1.27, and 1.29, respectively. Using the calibration curve in Figure 4.23 and Equation 3.8, it was determined that the batch adsorption values for GC 468 were 0.034, 0.013, and 0.011 mg/g, respectively. This does not follow Langmuir type adsorption. One reason, the adsorption does not show Langmuir behavior is the adsorption values are extremely low, and error exists in this method.

Adsorption was measured for GC 580 solutions 0.1, 0.5, and 1 wt% of surfactant; the UV-vis adsorbance was 0.4575, 0.43, and 0.4175, respectively. The calibration curve was generated using 0.001, 0.002, 0.004, 0.006, and 0.008 wt% solutions of GC 580. Using the calibration curve in Figure 4.24 and Equation 3.8, it was determined that the batch adsorption values for GC 580 were 0.007, 0.009, and 0.01 mg/g. The adsorption for GC 580 follows Langmuir behavior.

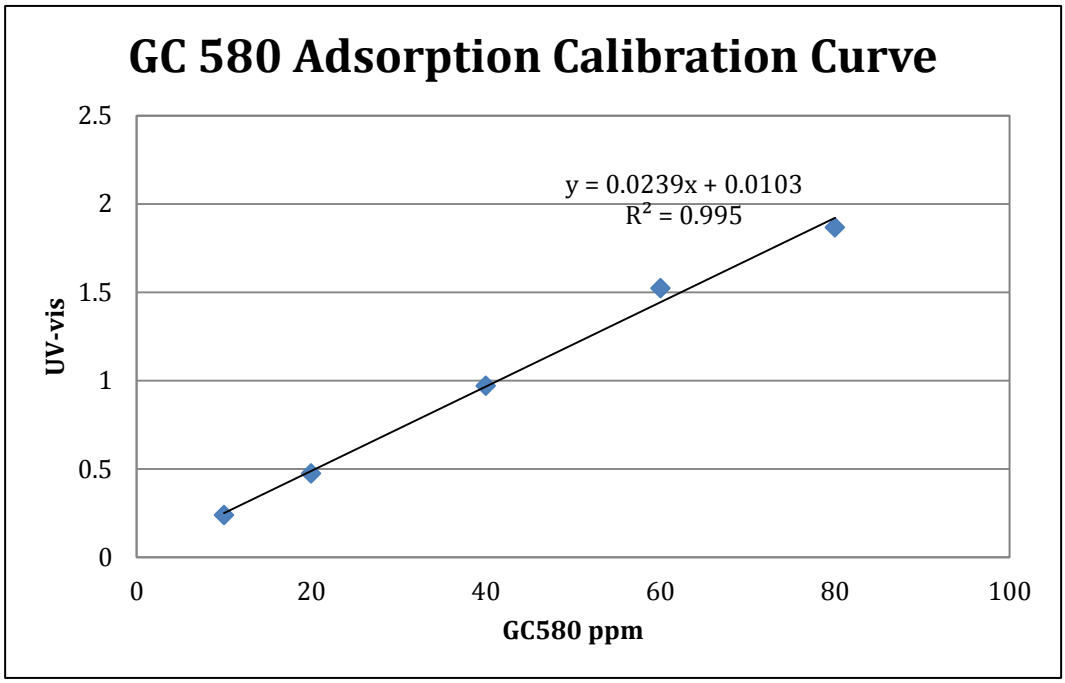

Figure 4. 24: Calibration curve for GC 580 using UV-vis.

Lastly, a calibration curve was generated for CTAB using 0.0005, 0.001, 0.0015, and 0.002 wt% solutions of CTAB to determine CTAB batch adsorption using UV-vis. Batch adsorption was measured for CTAB solutions of 0.1, 0.5, and 1 wt% CTAB; the UV-vis absorbance were 1.29, 1.405, and 1.416, respectively. Using the CTAB calibration curve in Figure 4.25 and Equation 3.8, the adsorption of CTAB on Texas Cream Limestone was determined to be 0.031, 0.019, and 0.018 mg/g, respectively.

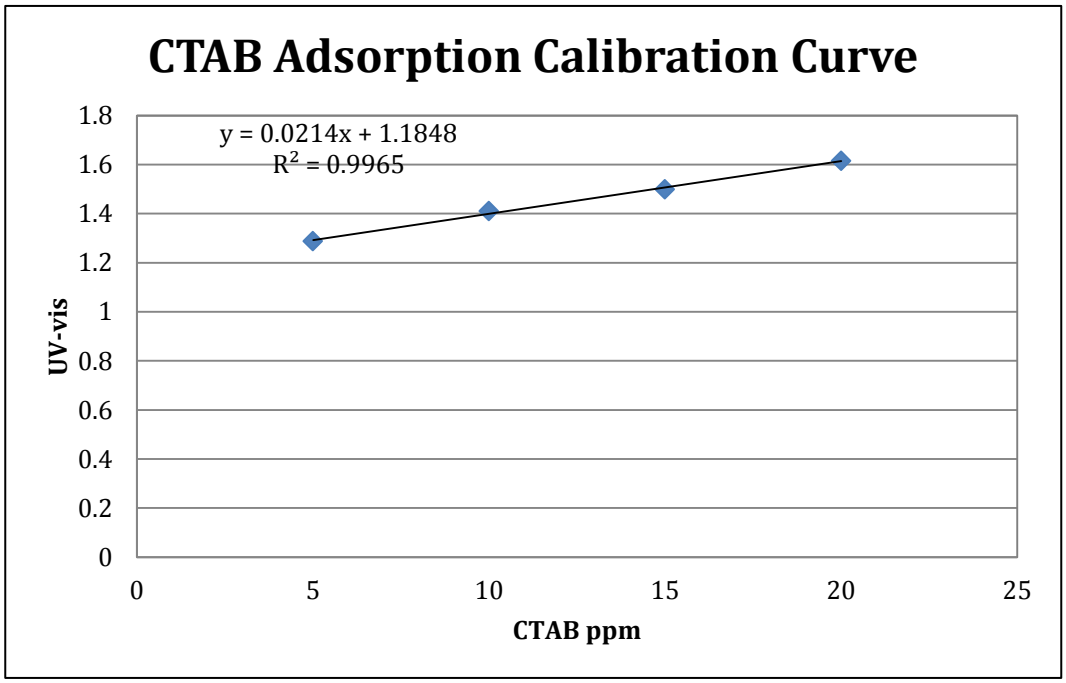

Figure 4. 25: Calibration curve for CTAB using UV-vis.

Table 4.19 contains a summary of the batch adsorption results for each surfactant at three different concentrations. As seen in the table below, the three cationic surfactants had significantly lower adsorption on limestone than anionic surfactant. The anionic surfactant had more than 10 times more adsorption than GC 580 at all the surfactant concentrations tested, and 10 times more adsorption than GC 468 and CTAB at higher surfactant concentrations, 0.5 and 1.0 wt%. These results show that cationic gemini surfactants are much better surfactants to use for carbonate reservoirs. Far less cationic surfactant will be consumed during EOR processes in laboratory and core applications, and they do not require the use of alkali to reduce the amount of surfactant lost to

adsorption, unlike conventional anionic surfactants. This could be particularly useful in applications when the typical alkali, sodium carbonate, is not effective, such as in the presence of anhydrite. Many studies are being conducted to reduce anionic surfactant adsorption in carbonate reservoirs, especially those that contain gypsum and anhydrite, using various alkali materials such as sodium polyacrylate (ShamsiJazeyi, 2013), sodium metaborate, and ammonium hydroxide (Sharma et al, 2014).

	GC 580	GC 468	CTAB	AS-40
0.1 wt%	0.007 mg/g	0.034 mg/g	0.031 mg/g	0.14 mg/g
0.5 wt%	0.009 mg/g	0.013 mg/g	0.019 mg/g	0.19 mg/g
1.0 wt%	0.010 mg/g	0.011 mg/g	0.018 mg/g	0.26 mg/g

Table 4. 18: Summary of batch adsorption studies for each of the four surfactants studied at three different concentrations. All batch adsorption studies were done at 60^{o}C and at the injection brine salinity.

Even though the use of alkalis reduce the amount of anionic surfactant adsorption in carbonate reservoirs during ASP floods, they would not be effective to use during CO_2 foam floods. Because the CO_2 would decrease the pH to below 6, surfactant adsorption would increase wherever CO_2 sweeps the reservoir, nulling the beneficial effects of alkali.

4.1.4.5 Wettability Alteration

Preliminary wettability alteration experiments were performed on calcite chips. Both cationic gemini surfactants were tested for all three crude oils. Figure 4.26a shows the calcite chip aged with Crude A immersed in 0.5% GC 468 aqueous solution with 1% $CaCl_2$ and 1% $MgCl_2$. Figure 4.26b shows the calcite chip aged with Crude A in 0.5% GC 580 aqueous solution with 2% NaCl, 0.5% $CaCl_2$, and 0.5% $MgCl_2$. Figure 4.27a shows the calcite chip aged with Crude B in 0.5% GC 468 with 1% $CaCl_2$ and 1% $MgCl_2$. Figure 4.27b shows the calcite chip aged with Crude B in 0.5% GC 580 with 2% NaCl, 0.5% $CaCl_2$, and 0.5% $MgCl_2$. Figure 4.28a shows the calcite chip aged with Crude C in 0.5% GC 468 with 1% $CaCl_2$ and 1% $MgCl_2$. Figure 4.28b shows the calcite chip aged with Crude C in 0.5% GC 580 with 2% NaCl, 0.5% $CaCl_2$, and 0.5% $MgCl_2$.

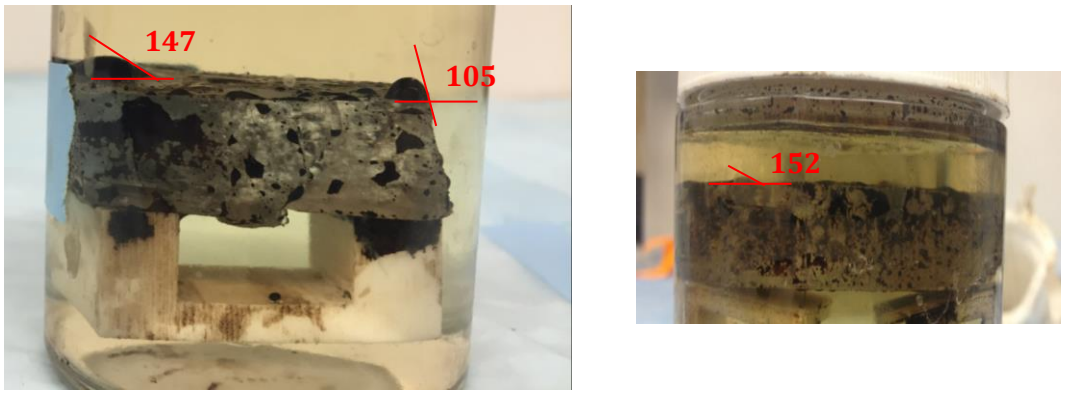

Figure 4. 26: a) Calcite chip aged in Crude A in GC 468, b) Calcite chip aged in Crude A in GC 580.

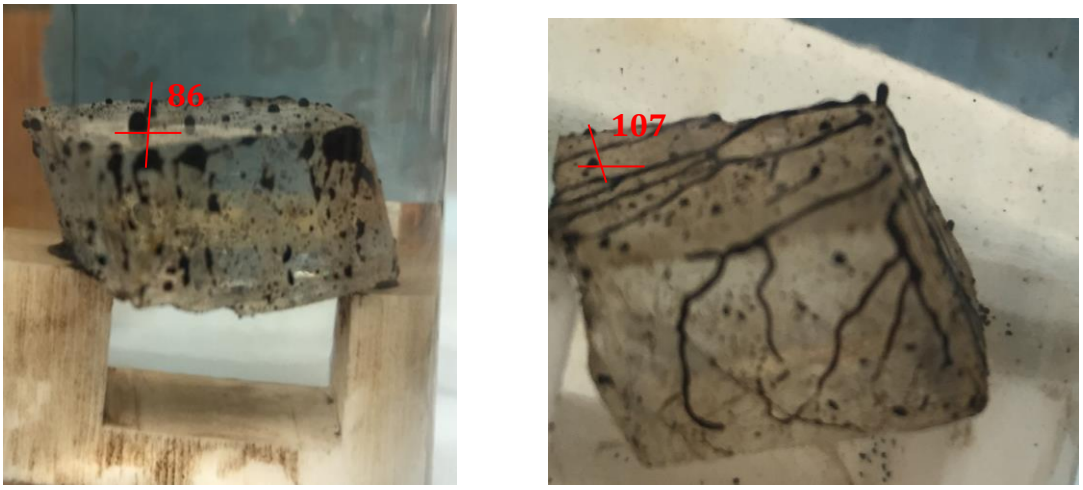

Figure 4. 27: a) Calcite chip aged in Crude B in GC 468. b) Calcite chip aged in Crude B in GC 580.

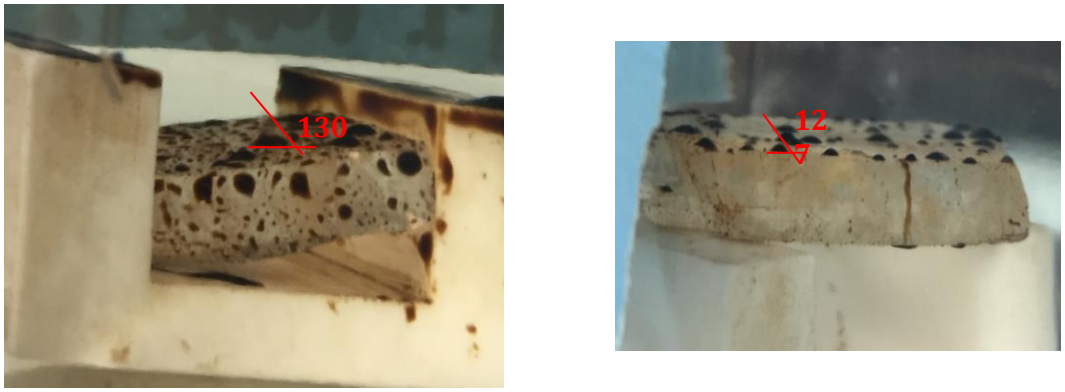

Figure 4. 28: a) Calcite chip aged in Crude C in GC 468, b) Calcite chip aged in Crude C in GC 580.

For Crude A, neither GC 580 nor GC 468 are capable of reducing the oil contact angle below 90^o. GC 468, however, results in a lower contact angle than GC 580. Crude B in GC 468 results in a contact angle less than 90^o. Crude B in GC 580, still results in a contact angle greater than 90^o. Like with Crude A, neither GC 468 nor GC 580 is able to reduce the contact angle to below 90^o. With Crude C, unlike Crude A and B, GC 580 results in the lower contact angle; however, Crude C in both GC 468 and GC 580 has contact angles greater than 125^o.

4.2 COREFLOODS IN THE ABSENCE OF OIL

Corefloods in the absence of oil were performed using varying concentrations of GC 468, GC 580, and CTAB. The foam quality was also varied for the three cationic surfactants.

4.2.1 GC 468

Core floods in the absence of oil were performed to determine if GC 468 co-injected with CO_2 would form foam in porous media and to determine the effects of surfactant concentration and foam quality on foam strength. The core properties for the experiments done in the absence of oil can be seen in Table 4.20. The experimental conditions are listed in Table 4.21.

Texas Cream Properties	
Length (in)	9
Diameter (in)	1.48
Porosity (%)	27%
Permeability	38 mD

Table 4. 19: Texas Cream Limestone properties for coreflood experiments performed in the absence of oil.

Experimental Conditions	
Temperature	60^{o}C
Back Pressure	~100 psi
Total Flow Rate	4 ft/day

Table 4. 20: Experimental conditions of corefloods performed in the absence of oil.

Brine was injected into the core at 4 ft/day until the pressure drop reached a constant pressure at 2.7 psi. The injection fluid was switched to CO_2. CO_2 was injected at 4 ft/day until the pressure drop reached a constant pressure of 2 psi. CO_2 and brine were co-injected at 90% quality at 4 ft/day to give a baseline for CO_2 and surfactant co-injection. The brine and CO_2 co-injected reached a steady-state pressure of 3.5 psi.

One pore volume of 0.1% GC 468 with 1% $CaCl_2$ and 1% $MgCl_2$ was injected to satisfy adsorption. CO_2 and the 0.1% surfactant solution were co-injected at 90% quality at 4 ft/day until the pressure drop stabilized around 7.2 psi. The pressure drop during a co-injection of surfactant and CO_2 was double the pressure drop during the co-injection

of brine and CO_2 at the same volume ratio, indicating that foam is forming, increasing the pressure drop across the core. The formation of foam was confirmed using the visual cell at the inlet of the core.

One pore volume of 0.25% GC 468 with 1% $CaCl_2$ and 1% $MgCl_2$ was injected into the core to satisfy adsorption. The 0.25% surfactant solution was co-injected with CO_2 at 90% quality until the pressure stabilized around 7.4 psi. This pressure drop is essentially the same pressure drop as seen with 0.1% surfactant solution.

One pore volume of 0.5 % GC 468 with 1% $CaCl_2$ and 1% $MgCl_2$ was injected into the core to satisfy adsorption. The 0.5% solution was then co-injected with CO_2 at 90% quality. Once again, the pressure stabilized around 7.0 psi, suggesting that there is little to no effect of GC 468 concentration on foam strength in the absence of oil. The results of these experiments in the absence of oil can be seen in Figure 4.28. This is different than typical literature results where increasing surfactant concentration results in increased foam strength. Perhaps not a large enough range of surfactant concentrations was studied to see an effect of surfactant concentration.

The effect of quality on foam strength was also tested in the absence of oil in the same core as listed in the table above. The ratio of 0.5% GC 468 with 1% $CaCl_2$ and 1% $MgCl_2$ and CO_2 was varied from 70% to 95% in increments of 5%. The effects of quality on foam strength can be seen in Figure 4.29. As seen in the figure, when foam was injected at 70% quality, the pressure drop reached steady state around 9.0 psi. When the quality was increased to 75%, the steady-state pressure drop increased to approximately 11.8 psi. The quality was increased to 80%, and the steady-state pressure increased to 14.5 psi. The steady-state pressure drop across the core continued to increase as the foam quality was increased to 85% quality. At 85% quality, the foam strength reached a

maximum, as the pressure drop reached 16 psi. After 85% quality, however, the pressure drop decreased with further increases in the quality. At 90% quality, the pressure drop stabilized around 8.4 psi. When the quality was further increased to 95%, the steady-state pressure drop decreased further to 7.0 psi. This apparent optimum quality for foam strength is also seen in literature results (Zeng et al., 2015. Because the foam was the strongest at 85% quality, the formulation of 0.5% GC 468 with 1% $CaCl_2$ and 1% $MgCl_2$ co-injected with CO_2 at 85% quality for foam corefloods performed in the presence of oil.

The core was cleaned by injecting 8 pore volumes of 0.5% NaCl at 5 ft/day, followed by 10 pore volumes of methanol mixed with 0.5% NaCl at equal volume ratios, followed by 10 pore volumes of 0.5% NaCl. The core was dried in the oven overnight before vacuuming and the brine saturation for the next set of coreflood experiments.

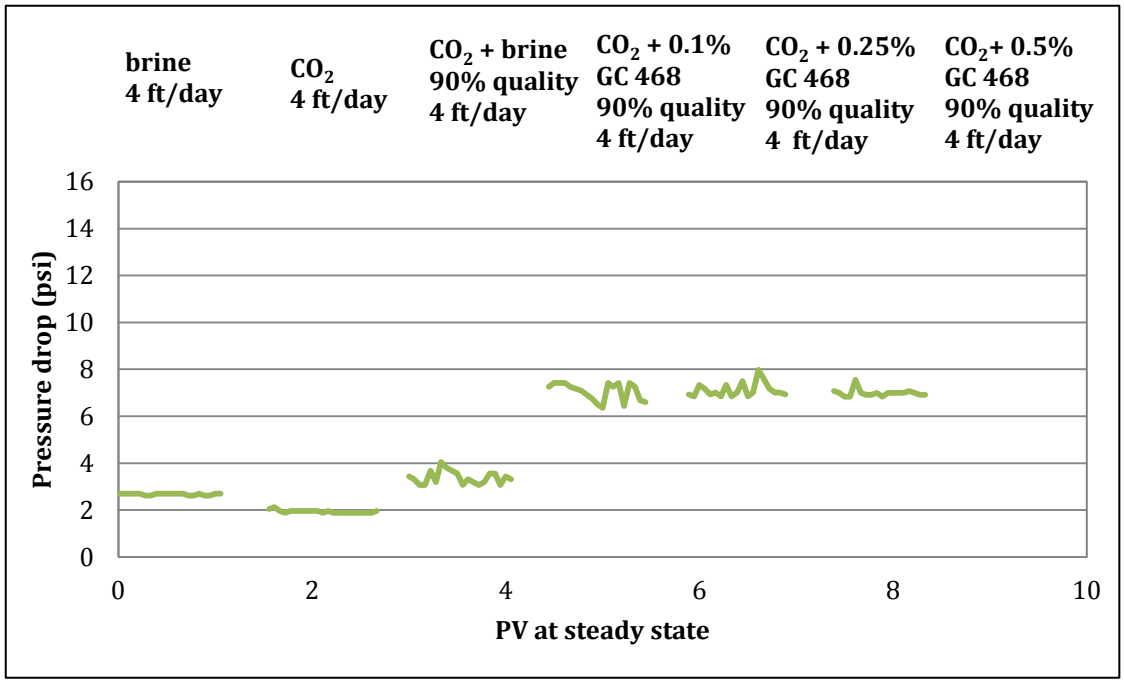

Figure 4. 29: Core flood experiment in the absence of oil with GC 468 with 1% $CaCl_2$ and 1% $MgCl_2$. The flow rate was 4 ft/day. The steady state pressure drop is plotted. This experiment looks at the effect of surfactant concentration on pressure drop during CO_2 and surfactant co-injection at 90% quality.

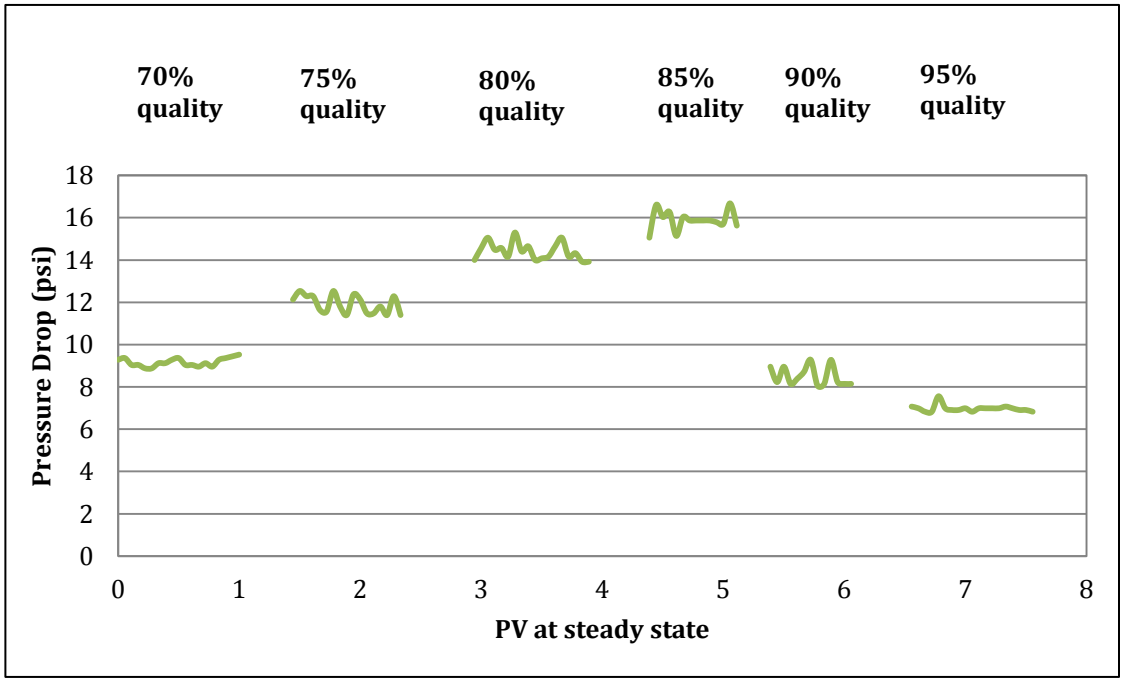

Figure 4. 30: Core flood experiment in the absence of oil with 0.5% GC 468 with 1%$CaCl_2$ and 1%$MgCl_2$. The flow rate was 4 ft/day. The pressure drop plotted is the pressure drop at the steady state. This experiment looks at the effect of the ratio of CO_2 to surfactant solution on the pressure drop across the core.

4.2.2 GC 580

The effect of surfactant concentration on foam strength was determined by changing the surfactant concentration co-injected with CO_2 in porous media with no oil present. Another objective of these experiments in the absence of oil was to show that the surfactant and CO_2 were forming foam. To show foam formation, a visual cell was placed after the sandpack, before the core. In addition, the pressure drop of CO_2 co-injected with brine was compared to the pressure drop of CO_2 co-injected with surfactant solution of varying surfactants. If foam could be seen in the porous media and the pressure drop of the CO_2 and surfactant co-injection was higher than the CO_2 and brine co-injection, it

was assumed that foam was in the porous media. The properties of the core and the experimental conditions for this experiment are in Table 4. 20 and Table 4.21.

Brine was injected at 4 ft/day until the pressure reached steady-state for one pore volume. The steady-state pressure for brine was approximately 2.6 psi. Since the pressure drop for brine was the same as the previous brine injection, it can be assumed that the core was completely cleaned and all previous surfactant had been removed from the core. The injection fluid was switched to CO_2 at an injection pressure of 100 psi set by a back pressure regulator. After the pressure reached steady-state for 1 pore volume at 1.4 psi, brine and CO_2 at 90% quality was injected. The steady state pressure for brine and CO_2 co-injected at 90% quality is 4.8 psi. The co-injection pressure of brine and CO_2 is higher than that of either brine or CO_2 because the relative permeabilities of CO_2 and of brine decrease with the introduction of a second phase.

One pore volume of 0.1% GC 580 solution was injected to satisfy adsorption. 0.1% GC 580 with 2%NaCl, 0.5% $CaCl_2$, and 0.5% $MgCl_2$ was co-injected with CO_2 at 90% quality until the pressure reached steady state at 4.9 psi. Since there is little pressure increase between the CO_2 and brine co-injection and the CO_2 and 0.1% GC 580 co-injection, it appears that no foam forms in porous media with only 0.1% surfactant solution.

One pore volume of 0.25% GC 580 was injected at 4 ft/day to satisfy adsorption. Then, CO_2 and 0.25% GC 580 were co-injected at 90% quality until the pressure reached steady state at 8.6 psi. The pressure drop of CO_2 and 0.25% surfactant was almost double the CO_2 and brine co-injection, indicating that foam was most likely present in the core. Foam could also be seen in the visual cell at the inlet of the core, confirming the presence of foam.

The last surfactant concentration tested was 0.5% GC 580. After one pore volume of 0.5% GC 580 was injected to satisfy adsorption, CO_2 and 0.5% GC 580 were co-injected at 90% quality until steady state was reached at 11.3 psi. The results from these experiments can be seen in Figure 4.30. As seen in the figure, the pressure drop across the core increases with increasing surfactant concentration. This is consistent with Apaydin and Kovscek (2000) who found that decreasing surfactant concentration results in an increase in gas mobility, decrease in displacement efficiency, and decrease in foam strength.

Tests were also done to determine the effect of foam quality on the formation of foam in porous media. For these experiments, the co-injection of CO_2 and 0.5% GC 580 at 4 ft/day was varied from 70% quality to 95% quality in increments of 5%. The results of these experiments can be seen in Figure 4.31.

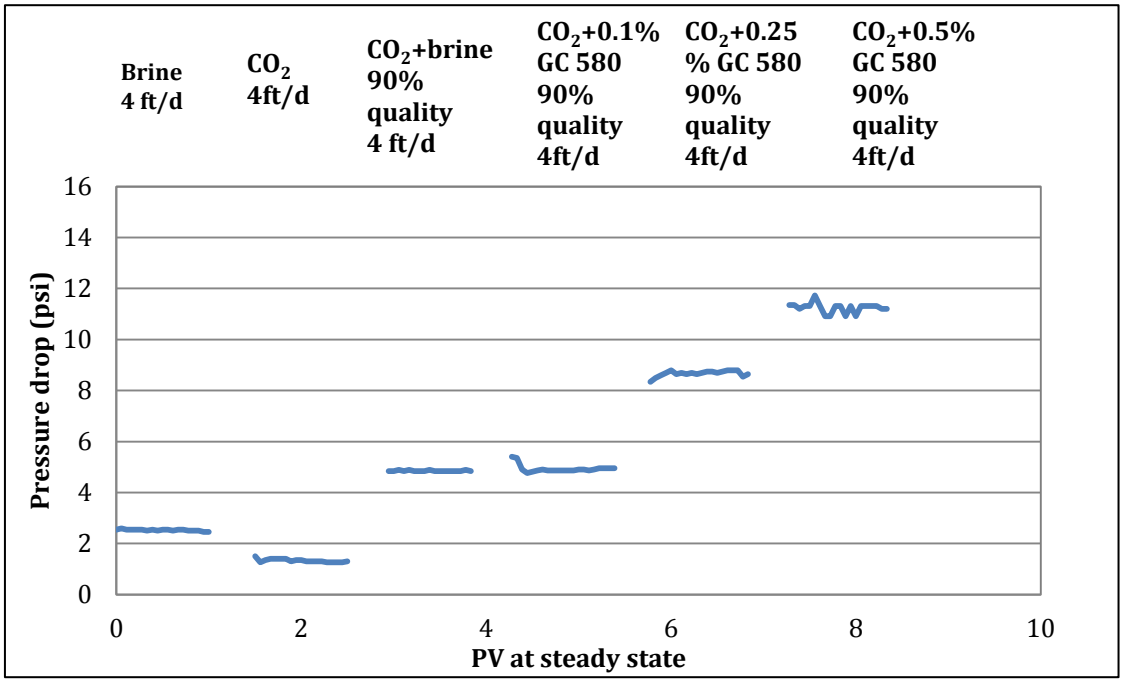

Figure 4. 31: Core flood experiment in the absence of oil with GC 580 with 4%NaCl, 1%$CaCl_2$, and 1%$MgCl_2$. The flow rate was 4 ft/day. The steady state pressure drop is plotted. This experiment looks at the effect of surfactant concentration on pressure drop during CO_2 and surfactant co-injection.

As seen in the figure, the pressure drop at 70% quality reaches steady state at 4.7 psi, the same pressure as CO_2 and brine co-injection, indicating that very little, if any, foam is forming at this quality. The quality was increased to 75%, where it reached a steady-state pressure of 4.9 psi, also suggesting that very little, if any foam, is formed at 75% quality. When the quality is increased to 80%, however, the steady state pressure increases to 11.4 psi, suggesting a stronger foam formation. This was verified by seeing foam in the visual cell at the core inlet. When the quality was increased to 85%, the steady state pressure increased to 12.4 psi. The quality was increased to 90%; instead of seeing another increase in steady state pressure as expected, the pressure drop decreased

to 11.3 psi. The last quality tested was 95% quality. The steady state pressure for 95% quality was dramatically reduced from that of 90% with a pressure of 5.6 psi. The pressure drop at 95% was similar to the pressure drop at 70% and 75% quality, indicating an optimum foam quality to produce strong foam. A similar trend of increasing pressure drop for increasing quality before reaching an optimum quality after which a decrease in pressure drop is seen with increasing quality is found in many studies. Zeng et al. (2015) found that the pressure drop for foam formed from AOS C14-16 and CO_2 increased with increasing pressure drop until 80% quality then proceeded to decrease with an increase in quality. For GC 580, the strongest foam was formed at 85% quality; therefore, for foam floods in the presence of oil, a quality of 85% was selected. The core was cleaned by the same method as described in 4.1.5.1.

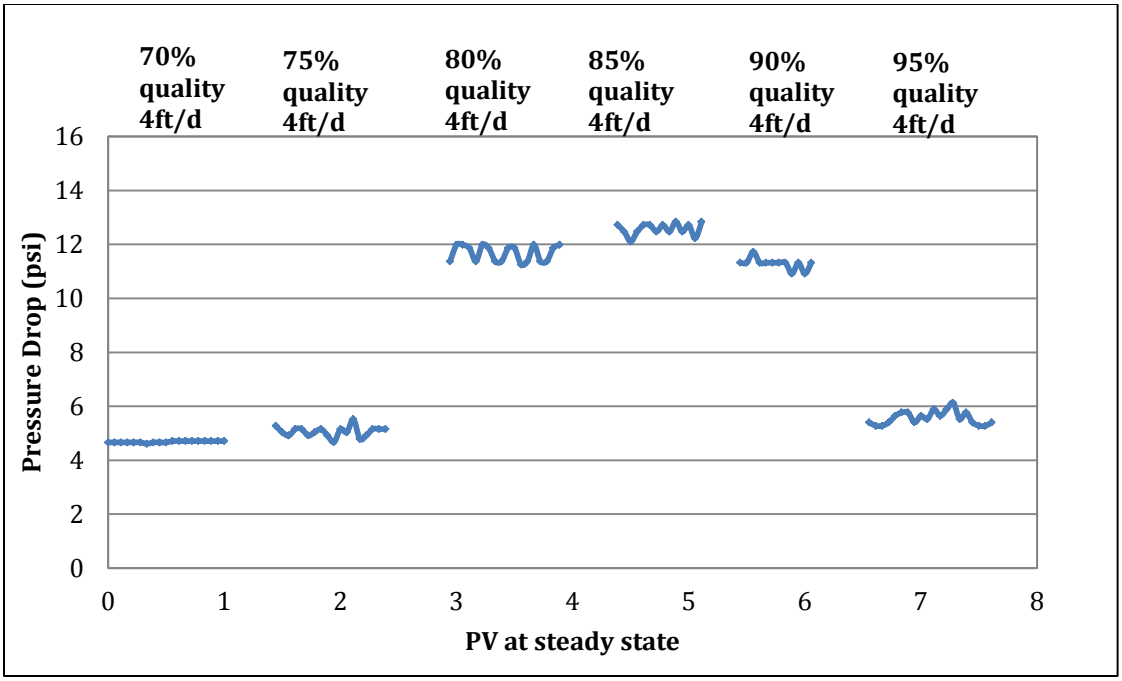

Figure 4. 32: Core flood experiment in the absence of oil with 0.5% GC 580 with 4%NaCl, 1%$CaCl_2$, and 1%$MgCl_2$. The flow rate was 4 ft/day. The steady state pressure drop is plotted. This experiment looks at the effect of ratio of CO_2 to surfactant during co-injection on pressure drop.

4.2.3 CTAB

Corefloods in the absence of oil were performed with CTAB to compare the foam strength of this conventional cationic surfactant to the two novel cationic gemini surfactants. As with the two cationic gemini surfactants, a series of injections at 4 ft/day were performed. The core properties are listed in Table 4.20, and the experimental conditions are listed in Table 4.21. Brine was injected at 4 ft/day and reached a steady-state pressure of 2.7 psi, the same pressure as the two prior water floods, indicating that the core had been completely cleaned. CO_2 was then injected at 4 ft/day and resulted in a steady-state pressure drop of 1.3 psi, similar to the other two CO_2 injections. When CO_2 and brine were co-injected at 90% quality, the pressure stabilized around 4.0 psi, in

between the other two brine-CO_2 injections. One pore volume of a solution containing 0.1% CTAB with 4% NaCl, 1% $CaCl_2$, and 1% $MgCl_2$ was injected to satisfy adsorption. The surfactant solution was co-injected with CO_2, and the pressure reached steady-state around 7.0 psi. This is the same pressure drop as seen with 0.1% GC 468 and 2 psi higher than the pressure drop seen with 0.1% GC 580. At low surfactant concentrations, the foam strength of GC 468 is comparable to a conventional surfactant CTAB.

One pore volume of 0.25% CTAB solution with 4% NaCl, 1% $CaCl_2$, and 1% $MgCl_2$ was injected to satisfy adsorption. The 0.25% surfactant solution was co-injected with CO_2 at 90% quality at 4 ft/day. Instead of seeing an increase in pressure drop as seen when the concentration of GC 468 and GC 580 were increased, the pressure drop of 0.25% CTAB foam was decreased to 5.0 psi. The pressure drop for 0.25% CTAB co-injected with CO_2 at 90% quality was lower than the pressure drop at the same surfactant concentration of both GC 468 and GC 580.

Lastly, the surfactant solution was increased to 0.5% CTAB with 4% NaCl, 1% $CaCl_2$, and 1% $MgCl_2$. After one pore volume of surfactant solution was injected, 0.5% CTAB with 4% NaCl, 1% $CaCl_2$, and 1% $MgCl_2$ was co-injected with CO_2 at 90% quality. Once again, the pressure drop decreased to 3.8 psi. The pressure drop for the 0.5% foam was similar to the pressure drop of brine and CO_2 co-injected at 90% quality, indicating CTAB does not form strong foam in porous at 0.5% surfactant concentration. This trend of decreasing pressure drop with increasing surfactant concentration has been seen in literature. Tsau and Grigg (1997) found that some commercial surfactants reach an optimum foam stability near CMC. Above CMC, some surfactants show a decrease in foam stability. The effects of surfactant concentration on foam strength for each cationic surfactant are shown in Figure 4.33. As seen in the figure, the two cationic gemini

surfactants may be better at forming foam in porous media than the conventional cationic surfactant CTAB.

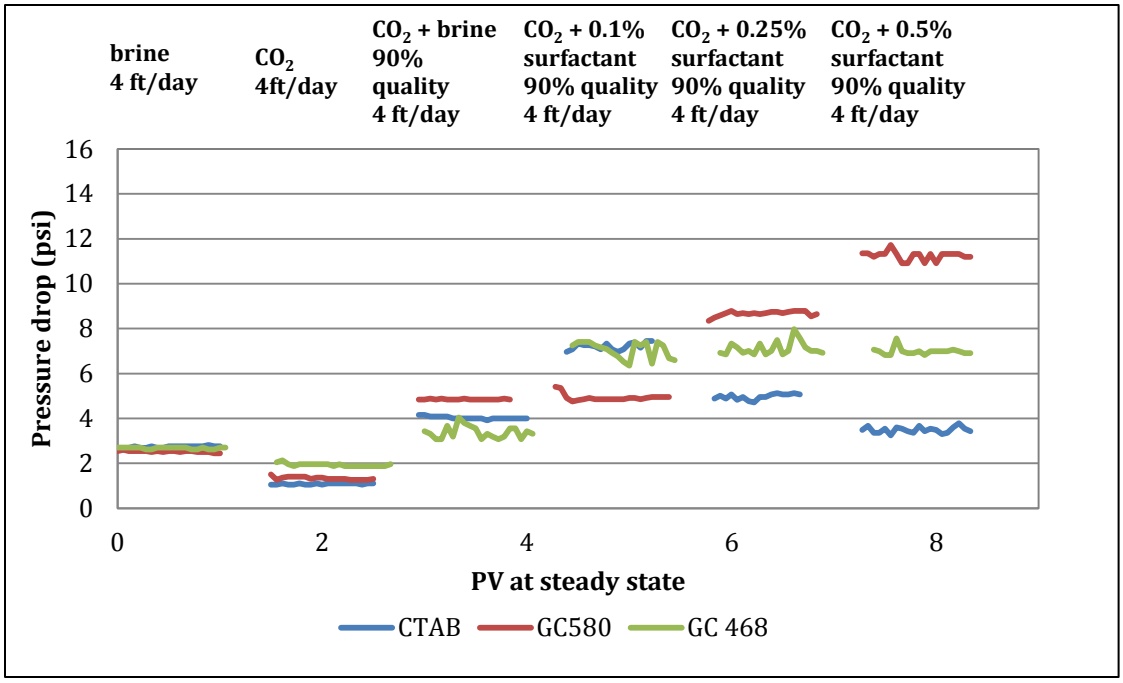

Figure 4. 33: Core flood experiment in the absence of oil with surfactants in 4% NaCl, 1% $CaCl_2$, and 1% $MgCl_2$. The flow rate was 4 ft/day. The pressure drop plotted is the pressure drop at the steady state. CO_2 and surfactant solution are co-injected at 90% quality. CTAB is compared to the two cationic gemini surfactants, GC 468 and GC 580 at different concentrations

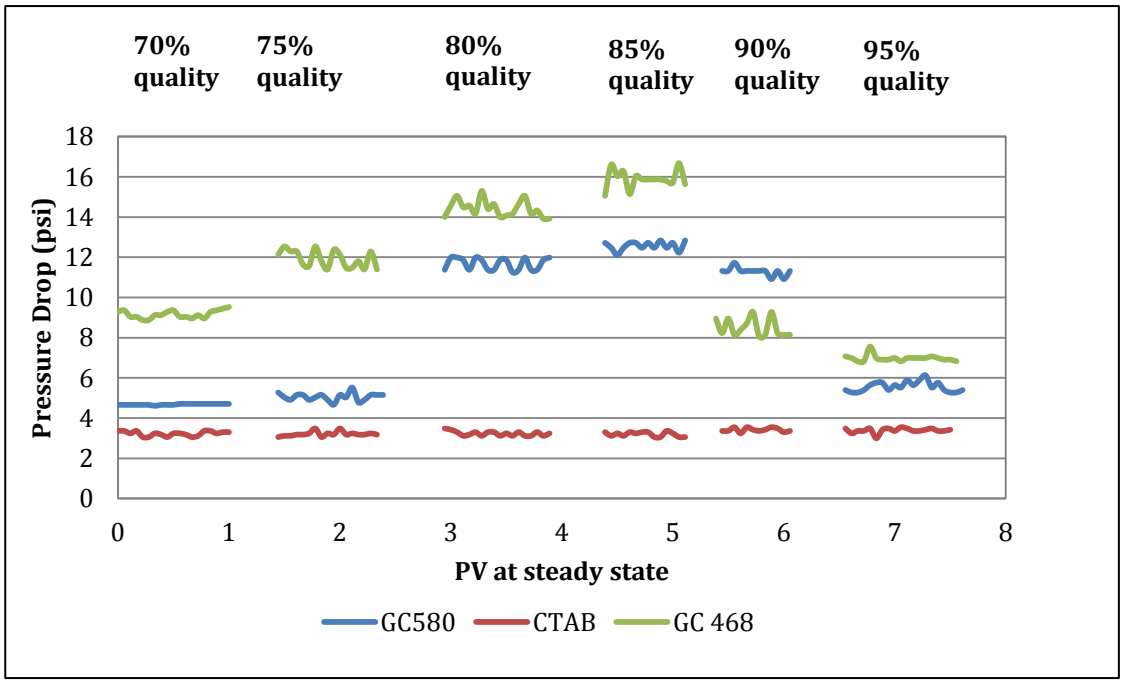

Figure 4. 34: Core flood experiment in the absence of oil with 0.5% surfactant with 4% NaCl, 1%$CaCl_2$, and 1%$MgCl_2$. The flow rate was 4 ft/day. The pressure drop plotted is at the steady state. This experiment looks at the effect of ratio of CO_2 to surfactant solution during co-injection on pressure drop. CTAB is compared to the two cationic gemini surfactants, GC 468 and GC 580.

The effect of quality on foam strength for CTAB was also tested and compared to the two gemini surfactants, as seen in Figure 4.34. The quality was varied from 70% to 95% in increments of 5%. The surfactant solution contained 0.5% CTAB with 4% NaCl, 1% $CaCl_2$, and 1% $MgCl_2$. As seen in the figure, the pressure drop did not change with changes in quality. Most likely, this is because no foam was forming with the 0.5% surfactant solution. To see the effects of quality on CTAB foam strength, a concentration closer to CMC should have been used. However, for these parameters, the novel cationic geminis have better foam formation in porous media.

4.2.4 Mobility Reduction Factor

The pressure drops from the corefloods in the absence of oil with GC 468, GC 580, and CTAB were converted to a mobility reduction factor, MRF, using Equation 4.4. The mobility reduction factor is used in place of a foam viscosity because the differences in pressure drops may be a result of changes in relative permeability, as well as changes in foam viscosity.

$$MRF = \frac{\Delta P_{foam}}{\Delta P_{baseline}}. \tag{4.4}$$

Figure 4.35 shows the mobility reduction for GC 468, GC 580, and CTAB at varying surfactant concentrations: 0.1%, 0.25%, and 0.5% surfactant. As seen in the figure, GC 468 has a higher mobility reduction factor than CTAB at all three concentrations tested. GC 580 also has a higher mobility reduction factor than CTAB at 0.25% and 0.5% surfactant concentrations. The cationic gemini surfactants will be more effective at reducing the mobility ratio and increasing the sweep efficiency of the foam in porous media.

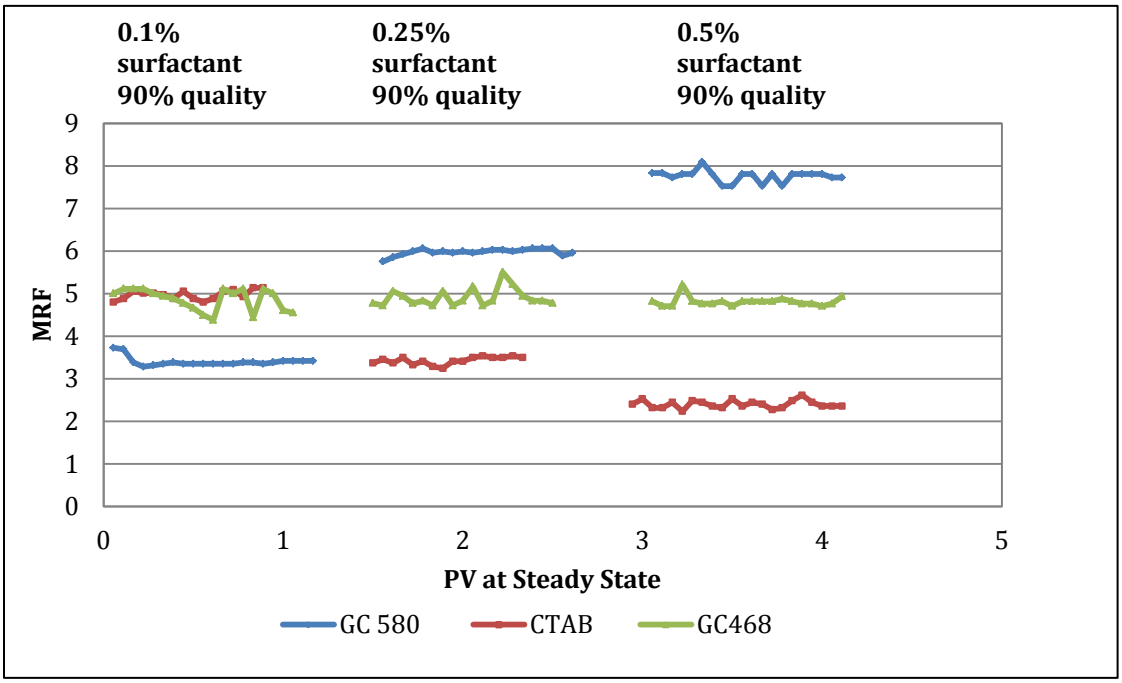

Figure 4. 35: The mobility reduction factor is compared for all three cationic surfactants. The effect of surfactant concentration is also shown.

The mobility reduction factor was also calculated at varying foam qualities for each of the three cationic surfactants. These results are shown in Figure 4.36. As seen in the figure, the two novel cationic gemini have higher mobility reduction factors than CTAB at all foam qualities. Both GC 468 and GC 580 have the highest mobility reduction factor at 85% quality; therefore, 85% quality should yield the highest sweep efficiency during coreflood experiments with oil.

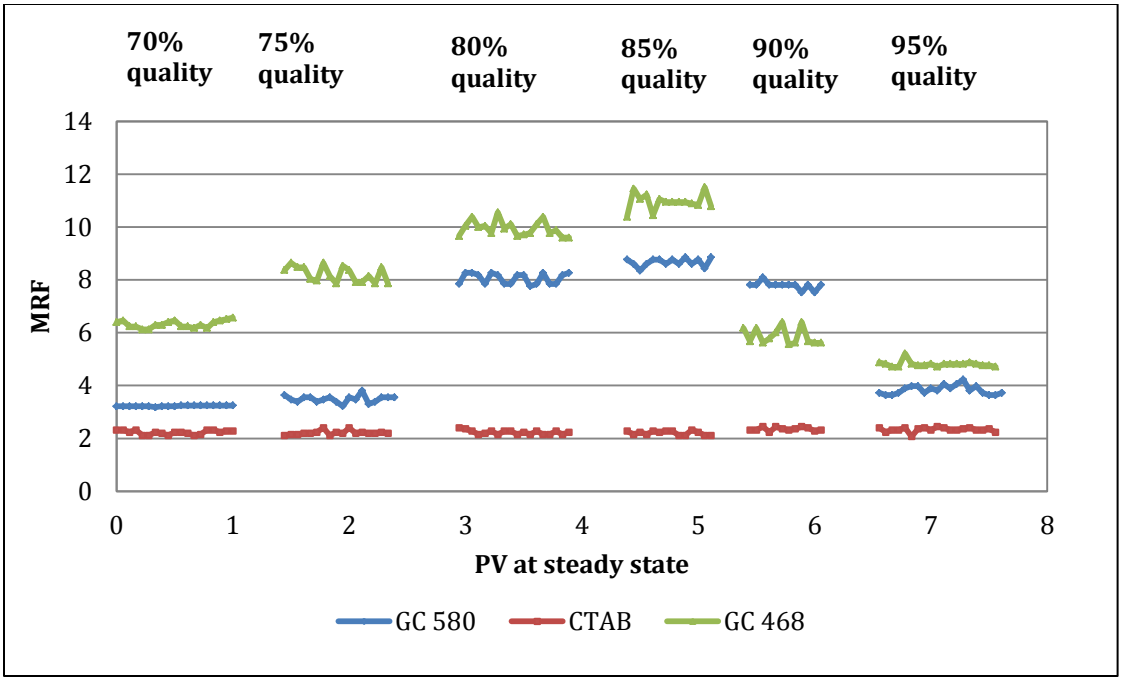

Figure 4. 36: The mobility reduction factor is compared for all three cationic surfactants. The effect of CO_2 and surfactant ratio is also shown.

4.3 COREFLOODS IN THE PRESENCE OF OIL

A series of corefloods in the presence of oil were performed to test the cationic gemini surfactants as potential surfactants for enhanced oil recovery using CO_2-foam. GC 468 and GC 580 were both used for water-wet limestones saturated with a mineral oil. They also were used for water-wet limestones saturated with Crude A, diluted to 10 cP. Lastly, GC 468 was used for an oil-wet limestone saturated with Crude A, at 100 cP.

4.3.1 Coreflood 1: GC 468 with Mineral Oil (Water wet)

A Texas Cream limestone was saturated with mineral oil to ensure the core was water-wet. The core properties are listed in Table 4.22, and the experimental conditions are listed in Table 4.23.

Coreflood 1: Core Properties	
Length	1.48 in
Diameter	11 in
Porosity	28%
Brine Permeability	20.5 mD
Initial Oil Saturation	77.3%

Table 4. 21: Core properties for Coreflood 1.

Coreflood 1: Experimental Conditions	
Temperature	60^{o}C
Back Pressure	~100 psi
Oil viscosity (T=60^{o}C)	11 cP
Foam quality	86%
Flow Rate	1 ft/day

Table 4. 22: Experimental conditions for Coreflood 1.

Table 4.24 shows a summary of the coreflood results. Figure 4.37 shows the oil recovery and pressure drop as a function of pore volumes injected. As seen in the figure, the water flood at 1 ft/day recovered 58.6% of OOIP. The waterflood rate was increased to 5 ft/day, and no additional oil was recovered. One pore volume of 0.5% GC 468 with 1% $CaCl_2$ and 1% $MgCl_2$ was injected to satisfy adsorption. As seen in the figure and results table, no additional oil was recovered during the surfactant flood because mineral oil is inactive and the surface tension between surfactant and mineral oil is over 3

dynes/cm. Surfactant and CO_2 were co-injected at 86% quality and 1 ft/day. After almost one pore volume of foam injection, additional oil recovery was seen. After three pore volumes of foam injection, an additional 15.9% OOIP was recovered.

Figure 4.38 shows the oil, water, and gas cuts as a function of pore volumes injected. The gas cut was calculated by measuring the volumetric flow rate at atmospheric pressure, converting to 100 psi, and dividing by the total flow rate of oil, water, and gas. As seen in the figure, water break through occurred around 0.35 PV. Once the foam flood began, it took 0.42 PV of foam injection before gas breakthrough was seen. The addition of surfactant greatly slowed the breakthrough time of CO_2. Even after gas breakthrough, more oil recovery still occurred for another 2 PV of foam injection, showing that the foam was sweeping previously unswept regions of the core. Since the pressure drop during the foam flood is less than the pressure drop during the water and surfactant floods, it appears that oil destabilizes the foam upon entering the core.

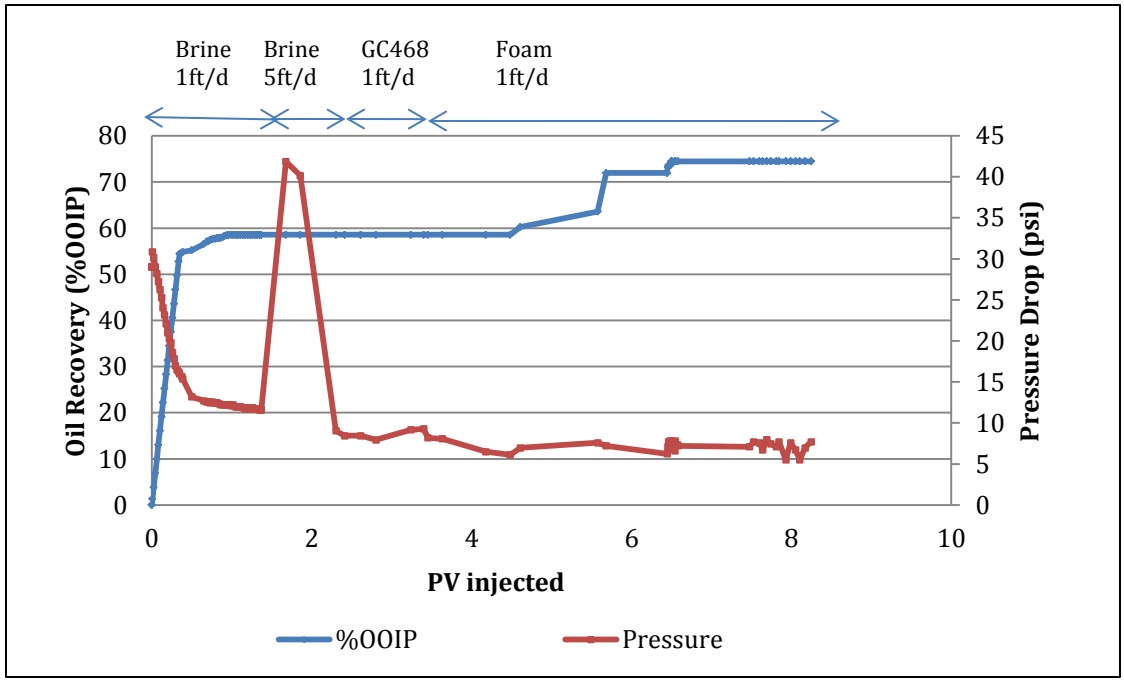

Figure 4. 37: The pressure drop and oil recovery are shown as a function of pore volumes injected for Coreflood 1. Brine is injected at 1 ft/day, followed by brine injection at 5 ft/day, surfactant injection at 1 ft/day, and finally a foam injection at 86% quality at 1 ft/day.

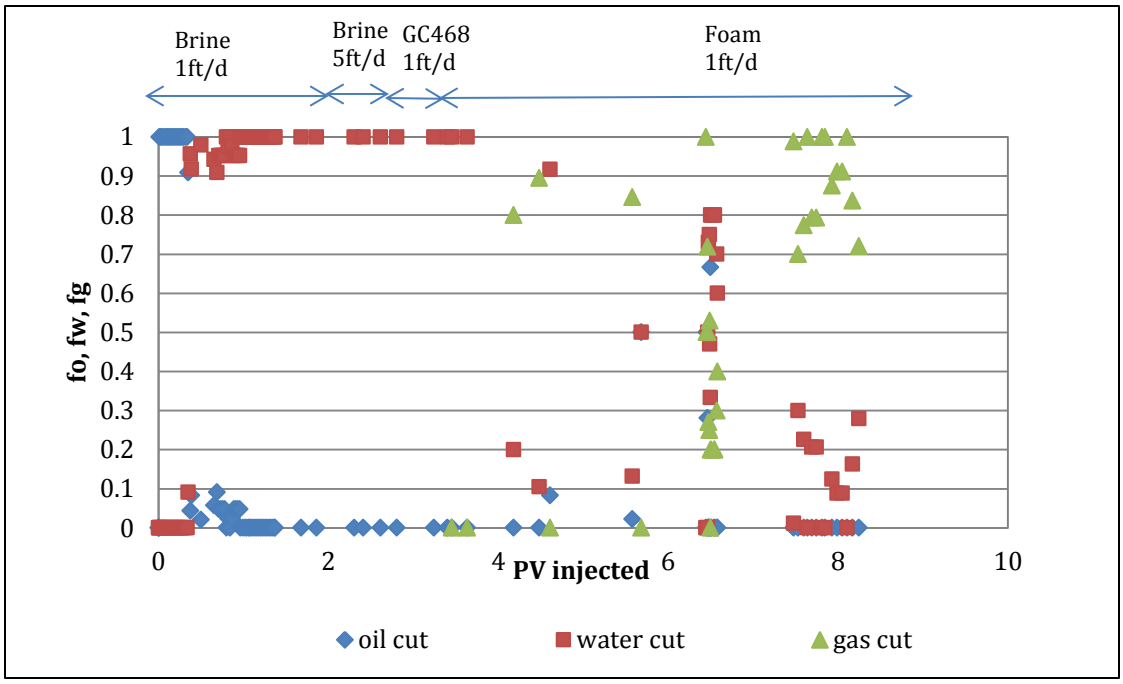

Figure 4. 38: The oil, water, and gas cuts during Coreflood 1.

Coreflood 1: Summary of Results		
Water flood 1 ft/day	1.4 PV	58.6% OOIP
Water flood 5 ft/day	1 PV	0% OOIP
0.5% GC 468	1 PV	0% OOIP
86% quality foam flood	4.8 PV	15.9% OOIP
	Total oil recovery	74.5% OOIP74.5%

Table 4. 23: Summary of oil recovery during Coreflood 1.

4.3.2 Coreflood 2: GC 468 with Crude A (Water Wet)

A second coreflood was performed on a Texas Cream Limestone core saturated with Crude A. The core was not aged, so the core was water wet. The core properties are listed in Table 4. 25 and the experimental conditions are listed in Table 4.26.

Coreflood 2: Core Properties	
Length	1.475 in
Diameter	11.75 in
Porosity	28.6%
Brine Permeability	32.5 mD
Initial Oil Saturation	47 %

Table 4. 24: Texas Cream Limestone properties for Coreflood 2.

Core Flood 2: Experimental Conditions	
Temperature	60^{o}C
Back Pressure	~100 psi
Oil viscosity (T=60^{o}C)	7 cP
Foam quality	86%
Flow Rate	1 ft/day

Table 4. 25: Experimental conditions for Coreflood 2.

As with Coreflood 1, a waterflood at 1 ft/day was performed, followed by a waterflood at 5 ft/day, followed by 1 PV of surfactant injection at 1 ft/day, and lastly, a foam flood was performed. A summary of the results of this coreflood can be seen in Table 4.27. Figure 4.39 shows the percent oil recovery and pressure drop across the core as a function of pore volumes injected. As seen in the figure, the waterflood at 1 ft/day recovered 35% of OOIP. When the waterflood flow rate was increase to 5 ft/day, no further oil was recovered, confirming that the core was water wet and no capillary end effects were seen. One pore volume of 0.5% GC 468 with 1% $CaCl_2$ and 1% $MgCl_2$ was injected to satisfy adsorption. 3.2% OOIP was recovered during the surfactant flood. One possible reason for oil recovery during this surfactant flood, but none during the mineral oil experiment is the lower interfacial tension between GC 468 and Crude A (approximately 0.1 dynes/cm) compared to GC 468 and mineral oil (approximately 10 dynes/cm). During the foam flood at 86% quality, an additional 9% OOIP was recovered after 2 PV of surfactant and CO_2 co-injection. After 2 PV of foam injection, no more oil

was recovered. Once again, the foam pressure is less than the waterflood pressure, suggesting that the foam is breaking down in the presence of oil.

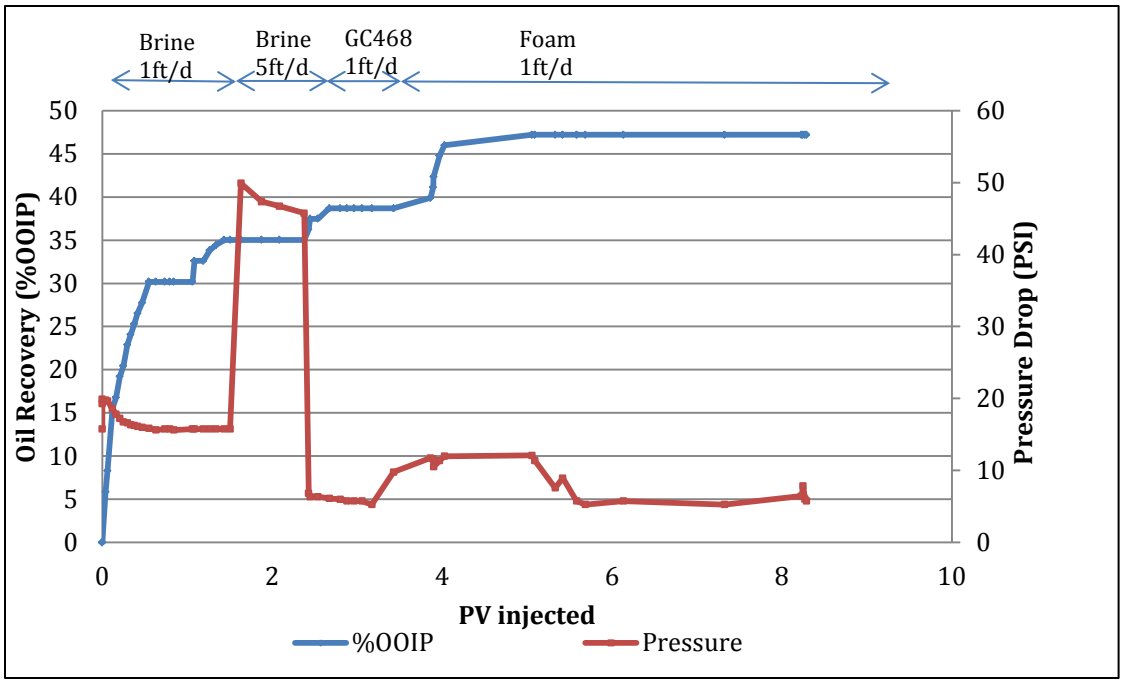

Figure 4. 39: The pressure drop and oil recovery are shown as a function of pore volumes injected for Coreflood 2. Brine is injected at 1 ft/day, followed by brine injection at 5 ft/day, surfactant injection at 1 ft/day, and finally a foam injection at 86% quality at 1 ft/day.

Figure 4.40 shows the ratio oil, water, and gas recovered during various stages of the coreflood. As seen in the figure below, the oil cut was low during the entire waterflood. Because the flood did not begin at residual water saturation, water and oil were recovered from the beginning of the water flood. During the surfactant flood, the oil cut was still lower than the water cut. During the foam flood, the oil recovery began just

before gas break through and continued for a little bit after gas break through. Gas breakthrough occurred at 0.54 PV. After gas break through, more water was recovered; however, no additional oil was recovered. The cumulative oil recovery was 47.2% OOIP with 12.2% OOIP occurring after the water flood. One reason for a lower recovery with Crude A than with mineral oil despite the higher foam stability with Crude A is the foam flood with the mineral oil was performed at a lower oil saturation. The waterflood during the mineral oil coreflood had much higher oil recovery, reducing the oil saturation below critical oil saturation, providing a better environment for foam formation, and therefore, increased sweep efficiency. Studies have observed that increases in oil saturation results in a decrease in the pressure gradient in oil-destabilized flowing foam (Myers and Radke, 2000). Since the waterflood was less effective in reducing oil saturation, Coreflood 2 had a higher oil saturation, and therefore a more destabilizing effect on the foam.

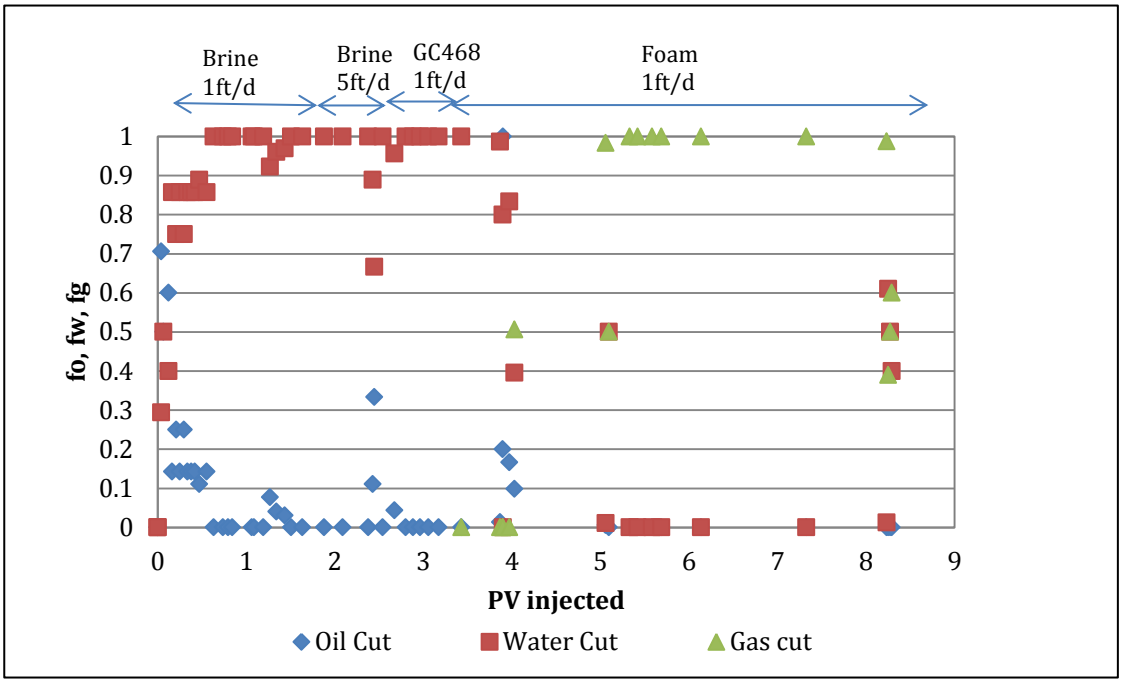

Figure 4. 40: The oil, water, and gas cuts during Coreflood 2.

Coreflood 2: Summary of Results		
Water flood 1 ft/day	1.6 PV	35% OOIP
Water flood 5 ft/day	1 PV	0% OOIP
0.5% GC 468	1 PV	3.2% OOIP
86% quality foam flood	4.9 PV	9% OOIP
	Total oil recovery	47.2 %OOIP

Table 4. 26: A summary of oil recovery during Coreflood 2.

4.3.3 Coreflood 3: GC 468 with Crude A (Oil Wet)

A third coreflood was performed on a Texas Cream Limestone core saturated with Crude A. The core was aged in an oven at 80°C for one month, making the core oil wet. The core properties are listed in Table 4.28, and the experimental conditions are listed in Table 4.29.

Coreflood 3: Core Properties	
Length	1.475 in
Diameter	11.75 in
Porosity	23.4%
Brine Permeability	12.5 mD
Initial Oil Saturation	65.9%

Table 4. 27: Texas Cream Limestone properties for Coreflood 3.

Core Flood 3: Experimental Conditions	
Temperature	60°C
Back Pressure	~100 psi
Oil viscosity (T=60°C)	43 cP
Foam quality	86%
Flow Rate	1 ft/day

Table 4. 28: Experimental conditions for Coreflood 3.

A waterflood at 1 ft/day was performed, followed by a waterflood at 4 ft/day, followed by 1 PV of surfactant injection at 1 ft/day, and lastly, a foam flood was performed. The second waterflood was performed at 4 ft/day rather than 5 ft/day due to pressure constraints of the coreholder. A summary of the results of this coreflood can be seen in Table 4.30. Figure 4.41 shows the percent oil recovery and pressure drop across the core as a function of pore volumes injected. Figure 4.42 shows the oil, water, and gas cuts throughout the flood. As seen in the figure, the waterflood at 1 ft/day recovered 33% of OOIP. When the waterflood flow rate was increase to 4 ft/day, no further oil was recovered; no capillary end effects were seen. One pore volume of 0.5% GC 468 with 1% $CaCl_2$ and 1% $MgCl_2$ was injected to satisfy adsorption. 1% OOIP was recovered during the surfactant flood. During the foam flood at 86% quality, an additional 13% OOIP was recovered after 6 PV of surfactant and CO_2 co-injection. Unlike the water-wet floods, where oil recovery was only seen at the beginning of the foam flood, oil was recovered throughout the foam flood. This could be a result of wettability alteration. The total oil recovery was 47% OOIP, with 14% OOIP occurring after the waterflood. As seen in Figure 4.42, it took almost 0.5 PV of foam injection before gas breakthrough. The pressure drops are much higher in this coreflood than the other corefloods because the oil viscosity is 47 cP rather than 7-11 cP, and the permeability is only 12 mD instead of 20-30 mD. However, these pressure drops are too high, and in a field, the injection rate would have be reduced.

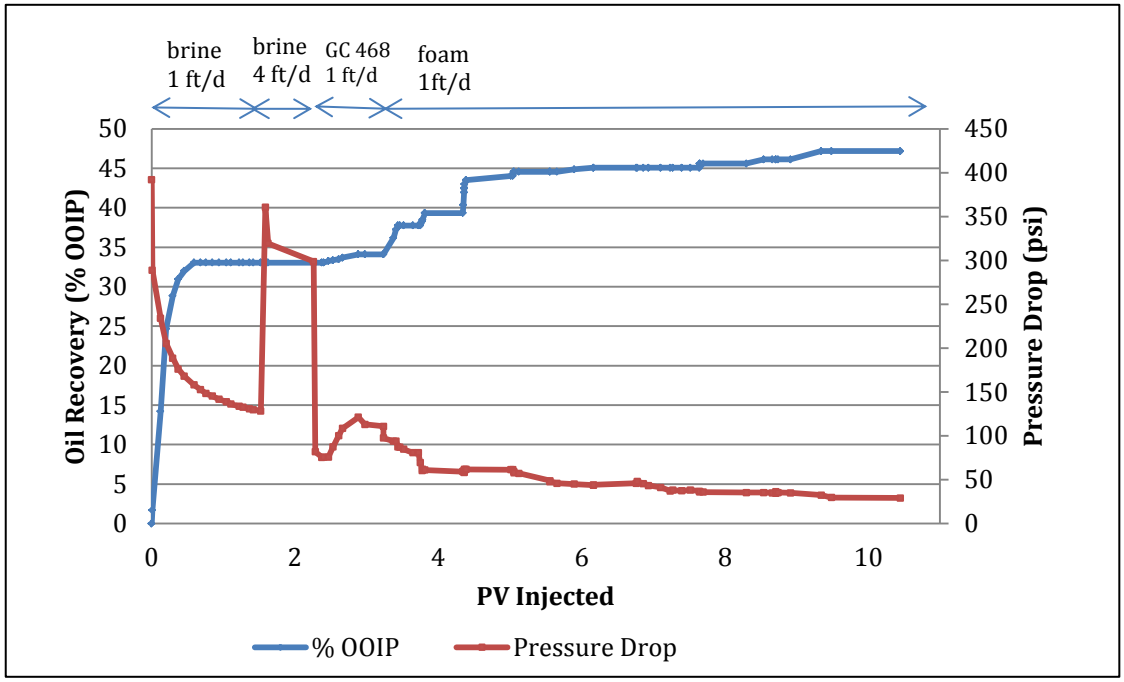

Figure 4. 41: The pressure drop and oil recovery are shown as a function of pore volumes injected for Coreflood 3. Brine is injected at 1 ft/day, followed by brine injection at 4 ft/day (because this coreholder should not be subjected to more than 400 psi), surfactant injection at 1 ft/day, and finally a foam injection at 86% quality at 1 ft/day.

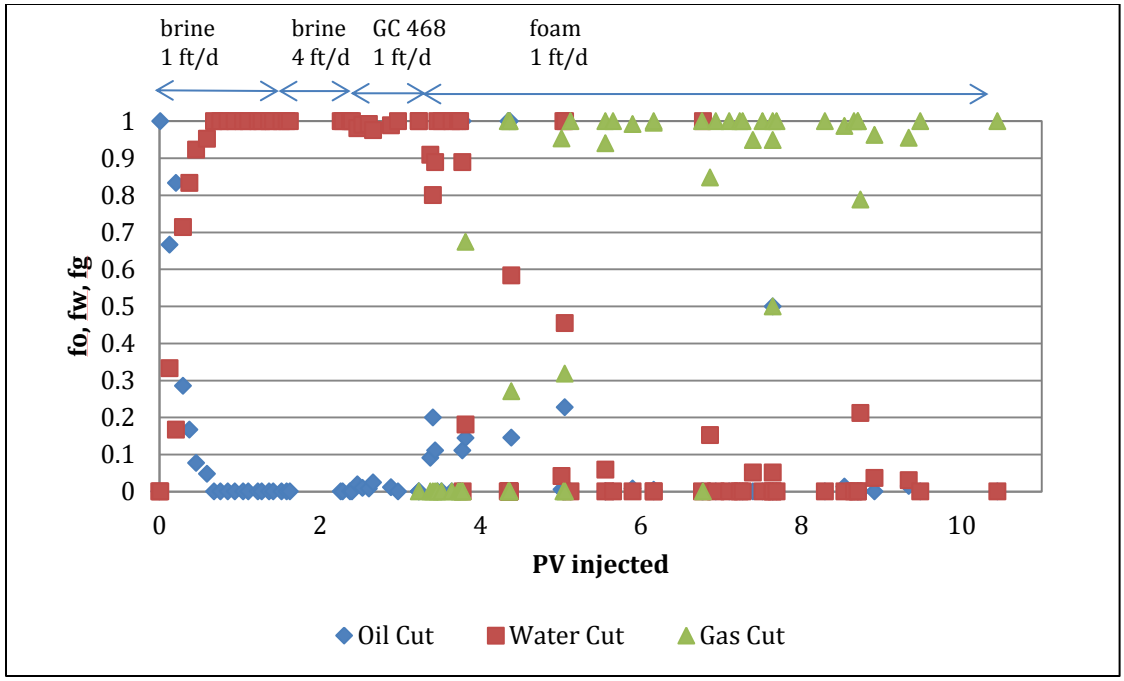

Figure 4. 42: The oil, water, and gas cuts during Coreflood 3.

Coreflood 3: Summary of Results		
Water flood 1 ft/day	1.57 PV	33% OOIP
Water flood 4 ft/day	1 PV	0% OOIP
0.5% GC 468	1 PV	1% OOIP
86% quality foam flood	7.2 PV	13% OOIP
	Total oil recovery	47% OOIP

Table 4. 29: A summary of oil recovery during Coreflood 3.

4.3.4 Coreflood 4: GC 580 with Mineral Oil (Water wet)

The core properties for the Texas Cream limestone used in the water wet coreflood with mineral oil are in Table 4.31, and the experimental conditions are listed in Table 4.32.

Coreflood 4: Core Properties	
Length	1.48 in
Diameter	11.75 in
Porosity	27%
Brine Permeability	20.9 mD
Initial Oil Saturation	70.3%

Table 4. 30: Texas Cream Limestone properties for Coreflood 4.

Coreflood 4: Experimental Conditions	
Temperature	60^{o}C
Back Pressure	~100 psi
Oil viscosity (T=60^{o}C)	11 cP
Foam quality	86%
Flow Rate	1 ft/day

Table 4. 31: Experimental conditions for Coreflood 4.

A summary of the coreflood results are shown in Table 4.33, and Figure 4.43 shows the oil recovery and pressure drop during the flood as a function of pore volumes injected. As seen in the figure below, brine was injected at 1 ft/day until no more oil was recovered. The waterflood recovered 41.6% OOIP. The waterflood flow rate was increased to 5 ft/day, and no additional oil was recovered. One pore volume of 0.5% GC 580 with 2% NaCl, 0.5% $CaCl_2$, and 0.5% $MgCl_2$ was injected to satisfy adsorption. No additional oil was recovered during the surfactant flood. After the surfactant flood, the foam flood at 86% quality was started at 1 ft/day. Very little oil, only 3.1% OOIP was recovered during the foam flood. The gas breakthrough occurred fairly early for a foam flood, after 0.26 PV of foam injection. Because so little oil was recovered and gas breakthrough occurred early, it was thought that the flow rate may have been too slow for foam formation. As a result, the flow rate was increased to 4 ft/day. At 4 ft/day, another 3.1% OOIP was recovered. The cumulative oil recovery from waterflood, surfactant flood, and foam flood was 47.8% OOIP. One explanation for the poor oil recovery from foam is the greatly destabilizing effect of mineral oil on GC 580 foam stability. Mineral oil decreased the bulk foam stability almost instantaneously in the bulk phase. It is possible that the mineral oil also ruptured the foam upon entering porous media, preventing foam from propagating through the core.

Figure 4.44 contains the oil, water, and gas cuts. It can be seen that the oil recovery occurred twice during the foam flood, once during the 1 ft/day foam flood and once during the 4 ft/day foam flood.

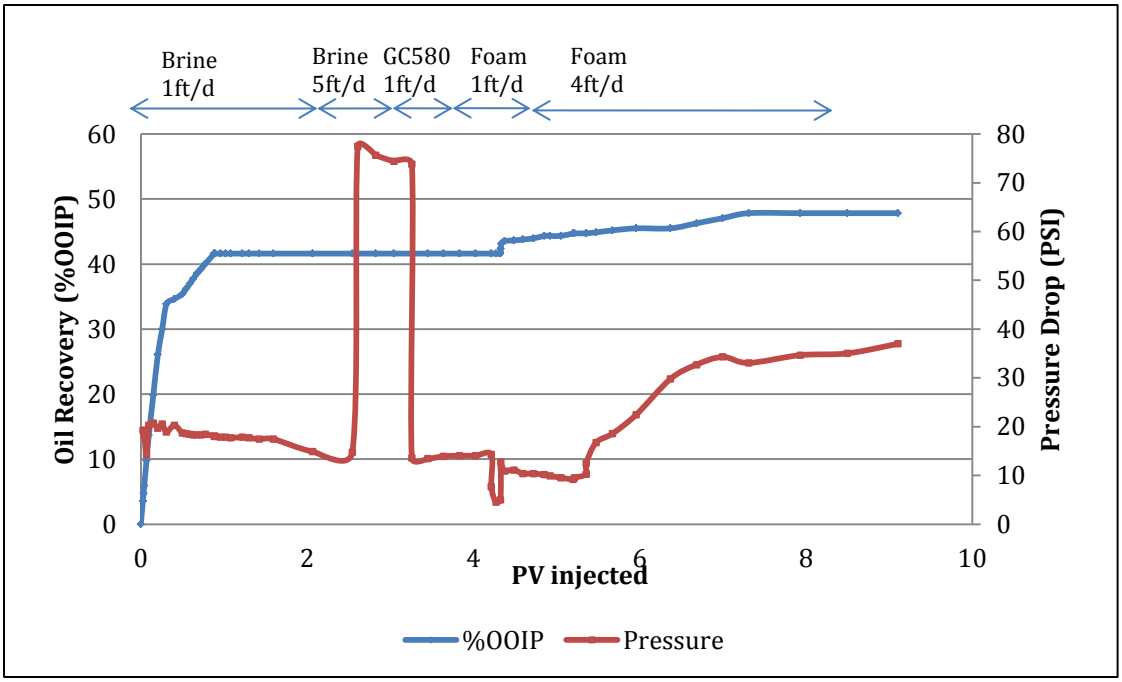

Figure 4. 43: The pressure drop and oil recovery are shown as a function of pore volumes injected for Coreflood 4. Brine is injected at 1 ft/day, followed by brine injection at 5 ft/day, surfactant injection at 1 ft/day, and finally a foam injection at 86% quality at 1 ft/day. Since the 1 ft/day foam flood did not recover much, the foam flood rate was increased to 4 ft/day.

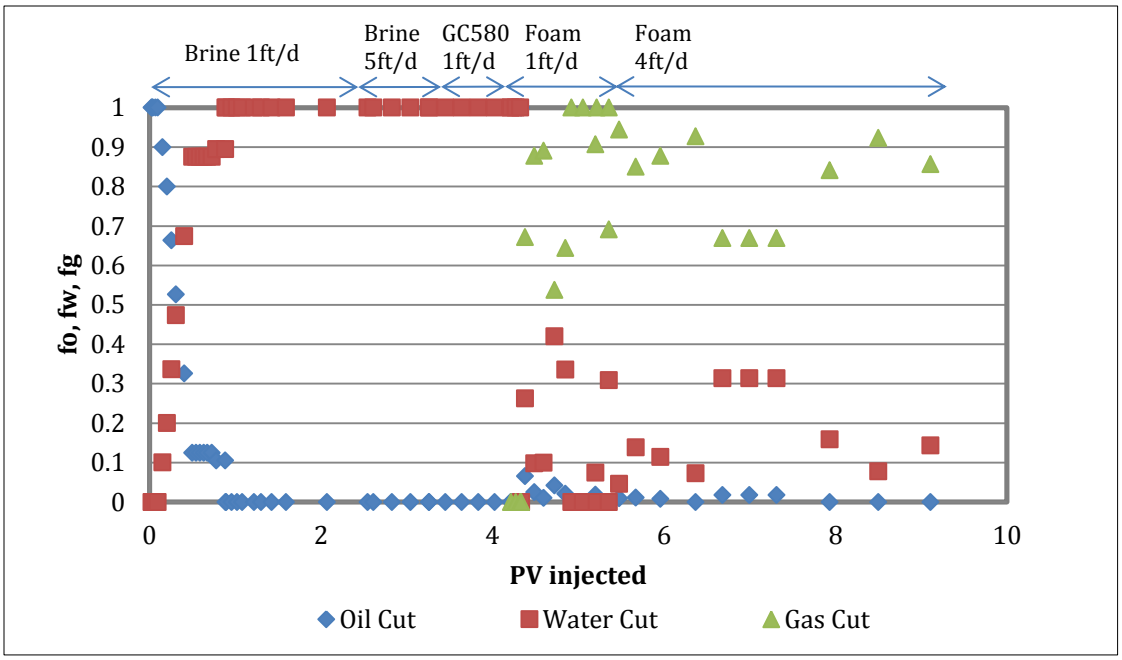

Figure 4. 44: The oil, water, and gas cuts during Coreflood 4.

Core Flood 4: Summary of Results		
Water flood 1 ft/day	2.6 PV	41.6% OOIP
Water flood 5 ft/day	1 PV	0% OOIP
0.5% GC 580	1 PV	0% OOIP
86% quality foam flood 1 ft/day	1.2 PV	3.1% OOIP
86% quality foam flood 4 ft/day	3.75 PV	3.1% OOIP
	Total oil recovery	47.8% OOIP

Table 4. 32: A summary of oil recovery during Coreflood 4

4.3.5 Coreflood 5: GC 580 with Crude A (Water Wet)

A Texas Cream Limestone was saturated with Crude A, but the core was not aged, ensuring the core was water-wet. The properties of the core can be seen in Table 4.34. The experimental conditions for the coreflood are listed in Table 4. 35.

Coreflood 5: Core Properties	
Length	1.48 in
Diameter	11.75 in
Porosity	28%
Brine Permeability	23 mD
Initial Oil Saturation	48%

Table 4. 33: Texas Cream Limestone properties for Coreflood 5.

Coreflood 5: Experimental Conditions	
Temperature	60^{o}C
Back Pressure	~100 psi
Oil viscosity (T=60^{o}C)	7 cP
Foam quality	86%
Flow Rate	1 ft/day

Table 4. 34: Experimental conditions for Coreflood 5.

A summary of the coreflood results and a plot of oil recovery and pressure drop across the core as function of pore volumes injected can be seen in Table 4.36 and Figure 4.45 A plot containing the fraction of oil, water, and gas recovery as a function of pore volumes injected can be seen in Figure 4.46. As seen in the figure, brine was injected at 1 ft/day until no more oil was recovered. The waterflood recovered 39.9% OOIP. The waterflood rate was increased to 5 ft/day to ensure that there were no capillary end effects. No additional oil was recovered during the 5 ft/day waterflood, confirming that the core was water-wet. One pore volume of 0.5% GC 580 with 2% NaCl, 0.5% CaCl2, and 0.5% MgCl2 was injected at 1 ft/day to satisfy adsorption, during which 5.4% OOIP was recovered. After the surfactant injection, CO_2 and surfactant were co-injected at 86% quality and 1 ft/day flow rate. The foam flood recovered 3% OOIP before gas breakthrough, which occurred 0.43 PV after the foam injection began. After breakthrough, however, the foam flood continued to produce another 5.8% OOIP. The foam flood recovered a total of 8.8% OOIP. The waterflood, surfactant flood, and foam flood recovered 54.1% OOIP. The tertiary recovery of the coreflood with Crude A was substantially better than the tertiary recovery of the coreflood with mineral oil, indicating that the type of oil has an effect of foam stability in porous media. Once again, the pressure drop during the foam flood was lower than the pressure drop during the waterflood, indicating that the oil quickly destabilized the foam.

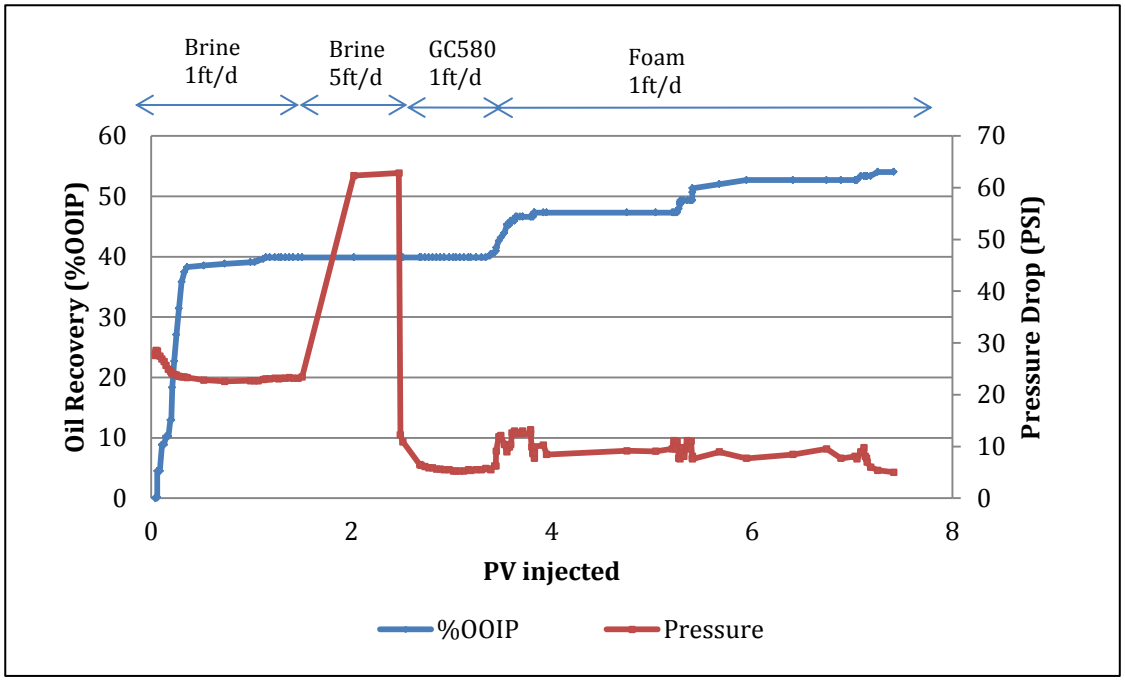

Figure 4. 45: The pressure drop and oil recovery are shown as a function of pore volumes injected for Coreflood 5. Brine is injected at 1 ft/day, followed by brine injection at 5 ft/day, surfactant injection at 1 ft/day, and finally a foam injection at 86% quality at 1 ft/day.

From Figure 4.45, it can be seen that oil recovery occurred during the 1 ft/day waterflood, the surfactant flood, and during the foam flood. During the foam flood, oil recovery can be seen at three separate times, suggesting that the foam was continuing to sweep new sections of the core, unlike the other water-wet corefloods where one main sweep was seen during the foam flood at 1 ft/day.

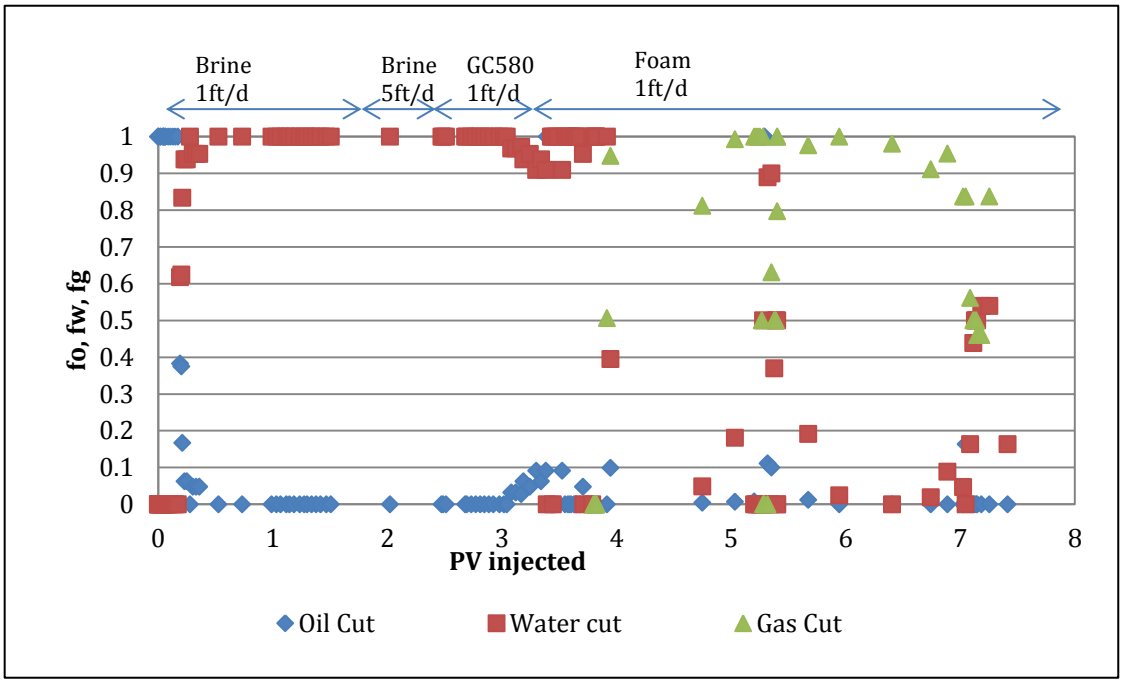

Figure 4. 46: The oil, water, and gas cuts during Coreflood 5.

Coreflood 5: Summary of Results		
Water flood 1 ft/day	2 PV	39.9% OOIP
Water flood 5 ft/day	1 PV	0% OOIP
0.5% GC 580	1 PV	5.4% OOIP
86% quality foam flood	4 PV	8.8% OOIP
	Total oil recovery	54.1% OOIP

Table 4. 35: A summary of oil recovery during Coreflood 5.

Chapter 5: Conclusions and Recommendations

ASP flooding using anionic surfactants are not suitable for many carbonate reservoirs. For example, common alkali cannot be used with hard formation brine. The anionic surfactant adsorption on carbonate rocks are high in the absence of high pH. Polymers plug low permeability reservoirs. Thus alternative methods of EOR need to be found for low permeability carbonate reservoirs. The goal of this work was to evaluate two novel cationic gemini surfactants for CO_2-foam flooding for EOR in carbonate reservoirs.

5.1 CONCLUSIONS

Experiments were first performed to characterize the surfactants in terms of aqueous stability, bulk foam stability, and adsorption. It was found that the cationic gemini surfactants are stable in brines at a range of temperatures and salinities. The shorter chain cationic gemini, GC 468, was stable from 25^{o}C up to 120^{o}C (the highest temperature tested) with 100,000 ppm salinity. The bulk foam stability was studied with and without oils at several salinities and temperatures. The bulk foam stability of the two cationic gemini surfactants was comparable to the bulk foam stability of a conventional cationic surfactant. It was found that increasing temperature resulted in a decrease in bulk foam stability, but pH had no effect on the bulk foam stability of these cationic gemini surfactants. Static adsorption was measured, and it was found that the cationic surfactants had 10 times less adsorption on crushed limestone than an anionic surfactant. The wettability alteration experiments showed that both cationic geminis are capable of changing an oil-wet calcite chip aged in Crude B to intermediate-wet. It is important for foam propagation that the rock is no longer oil-wet. Although water-wet conditions are ideal for foam propagation, foams can propagate in intermediate-wet reservoirs (Lescure

and Claridge, 1986). For Crude A and Crude C, however, these surfactants were not effective at wettability alteration and would require an additional surfactant for wettability alteration.

Core flood experiments were performed in the absence of oil to prove foam formation, determine the effect of surfactant concentration on foam strength, and to determine the quality at which the surfactants had the strongest foam. Both cationic gemini surfactants showed stronger foam than a conventional cationic surfactant. The foam strength increased with increasing gemini surfactant concentration. The strength of the foam increased with increasing quality from 70%-85%; after 85%, however, an increase in quality caused a decrease in foam strength. Due to this, a foam quality of 85% was chosen for foam floods in the presence of oil.

Two water-wet corefloods were performed with each surfactant. When using GC 468 during a coreflood with a limestone saturated with mineral oil, the foam flood recovered 15.9% OOIP after the water flood recovered 58.6% OOIP resulting in a total recovery of 74.5% OOIP. When the core was saturated with Crude A, the waterflood recovered 35% OOIP, and the GC 468 surfactant and foam flood recovered an additional 12.2% OOIP, resulting in a total recovery of 47.2% OOIP. When using GC 580 during a coreflood with a limestone saturated with mineral oil, the foam flood recovered an additional 6.2% OOIP after the waterflood recovered 41.6%, resulting in a total recovery of 47.8%. When the core was saturated with Crude A, the GC 580 surfactant and foam flood recovered an additional 14.2% OOIP after the waterflood recovered 39.9% OOIP, resulting in a total recovery of 54.1% OOIP.

One oil-wet coreflood was performed. The limestone was saturated with Crude A and aged for one month. The surfactant and foam flood recovered an additional 14%

OOIP after the waterflood recovered 33% OOIP, resulting in a total oil recovery of 47 % OOIP. The pressure drop during all the water-wet foam floods in the presence of oil was not too high, less than 15 psi/ft. Despite the lower pressure drop, the foam floods recovered an additional 6-16% OOIP, indicating the foam was sweeping unswept regions of the core, unlike polymers, which would have a significantly higher pressure drop than the waterflood. These results show that these novel cationic gemini surfactants could be a viable alternative to polymer flooding in carbonate reservoirs.

5.2 Recommendations and Future Work

The more experiments are recommended for further studies the use of cationic gemini surfactants for foam flooding in carbonate reservoirs. It would be beneficial to use Crude B in an oil-wet experiment since GC 468 showed favorable wettability alteration during calcite chip experiments. It would also be beneficial to vary the type of carbonate core to show these cationic surfactants can be used in a variety of reservoirs. Likewise, it would be valuable to add foam boosters to see if a stronger foam can be formed and further increase sweep efficiency. In addition to adding foam boosters, it could be valuable to look for synergistic surfactants for better wettability alteration. It could be beneficial to make shorter chain cationic gemini surfactants or shorter spacer to increase aqueous stability at higher salinity. Lastly, it would be valuable to evaluate heterogeneous systems (sand pack and core) to show foam does increase sweep efficiency.

Appendix A

Appendix A contains the aqueous stability results for GC 566 and GC 776.

Salinity	T=25°C	T=60°C	T=80°C	T=120°C
0% NaCl + 0% $CaCl_2$ + 0% $MgCl_2$	Cloudy	Hazy	Clear	Clear
0% NaCl + 1% $CaCl_2$ + 1% $MgCl_2$	Cloudy	Hazy	Clear	Clear
1% NaCl + 1% $CaCl_2$ + 1% $MgCl_2$	Cloudy	Hazy	Clear	Clear
4% NaCl + 1% $CaCl_2$ + 1% $MgCl_2$	Cloudy	Hazy	Hazy	Hazy
8% NaCl + 1% $CaCl_2$ + 1% $MgCl_2$	Cloudy	Hazy	Hazy	Hazy
10% NaCl + 0% $CaCl_2$ + 0% $MgCl_2$	Cloudy	Hazy	Hazy	Hazy
15% NaCl + 0% $CaCl_2$ + 0% $MgCl_2$	Cloudy	Hazy	Hazy	Hazy

Table A. 1: Aqueous stability GC 566 at a range of temperatures and salinities. GC 566 was only aqueously stable above 80°C at low salinities. The reservoir temperature for this study was 60°C; therefore, this surfactant was not studied further.

Salinity	T=25°C	T=60°C	T=80°C	T=120°C
0% NaCl + 0% $CaCl_2$ + 0% $MgCl_2$	Precipitates	Precipitates	Precipitates	Precipitates
0% NaCl + 1% $CaCl_2$ + 1% $MgCl_2$	Precipitates	Precipitates	Precipitates	Precipitates
1% NaCl + 1% $CaCl_2$ + 1% $MgCl_2$	Precipitates	Precipitates	Precipitates	Precipitates
4% NaCl + 1% $CaCl_2$ + 1% $MgCl_2$	Precipitates	Precipitates	Precipitates	Precipitates
8% NaCl + 1% $CaCl_2$ + 1% $MgCl_2$	Precipitates	Precipitates	Precipitates	Precipitates
10% NaCl + 0% $CaCl_2$ + 0% $MgCl_2$	Precipitates	Precipitates	Precipitates	Precipitates
15% NaCl + 0% $CaCl_2$ + 0% $MgCl_2$	Precipitates	Precipitates	Precipitates	Precipitates

Table A. 2: Aqueous stability of GC 776 at a range of temperatures and salinities. GC 776 is not aqueously stable at any temperatures or salinities evaluated; therefore it was not studied further.

Appendix B

Appendix B contains a few of the bulk foam stability results, showing the variability of each bulk foam stability test. Each experiment was performed three times to show the repeatability of foam formation and half-life at varying salinities, temperatures, and oils.

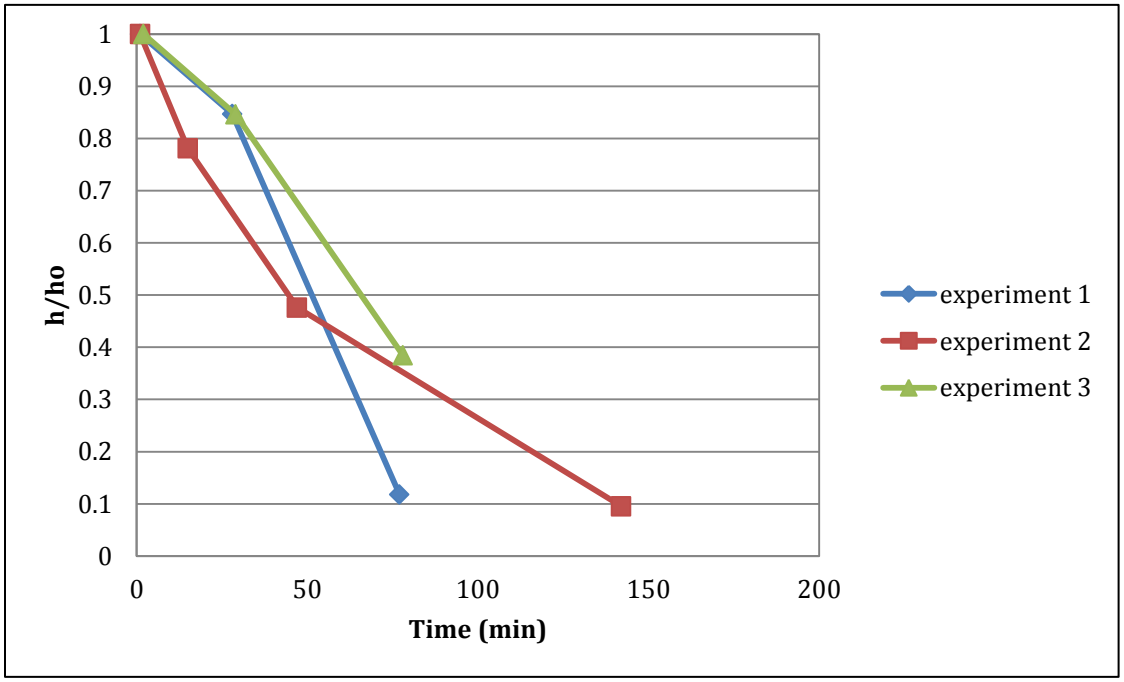

Figure B. 1: Bulk foam stability results of 0.25% GC 468 with 1% $CaCl_2$ and 1% $MgCl_2$ at T=60^{o}C. No oil was present.

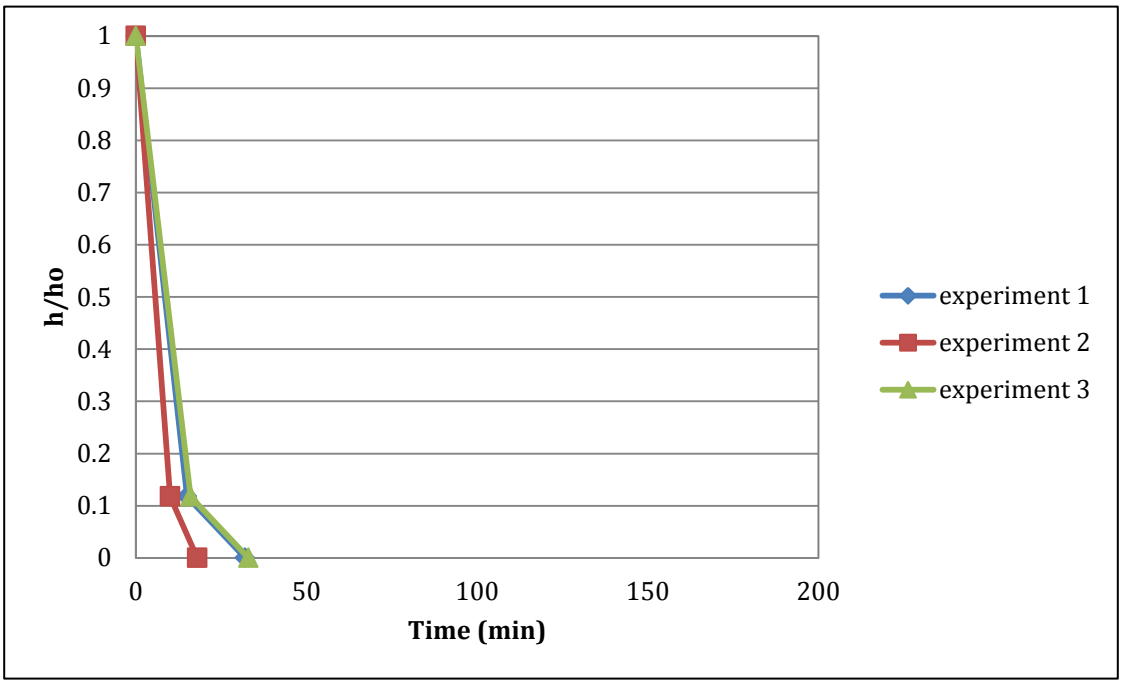

Figure B. 2: Bulk foam stability results of 0.25% GC 580 with 4% NaCl, 1% $CaCl_2$, and 1% $MgCl_2$ at T=25^{o}C in the presence of 1wt% decane.

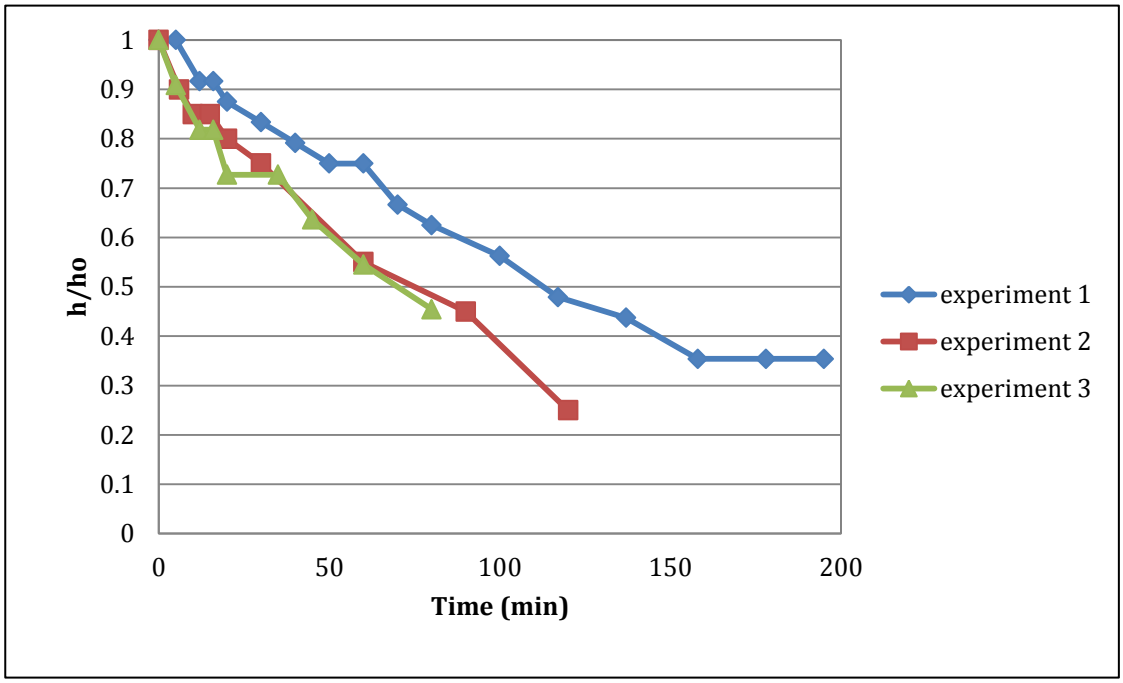

Figure B. 3: Bulk foam stability results of 0.25% GC 580 with 4% NaCl, 1% $CaCl_2$, and 1% $MgCl_2$ at T=25°C. No oil was present.

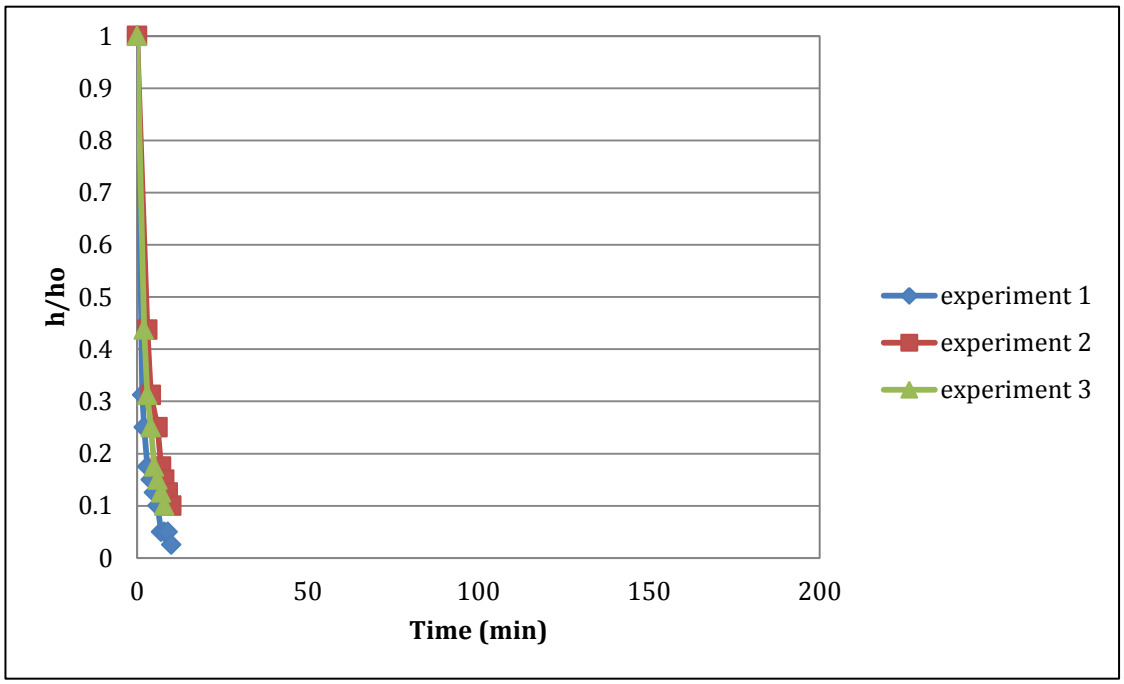

Figure B. 4: Bulk foam stability results of 0.25% GC 580 with 4% NaCl, 1% $CaCl_2$, and 1% $MgCl_2$ at T=25°C in the presence of 1 wt% mineral oil.

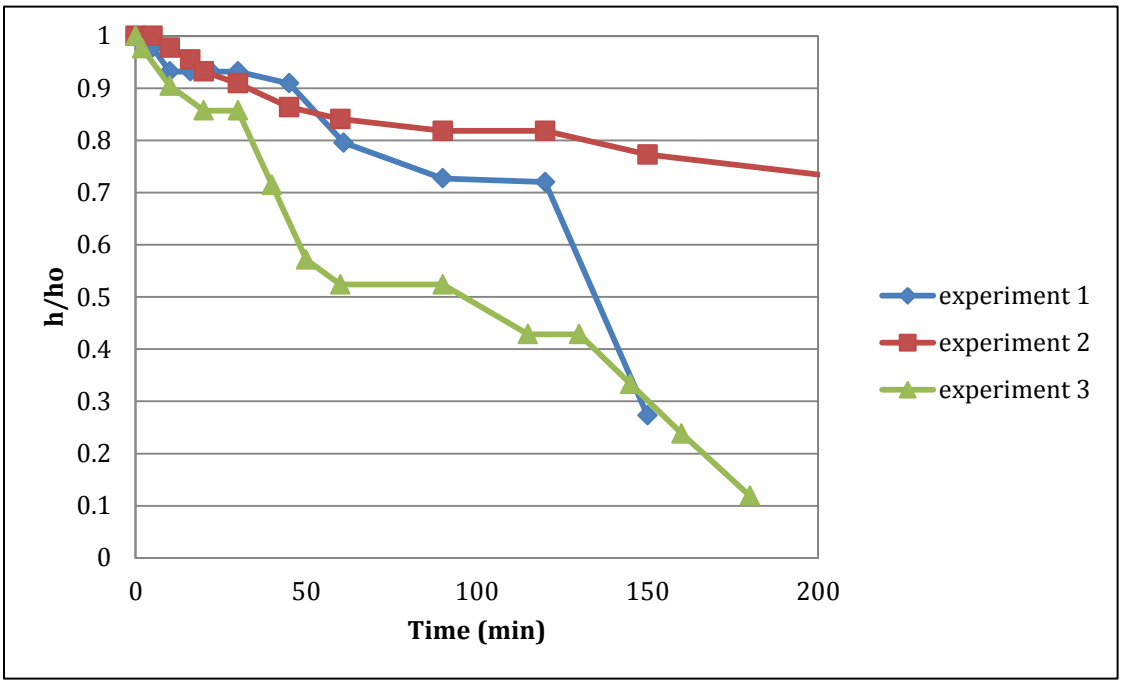

Figure B. 5: Bulk foam stability results of 0.25% GC 580 with 4% NaCl, 1% $CaCl_2$, and 1% $MgCl_2$ at T=25^{o}C in the presence of 1 wt% Crude A.

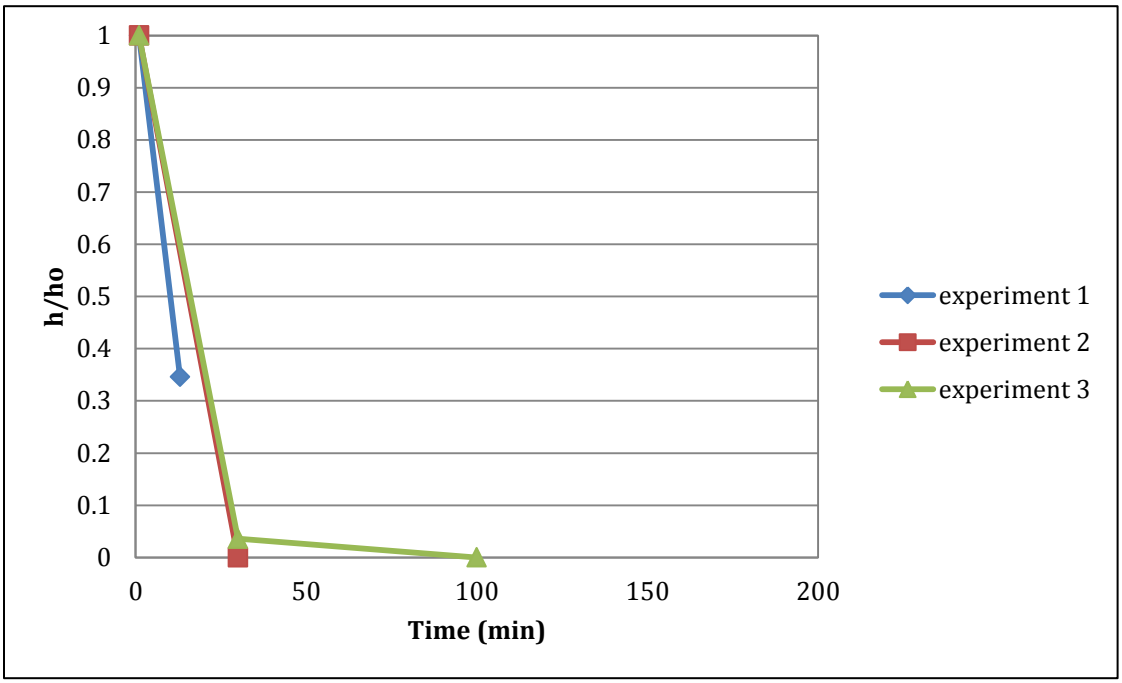

Figure B. 6: Bulk foam stability of 0.25% CTAB with 4% NaCl, 1% $CaCl_2$, and 1% $MgCl_2$ at T=60^{o}C. No oil was present.

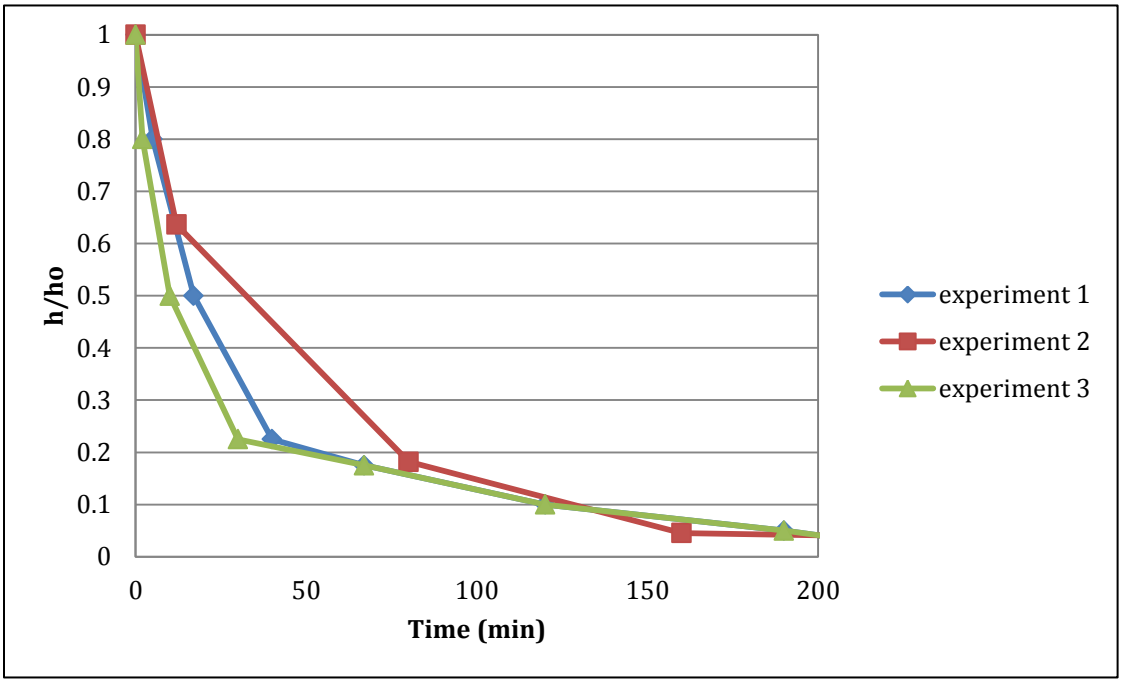

Figure B. 7: Bulk foam stability of 0.25% AS-40 at T=60°C. No salt is present and no oil is present

References

Apaydin, O., and Kovscek, A. (2001). Surfactant Concentration and End Effects on Foam Flow in Porous Media, TR-120.

Bullen, R. S., and Bratrud, T. F. (1976). Fracturing With Foam. *Petroleum Society of Canada*. doi:10.2118/76-02-02

Caenn, R., Burnett, D., and Chilingarian, G. (1989). Polymer Flooding. In *Enhanced Oil Recovery, II: Processes and Operations* (B ed., Vol. 17, pp. 157-186). New York: Elsevier Science.

Chambers, K.T. and Radke, C.J. (1990). Capillary Phenomena in Foam Flow Through Porous Media. *Interfacial Phenomena in Petroleum Recovery*, ed. N.R. Morrow, Chap. 6, 191-225. New York: Marcel Decker.

Chang, S.H., and Grigg, R. B. (1998). Effects of Foam Quality and flow Rate on CO2-Foam Behavior at Reservoir Conditions. *Society of Petroleum Engineers*. doi:10.2118/39679-MS

Chen, Y., Elhag, A. S., Poon, B. M., Cui, L., Ma, K., Liao, S. Y., and Johnston, K. P. (2012). Ethoxylated Cationic Surfactants for CO2 EOR in High Temperature, High Salinity Reservoirs. *Society of Petroleum Engineers*. doi:10.2118/154222-MS

Diamant, H. and Andelman, D. 2003. Models of Gemini Surfactants. In *Gemini Surfactants: Synthesis, Interfacial and Solution-phase Behavior, and Applications*, R. Zana and J. Xia (eds). New York: Marcel Dekker.

Falls, A. H., Shell Development Co., G. J. Hirasaki, Shell Development Co., et al. (1988). Development of a mechanistic Foam Simulator: The Population Balance and Generation by Snap-Off. *SPE Reservoir Engineering*, *3*: 884-892.

Farajzedah, R. Andrianov, A., Krastev, R., Hirasaki, G.J., and Rossen, W.R. (2012). Foam-Oil interaction in porous media: Implications for foam assisted enhanced oil recovery. *Advances in Colloid and Interface Science*. *183-184*: 1-13.

Friedmann, F., Chen, W. H., and Gauglitz, P. A. (1991). Experimental and Simulation Study of High-Temperature Foam Displacement in Porous Media. *Society of Petroleum Engineers*. doi:10.2118/17357-PA.

Hait, S.K., and Moulik, S.P. (2002). Gemini Surfactants: A Distinct Class of Self-Assembling Molecules. *Current Science*. *82*: 1101-1111.

Hirasaki, G. J., and Lawson, J. B. (1985). Mechanisms of Foam Flow in Porous Media: Apparent Viscosity in Smooth Capillaries. *Society of Petroleum Engineers*. doi:10.2118/12129-PA.

Homme, R. (1996). Foams: Theory, measurements, and applications. New York: Marcel Dekker.

Hutchins, R. D., and Miller, M. J. (2005). A Circulating Foam Loop for Evaluating Foam at Conditions of Use. *Society of Petroleum Engineers*. doi:10.2118/80242-PA

Jiménez, R., Soltero, J., Lopez-Dellamary, F., Palacios, G., and Puig, J. (2001). Unusual Hofmann Elimination under Mild Conditions in Polymerizable Cationic Surfactant Systems. *Langmuir, 18*, 3767-3772.

Kapetas, L., Vincent Bonnieu, S., Danelis, S., Rossen, W. R., Farajzadeh, R., Eftekhari, A. A., & Kamarul Bahrim, R. Z. (2015). Effect of Temperature on Foam Flow in Porous Media. *Society of Petroleum Engineers.* doi:10.2118/172781-MS

Kovscek, A.R. and C.J. Radke (1994). Fundamentals of Foam Transport in Porous Media. Foams: Fundamentals and Applications in the Petroleum Industry, *American Chemical Society*, *242*: 115-163.

Kruglyakov, P. and Vilkova, N. (1999). The relation between stability of asymmetric films of the liquid:liquid-gas type, spreading coefficient and surface pressure. *Colloid and Surface A*., *156*: 475-487.

Lake, L.W. (1989). Enhanced Oil Recovery. Upper Saddle River, New Jersey: Prentice Hall.

Lee, H. O., Heller, J. P., and Hoefer, A. M. W. (1991). Change in Apparent Viscosity of CO_2 Foam With Rock Permeability. *Society of Petroleum Engineers*. doi:10.2118/20194-PA

Lescure, B., and Claridge, E. (1986). CO_2 Foam Flooding Performance vs. Rock Wettability. *Proceedings of SPE Annual Technical Conference and Exhibition*.

Liu, Y., Grigg, R. B., and Bai, B. (2005). Salinity, pH , and Surfactant Concentration Effects on CO_2-Foam. *Society of Petroleum Engineers*. doi:10.2118/93095-MS

Lyons, W.C. and Plisga, G.J. (2011). Resevoir Engineering. Standard Handbook of Petroleum and Natural Gas Engineering. Houston: Gulf Professional Publishing.

Marsden, S.S. (1986). Foams in Porous Media. United States Department of Energy.

Montaron, B. (2005). Increasing Oil Recovery Factors: A Technical Challenge Key to Future World Energy Supply. ATP Conference, Paris, October, 2005.

Myers, T., and Radke, C. (2000). Transient Foam Displacement in the Presence of Residual Oil: Experiment and Simulation Using a Population-Balance Model. *Industrial & Engineering Chemistry Research Ind. Eng. Chem. Res*., 2725-2741.

Nguyen, Q. P., Alexandrov, A. V., Zitha, P. L., and Currie, P. K. (2000). Experimental and Modeling Studies on Foam in Porous Media: A Review. *Society of Petroleum Engineers*. doi:10.2118/58799-MS.

Nikolov, A. D., Wasan, D. T., Huang, D. W., and Edwards, D. A. (1986). The Effect of Oil on Foam Stability: Mechanisms and Implications for Oil Displacement by Foam in Porous Media. *Society of Petroleum Engineers*. doi:10.2118/15443-MS

Pope, G.A. (2007). Overiew of Chemical EOR. Casper EOR Workshop, Casper, 26 October.

Rossen, W.R. (1996). Foams in Enhanced Oil Recovery. Foams: Theory, Measurement, and Applications, ed. R.K. Prudhomme and S. Khan. New York: Marcel Dekker.

Schramm, L.L. (1994). Foams: Fundamentals and Applications in the Petroleum Industry. *American Chemical Society*. doi: 10.1021/ba-1994-0242.

Schlumberger. (2007). Carbonate Reservoirs: Meeting Unique Challenges to Maximize Recovery. Retrieved April 27, 2015, from http://www.slb.com/~/media/Files/industry_challenges/carbonates/brochures/cb_carbonate_reservoirs_07os003.pdf.

Schlumberger Market Analysis. (2007). Carbonate Reservoirs. (n.d.). Retrieved April 26, 2015, from http://www.slb.com/services/technical_challenges/carbonates.aspx.

Seethepalli, A., Adibhatla, B., and Mohanty, K.K. (2004). Wettability Alteration During Surfactant Flooding of Carbonate Reservoirs. Presented at the SPE/DOE Symposium on Improved Oil Recovery, Tulsa, 17-21 April. SPE-89423-MS. http://dx.doi.org/10.2118/89423-MS.

Shamsijazeyi, H., Hirasaki, G., and Verduzco, R. (2013). Sacrificial Agent for Reducing Adsorption of Anionic Surfactants. *Society of Petroleum Engineers.* doi:10.2118/164061-MS.

Sharma, H., Dufour, S., Arachchilage, G., Weerasooriya, U., Pope, G., & Mohanty, K. (2015). Alternative alkalis for ASP flooding in anhydrite containing oil reservoirs. Fuel, 407-420.

Sharma, M., & Shah, D. (1989). Use of Surfactants in Oil Recovery. Enhanced Oil Recovery, II: Processes and Operations (B ed., Vol. 17, pp. 256-208). New York: Elsevier Science.

Sharma, M.K., Shah, D.O., and Bringham, W.E. (1982). Surface properties of foaming agents and behavior of foam in porous media. *Ann. Conven. DOE-Contractor, Enhanced Oil Recovery Projects, San Francisco, Calif,. Jul 27-29*, pp. 74-84.

Spirov, P., Rudyk, S., and Khan, A. (2012). Foam Assisted WAG, Snorre Revisit with New Foam Screening Model. SPE J. doi:10.2118/150829-MS.

Tsau, J.-S., and Grigg, R. B. (1997). Assessment of Foam Properties and Effectiveness in Mobility Reduction for CO2-Foam Floods. *Society of Petroleum Engineers*. doi:10.2118/37221-MS.

Wang, L., and Langley, D. (1977). Identification and determination of ionic surface active agents. *Archives of Environmental Contamination and Toxicology, 5*, 447-456.

Zana, R., and Xia, J. (Eds.). (2004). Gemini Surfactants: Synthesis, Intefacial, and Solution-Phase Behavior and Applications. New York: Marcel Dekker.

Zeng, Y. (Director) (2015). Effect of Gas Type and Composition on Foam Rheology in Porous Media for EOR . AIChE Annual Meeting. Lecture conducted from , Salt Lake City.

Vita

Ruth Hahn was born in Knoxville, Tennessee. In 2009 she entered Trinity University, where she graduated with a B.S. in Engineering Science with a concentration in Chemical Engineering in 2013. In August, 2013, she entered the University of Texas at Austin and began her studies as a M.S. in Petroleum and Geosystems Engineering.

Email: ruthellenhahn@gmail.com

This thesis was typed by the author.